

Regeneration of the sea anemone
Nematostella vectensis: Dissecting the
interplay between local and systemic
responses

Stephanie Cheung

Regeneration of the sea anemone
Nematostella vectensis: Dissecting
the interplay between local and
systemic responses

Stephanie Cheung

Utrecht 2022

The work described in this thesis was performed at the European Molecular Biology Laboratory (EMBL) in Heidelberg, Germany within the framework of the research school Cancer Stem cells & Developmental biology (CS&D), which is part of the Utrecht Graduate School of Life Sciences (Utrecht University).

Cover and illustrations by Anniek Stokkermans and Stephanie Cheung
Printing: Proefschriftmaken

ISBN: 978-94-6423-962-1

Copyright © 2022 by Stephanie Cheung. All rights reserved. No part of this book may be reproduced, stored in a retrieval system or transmitted in any form or by any means without prior permission of the author.

**Regeneration of the sea anemone
Nematostella vectensis: Dissecting the
interplay between local and systemic
responses**

**Regeneratie van de zeeanemoon *Nematostella vectensis*: het
ontleden van het samenspel tussen lokale en systemische reacties**
(met een samenvatting in het Nederlands)

Proefschrift

ter verkrijging van de graad van doctor aan de
Universiteit Utrecht
op gezag van de
rector magnificus, prof.dr. H.R.B.M. Kummeling,
ingevolge het besluit van het college voor promoties
in het openbaar te verdedigen op

maandag 10 oktober 2022 des middags te 4.15 uur

door

Stephanie Cheung

geboren op 15 mei 1989
te Guangdong, China

Promotor:

Prof. dr. H.C. Korswagen

Co-Promotor:

Dr. A. Ikmi

Beoordelingscommissie:

Prof. dr. A. van Oudenaarden

Prof. dr. ir. J.P.W.M. Bakkers

Prof. dr. M. Boxem

Dr. T. Hiiragi

Prof. dr. E. Berezikov

Table of Contents

Chapter 1	General Introduction	7
Chapter 2	Spatial transcriptomics reveal gene expression and developmental landscapes of the primary polyp in a sea anemone	21
Chapter 3	Heat shock treatment initiates dormant regeneration in the sea anemone <i>Nematostella vectensis</i>	43
Chapter 4	Tentacle tip regeneration can proceed via two distinct mechanisms in <i>Nematostella vectensis</i>	63
Chapter 5	General Discussion	81
Addendum		89
	Nederlandse samenvatting	90
	English summary	92
	Acknowledgments/Dankwoord	94
	List of publications	98
	Curriculum vitae	99



“Scientific truth was not dogma, good for eternity, but a temporal quantitative entity that could be studied like anything else.”

- Robert M. Pirsig, *Zen and the Art of Motorcycle Maintenance*, p.140

Chapter 1

1

General Introduction

Stephanie Cheung

What is regeneration?

The topic of regeneration can be said to elicit a universal fascination among people. Indeed, who's imagination is not enticed by the idea of being able to regrow one's limb? However, what does it really mean to regenerate? In 1901 Thomas Hunt Morgan unified the many uses of the term "regeneration" into three distinct phenomena: egg and embryo regeneration, physiological regeneration, and restorative regeneration¹. In more recent literature, these phenomena may be referred to as "embryonic regulation" (the ability of embryos to compensate for cell or tissue lost), "homeostatic regeneration" (the periodic replacement of old cells or tissue not resulting from an acute injury such as skin renewal), and "restorative regeneration" (the regrowth of a lost body region as a result of acute injury or autotomy)². In this thesis, the term regeneration refers specifically to the study of restorative regeneration resulting from acute injury within the animal kingdom.

Within the category of restorative regeneration, there lies a hierarchy of regenerative complexity of structures that can be restored³. At the base lies cell regeneration, such as axonal regeneration in *C. elegans*, one of the simplest structures that can regenerate. Higher up is organ or tissue regeneration, such as skin regeneration of the spiny mouse *Acomys cahirinus*, followed by complex structure regeneration (which includes the restoration of lost limbs). At the top of the hierarchy is whole-body regeneration, which involves the restoration of a complete animal from a small tissue fragment or cluster of cells. Naturally, the categories higher on the hierarchy will also encompass properties of the lower categories. For example, complex structure regeneration incorporates cell, tissue, and organ regeneration. Thus, animals capable of whole-body regeneration are considered to possess the greatest regenerative ability.

The ability to regrow a body region following injury is a widespread phenomenon present across all phyla within the animal kingdom (Figure 1). From the freshwater cnidarian *Hydra* to salamander lizards, a large number of animal species have been shown to possess regenerative abilities⁴. Even humans are capable of regenerating its liver following partial hepatectomy⁵. However, the regenerative capacity of animals varies widely. *Hydra* polyps show the greatest regenerative capacity where complete polyps can be regenerated from clusters of dissociated single-cells⁶⁻⁸. Vertebrates such as the zebrafish (*Danio rerio*), in contrast, display more limited regenerative potential restricted to specific organ structures (i.e., heart, tail, fin)⁹. Interestingly, when the regenerative capacities of animals are put into the context of their phylogenetic positions, a general trend of anticorrelation between regenerative ability and anatomical complexity emerges^{4,10}. While there are many examples of this phylogenetic trend within different animal phyla, this trend is lacking within many animal classes. For example, different planarian flatworm species display very different regenerative abilities: *Schmidtea mediterranea* and *Dugesia japonica* can regenerate from tiny tissue fragments, while *Dendrocoelum lacteum*¹¹ possess anatomically limited regenerative abilities, and *Bdelloura candida* are almost entirely regeneration deficient^{12,13}. Thus, whether regeneration is an ancient evolutionary trait or an evolutionary adaptation remains to be clarified. The recent expansion of non-traditional model systems being studied in the field of regeneration will likely improve our understanding of the mechanisms driving regeneration.

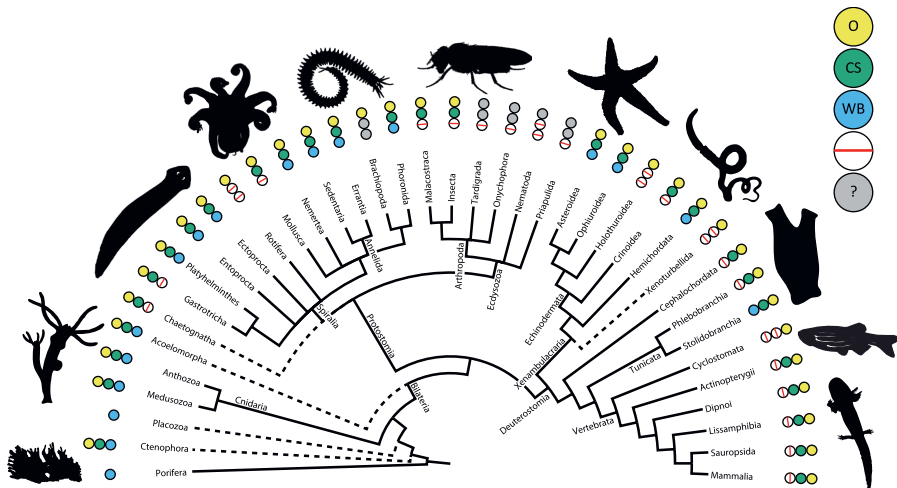


Figure 1. Mapping regenerative potential of various species on the metazoan phylogenetic tree. Most metazoan phyla include animals that are able to regenerate organs (O, yellow circles), and complex structures (CS, green circles). However, many vertebrate species either lack such regenerative abilities (struck-through circles) or their regenerative potential is unknown (? , gray circles). Whole-body regeneration (WB, blue circles) is widely observed among Cnidaria and Protostomia. Image copyright Springer Nature 2021. Adapted from Bideau, L. et al. Image reproduced with permission of the Licensor through Copyright Clearance Center.

Mechanisms of regeneration

Ever since the first regeneration experiments on *Hydra* in the 1700s, two major questions have been the focus of the regeneration field. How do animals regenerate? And why can some animals regenerate while others cannot? Despite an ever-growing body of literature on the topic, our understanding of how and why regeneration takes place remain poorly understood. On a mechanistic level, regeneration proceeds through three general modules: 1) wound healing, 2) regeneration initiation, and 3) morphogenesis³.

Wound healing is an ancient property of tissues found in both highly regenerative and non-regenerative animals. In regenerative tissues, wound closure typically occurs within the first few minutes to hours after amputation and is considered complete when re-epithelialization has occurred. Initial wound responses include reactive oxygen species (ROS) signaling, cell death, immune cell recruitment and extracellular matrix (ECM) remodeling^{14,15}. Inhibition of any of these processes leads to impaired wound closure and often blocks regeneration^{16–18}.

In regeneration competent tissues, successful wound then leads to regeneration initiation. In this step, regeneration has been divided into two distinct categories: regrowth resulting from cell proliferation (epimorphosis) and regrowth due to remodeling of existing tissue (morphallaxis)¹. Examples of strict morphallaxis are rare; the most commonly cited example being head regeneration in *Hydra* where treatment with cell-cycle inhibiting drugs did not prevent head regeneration^{19,20}. More detailed studies later identified a population of G2 paused cells located near the head that are poised to divide and differentiate after head

amputation²¹. The vast majority of animals undergo epimorphosis or a combination of both cell proliferation and tissue remodeling at the wound site²². A mass of undifferentiated and proliferative cells (called a blastema) can often be found under the wound epithelium at the onset of regeneration. The origin of these undifferentiated cells and their cellular plasticity varies widely across species. In the planarian *Schmidtea mediterranea*²³ and the hydrzoan *Hydractinia echinata*²⁴, resident adult stem cells proliferate and migrate to the wound site to form the blastema. Transplantation experiments of a single stem cell onto a stem-cell depleted host demonstrated the pluripotent nature of planarian stem cells²⁵. In axolotl, both resident stem cell populations and dedifferentiation of mature tissues contribute to the formation of the blastema. Muscle satellite cells migrate to the blastema and proliferate to form the new muscle tissue, while connective tissue cells dedifferentiate into a more homogeneous progenitor state and then redifferentiate in a lineage restricted manner^{26–28}.

The differentiation of these progenitors and their patterning of the new tissues constitutes the third module of regeneration: morphogenesis. This is perhaps the longest phase of regeneration, lasting from a few days (in the case of planaria and Hydra), to weeks (for Zebrafish and Xenopus), or even months (for salamanders). Morphogenesis during regeneration is in many ways akin to morphogenesis during embryonic development because both processes involve the orchestration of massive cellular growth and patterning. Moreover, body structures formed during development are the same structures that are reformed during regeneration. Early grafting experiments in axolotl using developing limb buds and limb blastemas suggested that patterning during limb growth is the same in both situations^{29,30}. However, more recent cellular and molecular studies showed that the spatial and temporal expression patterns of *Hox* genes vary significantly between limb development and regeneration^{31–33}. Gene expression analysis of embryonic tail buds and regenerating larval tails in *Xenopus laevis* showed that most of the genes they analyzed could be found at similar levels in both tissues. However, two bone morphogenetic protein (BMP)-antagonists, *chordin* and *noggin*, were only detected in the embryonic tail bud³⁴. More examples have been reported where regeneration seems to follow similar morphogenic events as that observed during embryonic development, however a number of molecular differences underlie the two processes^{35–38}. Thus, while it may be interesting to draw parallels between embryonic development and regeneration, the two processes should not be conflated.

Conventional model organisms used to study regeneration

Model organisms used to study regeneration span all ten major animal phyla. Among the many model systems available, four have emerged as the most well studied in the field of regeneration: *Hydra*, planarians, zebrafish, and salamanders (Figure 2).

Hydra was the first animal to be studied in the context of regeneration in 1740 by Abraham Trembley³⁹. Its renowned regenerative ability is unparalleled in the animal kingdom, with the ability to reform whole polyps from reagggregates of dissociated single cells⁷. Four different *Hydra* species (*H. vulgaris*, *H. oligactis*, *H. braueri*, and *H. viridissima*) have been used over the years, with *H. vulgaris* being the most commonly studied⁶. The *Hydra* polyp has a tube-like structure that can be divided into three anatomical regions (head, body column, and foot). Its entire body consists of two myoepithelial layers (gastrodermis and epidermis)

sandwiching a layer of extracellular matrix called the mesoglea⁴⁰. Three populations of resident adult stem cells can be found in the body column: myoepithelial epidermal stem cells (eESCs), myoepithelial gastrodermal stem cells (gESCs), and interstitial stem cells (ISCs). Each stem cell population are spatially restricted within the body column and gives rise to specific cell lineages^{41,42}. ISCs show the greatest cellular potency, giving rise to both somatic and germ cell lineages. The great ease of culturing Hydra polyps in the laboratory coupled with its short regeneration times (2-3 days for head regeneration) has made it a very popular system to use. The recent establishment of genetic techniques (stable transgenesis⁴³, gene knockdown by RNAi⁴⁴ and shRNA⁴⁵, CRISPR/Cas9 editing⁴⁶) has propelled this model organism into the omics era. However, the implementation of such methods remains difficult and so has not received wide adaptation. Sexual reproduction is also difficult to control and its embryonic stages are inaccessible behind a thick cuticle layer, severely limiting our understanding of the embryonic development of this species⁴⁷.

Planarian flatworms are also one of the oldest regeneration model systems and well known for its ability to regrow a whole worm from a tissue fragment 1/279th of its original size⁴⁸. There are hundreds of planarian species worldwide, with *Schmidtea mediterranea* being one of the most regenerative and also the most commonly studied. Unlike *Hydra*, planaria are triploblastic and have bilaterian symmetry. Pluripotent adult stem cells called neoblasts populate the entire body of Planaria except the very tip of the head and the pharynx, two structures that lack regenerative capacity when isolated from other tissues.²² Removal of the neoblasts by irradiation leads to eventual death of the animal and completely abolishes regeneration. Knockdown studies via RNAi of specific genes coupled with *in-situ* hybridization and immunohistochemistry has allowed for more mechanistic investigations into regeneration⁴⁹. Transcriptome and genome assemblies were also recently made available^{50,51}. Even a single-cell transcriptome atlas has been generated⁵². However, some key challenges remain. The pigmented bodies of planarians limit the feasibility of live tracking experiments, and the inaccessibility of planarian embryos has prevented the development of robust genetic and transgenic methods in this animal. Advances in these methods will be

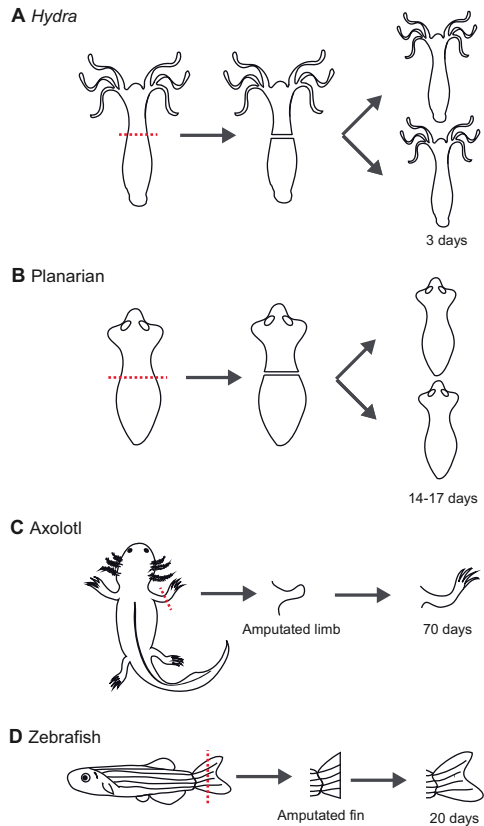


Figure 2. Schematics showing the regenerative capacity of four highly regenerative model organisms. Hydra (A) and planaria (B) exhibit remarkable whole-body regenerative abilities, while axolotl (C) and zebrafish (D) are capable of complex structure regeneration. The approximate length of time required to regenerate each structure is indicated below each regenerate. Image copyright John Wiley and Sons 2017. Adapted from Maddaluno, L. et al. Reproduced with permission of the Licensor through Copyright Clearance Center.

necessary to planarians to sustain their prominent position in the field of regeneration.

The zebrafish (*Danio rerio*), is probably the most studied vertebrate animal in regeneration. Initially established as a model organism for the study of developmental biology, the remarkable regenerative abilities of zebrafish were first reported in the 1990s^{53,54}. Zebrafish is used to study organ and limb regeneration, including regeneration of the fin⁵⁵, heart⁵⁶, liver⁵⁷, kidney⁵⁸ and skin⁵⁹. Although zebrafish entered the field of regeneration fairly recently, the abundance and ease of genetic and transgenic methods has pushed it to the forefront of regeneration research. Namely, the many inducible transgenic lines (i.e., heat shock, Gal4/UAS, Cre/Lox, TetOn/TetOff) allows for precise spatial and temporal control of specific genes during regeneration (cite). A wide range of “omics tools” has also become available in the recent years, including ChIPseq, Tomo-seq, single-cell RNAseq, proteomics, and metabolomics (cite). Despite its many advantages as a model system, the zebrafish still has its drawbacks. Live imaging of internal structures of the adult fish remains a challenge and the number antibodies compatible with immunohistochemistry is extremely limited⁹.

Regeneration in salamanders was first investigated in the 1700s by Lazzaro Spallanzani. Newts (such as *Notophthalmus viridescens*, *Cynops pyrrhogaster*, and *Pleurodeles waltl*) can regenerate more body parts than axolotls but their complex life cycles (consisting of both aquatic and terrestrial phases) make it difficult to establish laboratory colonies^{60,61}. The axolotl (*Ambystoma mexicanum*) however, is a fully aquatic animal that breeds well in captivity and thus has emerged as the salamander of choice for regeneration experiments. Unlike the other model systems described so far, the anatomy of the salamander is most similar to that of humans. Particularly when we consider the cellular composition and tissue patterning of the limb. This resemblance to human limbs makes it the most relevant model for regenerative medicine. Recent advances in the creating transgenic axolotls has allowed for lineage tracing of specific cell types during regeneration, revealing that somatic tissues near the wound dedifferentiate to form the blastema and redifferentiate to pattern the new limb^{26,62}. The axolotl genome is also fully assembled and annotated, paving the way for more mechanistic studies and genetic perturbations to challenge the regenerative abilities of this animal⁶³.

Aside from these four major model systems I described above, Arabidopsis, drosophila, xenopus, and mice were also used in the study of regeneration. However, their involvement was largely influenced by their dominance in the field of developmental biology rather than their regenerative abilities. As a result, these model systems have largely faded in recent literature. With the recent boom of sequencing methods and multi-omics approaches, a number of new model organisms have been curated specifically for their regenerative abilities and experimental advantages. The spiny mouse (*Acomys cahirinus*⁶⁴) and sea anemone (*Nematostella vectensis*⁶⁵) are among the most prominent recent additions to the field. Different species of planaria and newts that overcome the disadvantages of the current dominant species are also actively being set up.

Nematostella vectensis Is A Promising New Model Organism To Study Regeneration

Nematostella vectensis, a sea anemone capable of whole-body regeneration, has emerged as a powerful new model organism in the field of regeneration in the past decade. Naturally

found in estuaries where salt and temperature fluctuations are commonplace, *Nematostella* polyps can be easily reared at a range of temperatures (17-27°C) and salt conditions⁶⁶. Phylogenetically, *Nematostella vectensis* is closely related to *Hydra*, and morphologically shares similar features such as a tube-like body structure consisting of three major regions: head, body column, and physa (Figure 3a). As a diploblastic organism, the body tissue is composed of two epithelial layers with a layer of extracellular matrix in between called the mesoglea. *Nematostella* polyps show bilateral symmetry along two perpendicular body-axis called the oral-aboral axis and the directive axis. Invagination of tissue at the mouth forms the pharynx, which then connects to the mesenteries inside the body column. The mesentery tissue serves as the gut of the animal, with many cells involved in digestion and nutrient absorption and also contains the gonads in sexually mature animals. Despite its simple morphology, *Nematostella* contains a diverse array of cell types. Recent single-cell whole-animal RNA sequencing identified eight broad cell classes (cnidocytes, epithelium, progenitor, gland/secretory cells, retractor muscle, gastrodermis, digestive filaments, and neurons), with subtypes found in each class⁶⁷. Importantly, no resident adult stem cells have been identified to date.

The entire life cycle of *Nematostella* can be easily reared in the laboratory (Figure 3b). Spawning of male and female adults can be robustly controlled and the resulting egg and sperm are readily amenable to microinjection manipulations⁶⁸. Fertilized embryos enter a free-swimming larval stage that lasts about a week before undergoing metamorphosis into its polyp form. At this stage, the primary polyp consists of four primary tentacles and is capable of feeding by capturing live brine shrimp (*Artemia nauplii*). Sexual maturity is reached after approximately 3 months. The accessible nature of all the life stages of *Nematostella* make it an attractive model to directly compare mechanisms driving embryonic development and regeneration. *Nematostella* polyps are also capable of asexual reproduction by pinching off

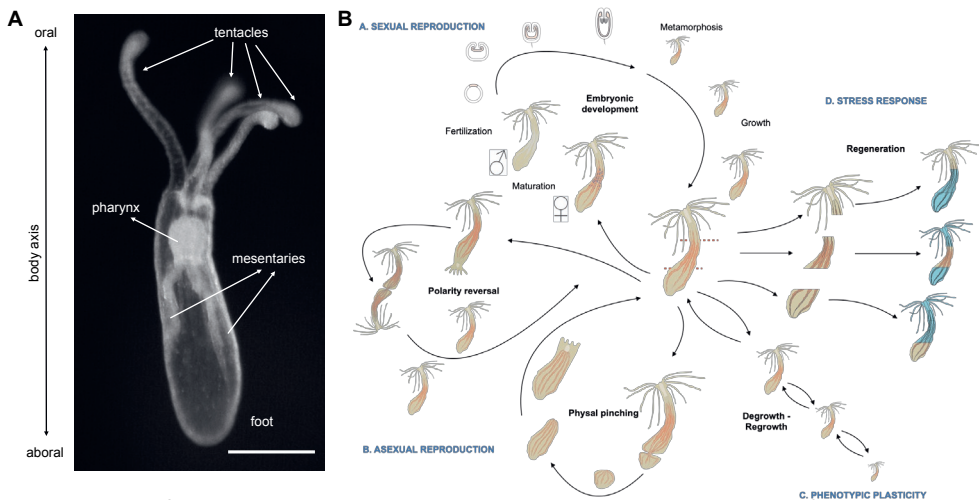


Figure 3. Image of a *Nematostella* primary polyp (A) with the body axis and major anatomical features marked. (Scale bar = 200 microns). Schematic (B) highlighting the various developmental trajectories and phenotypic plasticity of *Nematostella* polyps. Image copyright Company of Biologists 2021. Adapted from Rottinger, E. Reproduced with permission of the Licensor through Copyright Clearance Center.

a region of its body.

Transcriptome data of animals at various developmental stages are already available and a third annotated genome model was recently published⁶⁹. In contrast to *Hydra*, the *Nematostella* genome shows an unexpected level of conservation to bilaterians in terms of both gene complexity and genetic regulatory elements^{70,71}. The development of genomics tools such as mRNA or morpholino injections and transgenesis using meganuclease or CRISPR/Cas9 has allowed for more targeted studies into the mechanism of regeneration⁷²⁻⁷⁴ (cite). The robustness of these methods is evident when we look at the number of stable reporter and knock-out (KO) lines currently available (reviewed here⁷⁵). Other important molecular biology techniques such as immunohistochemistry and *in-situ* hybridization are also easily implemented at all life stages of this animal^{76,77}.

The advantages highlighted thus far showcase the power of this model in elucidating fundamental regeneration principles. However, given its phylogenetic position and the lack of morphological resemblance to humans, direct adaptation of any regeneration mechanisms to regenerative medicine is unlikely. Moreover, the lack of immune cells in *Nematostella* prevent the investigation of one of the key factors integral to vertebrate wound healing and regeneration: the immune system. However the advantages it offers to regenerative studies will surely place it in a prominent position alongside *Hydra* and planaria as a powerful invertebrate model for whole-body regeneration.

In summary, *Nematostella vectensis* is a promising new model system to study regeneration with four major advantages:

1. Capable of whole-body regeneration with a few days
2. Small and simple body morphology with complex cell composition
3. Accessibility of all life stages to manipulation and live imaging
4. Robust genetic and transgenic tools and resources

The main disadvantages of this model are:

1. Non-mammalian model
2. Anatomical and physiological differences to humans
3. No immune system yet identified

Outline of this Thesis

As I have highlighted in this general introduction, many advances have been made since the very first regeneration experiments in the 1700s, including the identification of stem cell populations and key signaling processes in a number of model organisms. Despite these advances, a molecular understanding of how regeneration is initiated remains in its infancy. Furthermore, the fundamental question of why some tissues can regenerate while others cannot remain elusive.

Recently, some studies have revealed that local wounding can cause wound-like responses in distant tissues across the body^{78,79}. Indeed, in Planarian worms, wounding first elicits a body-wide proliferative response followed by a secondary wound-localized response²³. Further scrutiny of gene expression changes as a result of wounding reveals that many genes not only change their expression levels but also their expression patterns after wounding⁸⁰. Taken

together, these results suggest that a more thorough understanding of what effects local wounding have on the rest of the body may provide greater insight into how regeneration is initiated within tissues. Furthermore, tracking of how genes change their expression pattern in addition to their level of expression could better inform us about the role of these genes in the process of regeneration. With the rapid advances in imaging and sequencing technologies, organism-wide monitoring of gene expression changes throughout the course of regeneration is no longer a far-fetched reality. The work presented in this thesis aims to compare local versus organism-level processes underlying regeneration using *Nematostella vectensis* as our model system.

In **Chapter 2**, we establish the first reference spatial transcriptomic atlas of a whole primary polyp along the oral-aboral axis. Using tomography RNA-seq (tomo-seq), we were able to identify eight gene clusters with discrete expression along the primary axis of the polyp. Validation of the expression patterns of various genes revealed that while many gene clusters marked the major anatomical regions of the animal (tentacles, head, body column, and foot), some genes showed expression that crossed anatomical boundaries (head and tentacle) while others were restricted to a sub-anatomical region (i.e., base of the tentacle). The tentacle tip was found to contain the largest number of genes with spatially restricted expression. Integrating the tip region marker genes with single-cell RNA-seq of tentacle tissue, we showed that the tip contains an enrichment of highly specialized cells called cnidocytes (or stinging cells).

Chapter 3 explores how gene expression of the polyp changes during foot regeneration across time and space. We apply tomo-seq to foot regenerating polyps at 4 different time points (12, 24, 48, 96hpa) and were able to capture dynamic gene expression changes across the animal. Interestingly, these transcriptional changes were not only restricted to the wound site but could also be detected in spatially distant tissues such as the tentacles. These results demonstrate that wounding causes body-wide transcriptional changes and suggests injury signals are propagated over very large distances. Furthermore, we were able to show that other stresses (i.e., heat shock and salt stress) are able to elicit similar transcriptional responses in *Nematostella*, suggesting the injury response may be part of a more general stress response.

In **Chapter 4**, we investigate tissue autonomous versus non-autonomous regeneration of the tentacle tip. We establish an *ex vivo* assay where detached tentacles are able to regenerate the tentacle tip. We identify the region proximal to the tip as essential for tip regeneration in the *ex vivo* system and found that this region contains an enrichment of precursor cells. When these precursor cells are present, cell proliferation and FGF signaling are dispensable for tip regeneration. When these cells are removed, *ex vivo* tip regeneration is blocked. *In vivo* tip regeneration is not blocked when this precursor population is removed, but requires FGF signaling. Taken together, we showed that the tentacle is capable of autonomous regeneration of the tip structure due to the presence of a precursor cell population.

I conclude this thesis in **Chapter 5**, where I integrate the findings of the previous chapters and discuss its implications toward general concepts governing regeneration.

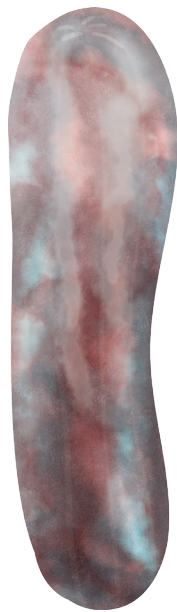
References

1. Morgan, T. H. *Regeneration*. (Macmillan, 1901).
2. Vervoort, M. Regeneration and Development in Animals. *Biol. Theory* **6**, 25–35 (2011).
3. Bideau, L., Kerner, P., Hui, J., Vervoort, M. & Gazave, E. Animal regeneration in the era of transcriptomics. *Cell. Mol. Life Sci.* **78**, 3941–3956 (2021).
4. Elchaninov, A., Sukhikh, G. & Fatkhudinov, T. Evolution of Regeneration in Animals: A Tangled Story. *Front. Ecol. Evol.* **9**, 1–14 (2021).
5. Katoonzadeh, A. Liver Regeneration. *Liver Pathophysiol. Ther. Antioxidants* **276**, 113–123 (2017).
6. Vogg, M. C., Galliot, B. & Tsiiris, C. D. Model systems for regeneration: Hydra. *Dev.* **146**, (2019).
7. Gierer, A. *et al.* Regeneration of Hydra from Reaggregated Cells. *Nat. new Biol.* **239**, 226–229 (1972).
8. Seybold, A., Salvenmoser, W. & Hobmayer, B. Sequential development of apical-basal and planar polarities in aggregating epitheliomuscular cells of Hydra. *Dev. Biol.* **412**, 148–159 (2016).
9. Marques, I. J., Lupi, E. & Mercader, N. Model systems for regeneration: Zebrafish. *Dev.* **146**, (2019).
10. Needham, A. E. Asexual propagation and regeneration. by M. A. Vorontsova and L. D. Liosner, Pergamon Press, London, 1960. pp. xxiv + 489, 70s. *Comp. Biochem. Physiol.* **2**, 221–229 (1961).
11. Morgan, T. H. Notes on Regeneration. *Biol. Bull.* 159–172 (1904).
12. H.V. BRØNDSTED D.Phil. *Planarian Regeneration*. (Pergamon Press, 1969). doi:<https://doi.org/10.1016/B978-0-08-012876-4.50024-3>
13. Ivankovic, M. *et al.* Model systems for regeneration: Planarians. *Dev.* **146**, 0–1 (2019).
14. Amiel, A. R. *et al.* Characterization of morphological and cellular events underlying oral regeneration in the sea anemone, *Nematostella vectensis*. *Int. J. Mol. Sci.* **16**, 28449–28471 (2015).
15. Kakebeen, A. D. & Wills, A. E. More than just a bandage: Closing the gap between injury and appendage regeneration. *Front. Physiol.* **10**, 1–11 (2019).
16. Dunnill, C. *et al.* Reactive oxygen species (ROS) and wound healing: the functional role of ROS and emerging ROS-modulating technologies for augmentation of the healing process. *Int. Wound J.* **14**, 89–96 (2017).
17. Strbo, N., Yin, N. & Stojadinovic, O. Innate and Adaptive Immune Responses in Wound Epithelialization. *Adv. Wound Care* **3**, 492–501 (2014).
18. Weinreich, J. *et al.* Rapamycin-induced impaired wound healing is associated with compromised tissue lactate accumulation and extracellular matrix remodeling. *Eur. Surg. Res.* **47**, 39–44 (2011).
19. Clarkson, S. G. Nucleic acid and protein synthesis and pattern regulation in hydra. I. Regional patterns of synthesis and changes in synthesis during hypostome formation. *J. Embryol. Exp. Morphol.* **21**, 33–54 (1969).
20. Clarkson, S. G. Nucleic acid and protein synthesis and pattern regulation in hydra. II. Effect of inhibition of nucleic acid and protein synthesis on hypostome formation. *J. Embryol. Exp. Morphol.* **21**, 55–70 (1969).
21. Buzgariu, W., Wenger, Y., Tcaciuc, N., Catunda-Lemos, A. P. & Galliot, B. Impact of cycling cells and cell cycle regulation on Hydra regeneration. *Dev. Biol.* **433**, 240–253 (2018).
22. Tanaka, E. M. & Reddien, P. W. The Cellular Basis for Animal Regeneration. *Dev. Cell* **21**, 172–185 (2011).
23. Wenmoser, D. & Reddien, P. W. Planarian regeneration involves distinct stem cell responses to wounds and tissue absence. *Dev. Biol.* **344**, 979–991 (2010).
24. Bradshaw, B., Thompson, K. & Frank, U. Distinct mechanisms underlie oral vs aboral regeneration in the cnidarian *Hydractinia echinata*. *Dev. Dyn.* **238**, 1111–1117 (2009).

25. Wagner, D. E., Wang, I. E. & Reddien, P. W. Clonogenic Neoblasts Are Pluripotent Adult Stem Cells That Underlie Planarian Regeneration. *Science* (80-.). **332**, 811–817 (2011).
26. Gerber, T. *et al.* Single-cell analysis uncovers convergence of cell identities during axolotl limb regeneration. *Science* (80-.). **0681**, eaaq0681 (2018).
27. Leigh, N. D. *et al.* Transcriptomic landscape of the blastema niche in regenerating adult axolotl limbs at single-cell resolution. *Nat. Commun.* **9**, (2018).
28. Sandoval-Guzmán, T. *et al.* Fundamental differences in dedifferentiation and stem cell recruitment during skeletal muscle regeneration in two salamander species. *Cell Stem Cell* **14**, 174–187 (2014).
29. Muneoka, K. & Bryant, S. V. Evidence that patterning mechanisms in developing and regenerating Limbs Are the Same. *Nature* **298**, 369–371 (1982).
30. Muneoka, K. & Bryant, S. V. Cellular contribution to supernumerary limbs resulting from the interaction between developing and regenerating tissues in the axolotl. *Dev. Biol.* **105**, 179–187 (1984).
31. Torok, M. A., Gardiner, D. M., Shubin, N. H. & Bryant, S. V. Expression of HoxD genes in developing and regenerating axolotl limbs. *Dev. Biol.* **200**, 225–233 (1998).
32. Carlson, M. R. J., Komine, Y., Bryant, S. V. & Gardiner, D. M. Expression of Hoxb13 and Hoxc10 in developing and regenerating axolotl limbs and tails. *Dev. Biol.* **229**, 396–406 (2001).
33. Christen, B., Beck, C. W., Lombardo, A. & Slack, J. M. W. Regeneration-specific expression pattern of three posterior Hox genes. *Dev. Dyn.* **226**, 349–355 (2003).
34. Sugiura, T. *et al.* Differential gene expression between the embryonic tail bud and regenerating larval tail in *Xenopus laevis*. *Dev. Growth & Differ.* **46**, 97–105 (2004).
35. Genikhovich, G., Kürn, U., Hemmrich, G. & Bosch, T. C. G. Discovery of genes expressed in Hydra embryogenesis. *Dev. Biol.* **289**, 466–481 (2006).
36. Fröbuis, A. C., Genikhovich, G., Kürn, U., Anton-Erxleben, F. & Bosch, T. C. G. Expression of developmental genes during early embryogenesis of Hydra. *Dev. Genes Evol.* **213**, 445–455 (2003).
37. Burton, P. M. & Finnerty, J. R. Conserved and novel gene expression between regeneration and asexual fission in *Nematostella vectensis*. *Dev. Genes Evol.* **219**, 79–87 (2009).
38. Lepper, C., Conway, S. J. & Fan, C. M. Adult satellite cells and embryonic muscle progenitors have distinct genetic requirements. *Nature* **460**, 627–631 (2009).
39. Trembley, A., Pronk, C., Schley, J. van der, Lyonet, P. & Bayer, F. M. *Mémoires pour servir à l'histoire d'un genre de polypes d'eau douce, à bras en forme de cornes*. (A Leide : Chez Jean & Herman Verbeek, 1744).
40. Sarras, M. P. *et al.* Extracellular matrix (mesoglea) of *Hydra vulgaris*. I. Isolation and characterization. *Dev. Biol.* **148**, 481–494 (1991).
41. Bode, H. R. The interstitial cell lineage of hydra: a stem cell system that arose early in evolution. *J. Cell Sci.* **109**, 1155–1164 (1996).
42. Campbell, R. D. & David, C. N. Cell cycle kinetics and development of *Hydra attenuata*. II. Interstitial cells. *J. Cell Sci.* **16**, 349–358 (1974).
43. Klimovich, A., Wittlieb, J. & Bosch, T. C. G. Transgenesis in Hydra to characterize gene function and visualize cell behavior. *Nat. Protoc.* **14**, 2069–2090 (2019).
44. Galliot, B., Miljkovic-Licina, M., Ghila, L. & Chera, S. RNAi gene silencing affects cell and developmental plasticity in hydra. *Comptes Rendus - Biol.* **330**, 491–497 (2007).
45. Klimovich, A. *et al.* Non-senescent Hydra tolerates severe disturbances in the nuclear lamina. *Aging (Albany, NY)*. **10**, 951–972 (2018).
46. Lommel, M., Tursch, A., Rustarazo-calvo, L., Trageser, B. & Thomas, W. Genetic knockdown and knockout approaches in Hydra. *BioRxiv* 1–19 (2017). doi:10.1101/230300
47. Martin, V. J., Littlefield, C. L., Archer, W. E. & Bode, H. R. Embryogenesis in Hydra. *Biol. Bull.* **192**, 345–363 (1997).
48. Morgan, T. H. Experimental studies of the regeneration of *Planaria maculata*. *Arch. für*

- Entwicklungsmechanik der Org.* **7**, 364–397 (1898).
49. Rouhana, L. *et al.* RNA interference by feeding in vitro–synthesized double-stranded RNA to planarians: Methodology and dynamics. *Dev. Dyn.* **242**, 718–730 (2013).
 50. Grohme, M. A. *et al.* The genome of *Schmidtea mediterranea* and the evolution of core cellular mechanisms. *Nature* **554**, 56–61 (2018).
 51. Adamidi, C. *et al.* De novo assembly and validation of planaria transcriptome by massive parallel sequencing and shotgun proteomics. *Genome Res.* **21**, 1193–1200 (2011).
 52. Fincher, C. T., Wurtzel, O., de Hoog, T., Kravarik, K. M. & Reddien, P. W. Cell type transcriptome atlas for the planarian *Schmidtea mediterranea*. *Science* (80-.). **360**, (2018).
 53. White, J. A., Boffa, M. B., Jones, B. & Petkovich, M. A zebrafish retinoic acid receptor expressed in the regenerating caudal fin. *Development* **120**, 1861–1872 (1994).
 54. Bernhardt, R. R., Tongiorgi, E., Anzini, P. & Schachner, M. Increased expression of specific recognition molecules by retinal ganglion cells and by optic pathway glia accompanies the successful regeneration of retinal axons in adult zebrafish. *J. Comp. Neurol.* **376**, 253–264 (1996).
 55. Nechiporuk, A. & Keating, M. T. A proliferation gradient between proximal and msxb-expressing distal blastema directs zebrafish fin regeneration. *Development* **129**, 2607–2617 (2002).
 56. Poss, K. D., Wilson, L. G. & Keating, M. T. Heart regeneration in zebrafish. *Science* (80-.). **298**, 2188–2190 (2002).
 57. Burkhardt-Holm, P., Oulmi, Y., Schroeder, A., Storch, V. & Braunbeck, T. Toxicity of 4-chloroaniline in early life stages of zebrafish (*Danio rerio*): II. Cytopathology and regeneration of liver and gills after prolonged exposure to waterborne 4-chloroaniline. *Arch. Environ. Contam. Toxicol.* **37**, 85–102 (1999).
 58. Reimschuessel, R. A fish model of renal regeneration and development. *ILAR J.* **42**, 285–291 (2001).
 59. Chen, C. H. *et al.* Multicolor Cell Barcoding Technology for Long-Term Surveillance of Epithelial Regeneration in Zebrafish. *Dev. Cell* **36**, 668–680 (2016).
 60. Joven, A., Elewa, A. & Simon, A. Model systems for regeneration: Salamanders. *Dev.* **146**, 0–2 (2019).
 61. Takahashi, M. K. & Parris, M. J. Life cycle polyphenism as a factor affecting ecological divergence within *Notophthalmus viridescens*. *Oecologia* **158**, 23–34 (2008).
 62. Currie, J. D. *et al.* Live Imaging of Axolotl Digit Regeneration Reveals Spatiotemporal Choreography of Diverse Connective Tissue Progenitor Pools. *Dev. Cell* **39**, 411–423 (2016).
 63. Smith, J. J. *et al.* A chromosome-scale assembly of the axolotl genome. *Genome Res.* **29**, 317–324 (2019).
 64. Maden, M. & Varholick, J. A. Model systems for regeneration: The spiny mouse, *Acomys cahirinus*. *Dev.* **147**, (2020).
 65. Darling, J. A. *et al.* Rising starlet: The starlet sea anemone, *Nematostella vectensis*. *BioEssays* **27**, 211–221 (2005).
 66. Hand, C. & Uhlinger, K. R. The unique, widely distributed, estuarine sea anemone, *Nematostella vectensis* Stephenson: A review, new facts, and questions. *Estuaries* **17**, 501–508 (1994).
 67. Sebé-Pedrós, A. *et al.* Cnidarian Cell Type Diversity and Regulation Revealed by Whole-Organism Single-Cell RNA-Seq. *Cell* **173**, 1520–1534.e20 (2018).
 68. Stefanik, D. J., Friedman, L. E. & Finnerty, J. R. Collecting, rearing, spawning and inducing regeneration of the starlet sea anemone, *Nematostella vectensis*. *Nat. Protoc.* **8**, 916–923 (2013).
 69. Zimmermann, B. *et al.* Sea anemone genomes reveal ancestral metazoan chromosomal macrosynteny. *bioRxiv* (2022). doi:10.1101/2020.10.30.359448
 70. Schwaiger, M. *et al.* Evolutionary conservation of the eumetazoan gene regulatory landscape. *Genome Res.* **24**, 639–650 (2014).

71. Rigo-Watermeier, T. *et al.* Functional conservation of *Nematostella* Wnts in canonical and noncanonical Wnt-signaling. *Biol. Open* **1**, 43–51 (2012).
72. Ikmi, A., McKinney, S. A., Delventhal, K. M. & Gibson, M. C. TALEN and CRISPR/Cas9-mediated genome editing in the early-branching metazoan *Nematostella vectensis*. *Nat. Commun.* **5**, 1–8 (2014).
73. Renfer, E., Amon-Hassenzahl, A., Steinmetz, P. R. H. & Technau, U. A muscle-specific transgenic reporter line of the sea anemone, *Nematostella vectensis*. *Proc. Natl. Acad. Sci. U. S. A.* **107**, 104–108 (2010).
74. Karabulut, A., He, S., Chen, C. Y., McKinney, S. A. & Gibson, M. C. Electroporation of short hairpin RNAs for rapid and efficient gene knockdown in the starlet sea anemone, *Nematostella vectensis*. *Dev. Biol.* **448**, 7–15 (2019).
75. Rottinger, E. *Nematostella vectensis*, an Emerging Model for Deciphering the Molecular and Cellular Mechanisms Underlying Whole-Body Regeneration. *Cells* **10**, 2692 (2021).
76. Genikhovich, G. & Technau, U. In situ hybridization of starlet sea anemone (*Nematostella vectensis*) embryos, larvae, and polyps. *Cold Spring Harb. Protoc.* **4**, 1–6 (2009).
77. Zenkert, C., Takahashi, T., Diesner, M. O. & Özbek, S. Morphological and molecular analysis of the *Nematostella vectensis* cnidom. *PLoS One* **6**, (2011).
78. Busse, S. M., McMillen, P. T. & Levin, M. Cross-limb communication during xenopus hindlimb regenerative response: Non-local bioelectric injury signals. *Dev.* **145**, (2018).
79. Payzin-Dogru, D. *et al.* Nerve-mediated amputation-induced stem cell activation primes distant appendages for future regeneration events in axolotl. *bioRxiv* (2021). doi:10.1101/2021.12.29.474455
80. Wenemoser, D., Lapan, S. W., Wilkinson, A. W., Bell, G. W. & Reddien, P. W. A molecular wound response program associated with regeneration initiation in planarians. *Genes Dev.* **26**, 988–1002 (2012).



“...it is questions with no answers that set the limits of human possibilities, describe the boundaries of human existence.”

- Milan Kundera, *The Unbearable Lightness of Being*, p.137

Chapter 2

Spatial transcriptomics reveal gene expression and developmental landscapes of the primary polyp in a sea anemone

2

Stephanie Cheung^{1*}, Danila Bredikhin^{2*}, Tobias Gerber^{1,2}, Petrus Steenbergen¹, Jacob M. Musser¹, Andrea B. Kohn³, Leonid L. Moroz^{3,4}, Pauline Hansen^{1,5}, Anniek Stokkermans¹, Hendrik C. Korswagen⁶, Oliver Stegle^{2,7#}, Aissam Ikmi^{1#}

¹ Developmental Biology Unit, European Molecular Biology Laboratory, Heidelberg 69117, Germany

² Genome Biology Unit, European Molecular Biology Laboratory, Heidelberg 69117, Germany

³ Whitney Laboratory for Marine Bioscience, University of Florida, St. Augustine, FL 32080

⁴ Dept of Neuroscience and Brain Institute, University of Florida, Gainesville, FL 32610, USA

⁵ Institute for Pharmacy and Molecular Biotechnology, Heidelberg University, Heidelberg 69120, Germany

⁶ Hubrecht Institute- KNAW (Royal Netherlands Academy of Arts and Sciences) and University Medical Center Utrecht, 3584 CT Utrecht, The Netherlands

⁷ Division of Computational Genomics and Systems Genetics, German Cancer Research Center (DKFZ), Heidelberg 69120, Germany

*These authors contributed equally

#Corresponding authors

Abstract

Spatially resolved transcriptomic maps provide valuable insight into understanding the organization and function of cells and tissues within an organism. The starlet sea anemone *Nematostella vectensis*, a diploblastic animal belonging to the cnidarian phylum, is particularly well suited for spatial transcriptomic profiling because of its small size, simple body plan, yet diverse cellular makeup^{1,2}. Here, we apply tomo-seq to generate the first organism-wide spatial transcriptomic atlas of homeostatic primary polyps of *Nematostella vectensis*. We identified novel gene clusters that mark distinct regions across the oral-aboral axis of the polyp. We also devised new computational approaches to identify genes with spatial expression patterns and align samples of different lengths. Lastly, we combine our spatial expression atlas with single cell RNA sequencing of tentacle tissue to reveal that the tentacle tip consists of two branches of actively differentiating stinging cell populations. We conclude that our spatial transcriptomic atlas of homeostatic polyps will serve as a valuable resource for identifying region-specific genes for use in further studies of tissue function and generation of tissue-specific transgenic constructs.

Introduction

Spatial transcriptomic atlases provide important insight into the organization and function of cells within an organism³⁻⁵. Transcriptome-wide analyses of gene expression profiles allow for large scale molecular characterization of tissues in time and space. Tomography RNA-sequencing (tomo-seq) is an attractive method that allows spatial transcriptomic profiling at the whole-organism scale⁶⁻⁹. This method combines the advantages of low-input RNA-sequencing with cryosectioning to preserve the spatial location of gene expression profiles across a single body axis. Importantly, the use of cryopreservation minimizes sample perturbation to preserve the natural transcriptomic state of the tissues. Spatially resolved transcriptomic maps of Zebrafish heart and embryos, and adult nematodes have already been reported using this method⁷⁻⁹. These unbiased investigations enable the identification of tissue regions with highly specialized roles and independently of anatomical boundaries.

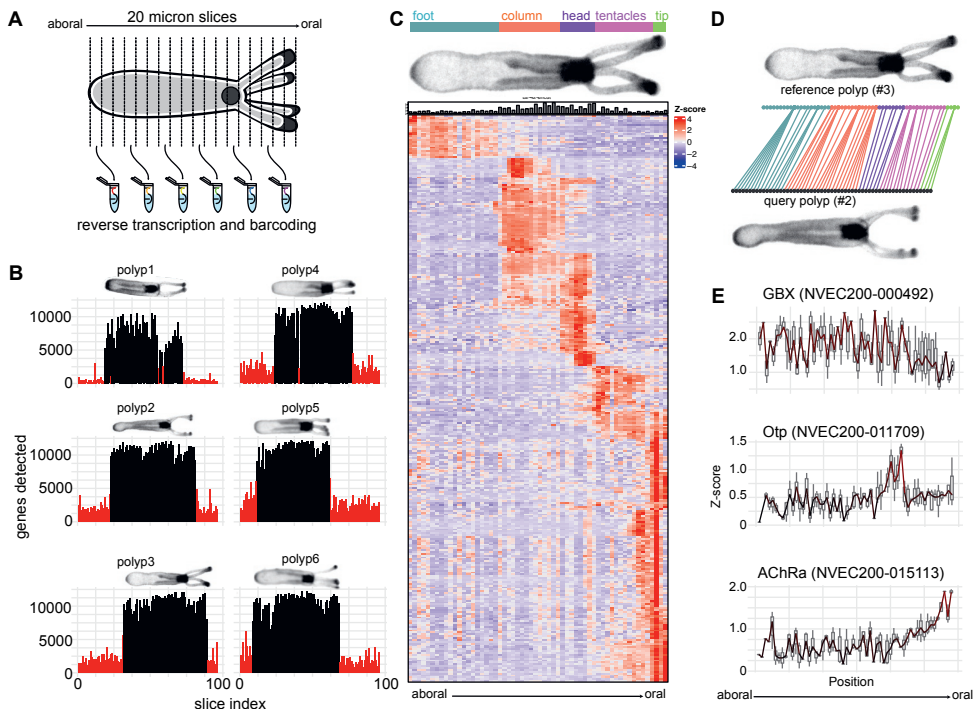


Figure 1. Spatial transcriptomics identify genes with highly variable
Figure 1. Spatial transcriptomics identify genes with highly variable expression patterns across space in homeostatic polyps. (a) Schematic showing the TOMO-seq method that combines RNA-seq with cryosectioning to achieve spatial gene expression atlases across a single body axis. (b) Images of the six homeostatic polyps are shown with their respective bar plots showing the total number of genes detected per slice. Slices with >6000 genes are shown in black, while slices with <6000 genes are colored red. (c) Image of the reference polyp and the approximate anatomical regions (foot, column, head, tentacles, tip) are marked by the different colored bars. Heat map shows the z-scores of anatomical region marker genes clustered by their expression pattern. (d) Example of how samples of different lengths are aligned to the reference polyp using dynamic time warping (see methods) to obtain a common coordinate space across samples. (e) Line plots showing the median z-scores of three genes (GBX, Otp, AChRa) with known spatial expression patterns are shown. Box plots show the spread of z-score values from all six polyps after alignment.

One model organism particularly suited for spatial transcriptomic profiling is the sea anemone *Nematostella vectensis*, a diploblastic animal belonging to the cnidarian phylum. Polyps from this species have a relatively simple tubular body plan yet contains a diversity of cell types along the main axis that runs from the tentacle tip to the foot (oral–aboral axis)^{1,2}. *Nematostella* polyps are also highly regenerative, capable of whole-body regeneration, however little is known about the cellular and molecular basis of its regenerative potential^{10–12}. Transcriptomic studies of *Nematostella* reported thus far have utilized methods that do not preserve the spatial context in which gene expression changes occur (i.e., bulk RNA-seq^{12,13}, microarray¹⁴, single-cell RNA-seq¹). Other studies that do preserve the spatial information have relied on microscopy-based techniques such as *in-situ* hybridizations^{15–17}, immunohistochemistry^{18,19}, and transgenic reporter constructs^{20,21}, where only a few genes could be interrogated at a time. While a transcriptome-wide analysis of spatial expression patterns in the *Nematostella* polyp is still missing, the generation of this resource would facilitate the identification of the molecular and cellular mechanism underling the biology of the polyp.

Here, we apply tomo-seq to *Nematostella vectensis* to generate a spatial transcriptomic atlas of homeostatic primary polyps. We identified novel gene clusters that mark distinct regions across the oral-aboral axis of the polyp. These regions mostly corresponded to the different anatomical regions within the polyp, but some gene clusters show expression that span multiple anatomical regions while others are restricted to a sub-anatomical region. We also devised new computational approaches to identify genes with spatial expression patterns and align samples of different lengths. The tentacle tip emerged as a region with the highest number of genes showing a spatially restricted expression pattern. Using single-cell RNA sequencing of tentacle tissue, we established that the rich repertoire of genes in the tip region is largely driven by the enrichment of highly specialized cells (i.e. cnidocytes) in this tissue. Using a cell cycle reporter construct, we further illustrate that the tentacle tip is a region with active differentiation of cnidocyte cells.

Results

Generation of spatially aligned transcriptomics maps along the oral-aboral axis of primary polyps

To characterize the spatial gene expression patterns of homeostatic polyps along the oral-aboral axis, we applied tomo-seq⁶ to unfed primary polyps (Figure 1a). Tomo-seq is a spatial transcriptomic method that combines cryosectioning of tissue with low-input RNA-sequencing to generate genome-wide transcriptomic atlases. Six total polyps were subjected to tomo-seq at a resolution of 20 microns. Fifty to sixty million reads were sequenced per sample, which mapped to ~14000 genes. Total genes per slice were used to determine sample boundaries (Figure 1b). A reference polyp was initially defined based on two criteria: 1) a high average gene count per slice and 2) no slices within the sample boundary were discarded due to low gene counts. To determine genes with high spatial expression variability, we identified the top 500 highly variable genes (HVGs) from the reference polyp. Hierarchical clustering of these 500 HVGs revealed 12 gene clusters with distinct spatial expression patterns. From these 500 HVGs, 284 genes showed consistent spatial expression patterns across all six polyps (by manual selection based on the z-scores for each gene). We expanded

this list by a few genes that mark the foot region, identifying in total 292 genes with distinct spatial expression patterns across the primary polyp. Clustering of these genes in the reference polyp revealed eight major gene clusters with expression patterns that reflected the spatial arrangement of major anatomical regions of the *Nematostella* polyp (Figure 1c). Interestingly, all genes identified with expression in the foot region show a graded expression across the foot. In contrast, genes expressed in the other areas of the polyp show both graded and sharp expression profiles.

In order to compare our tomo-seq results across all six samples, we then normalized the lengths of the six polyps by aligning each sample to the reference polyp via dynamic time warping²² (DTW; Figure 1d). DTW, a method commonly used in time series analyses, calculates the optimal match between two sequences whereby the order of the data must be maintained. Similar to time series data, where certain events occur in the same order but at

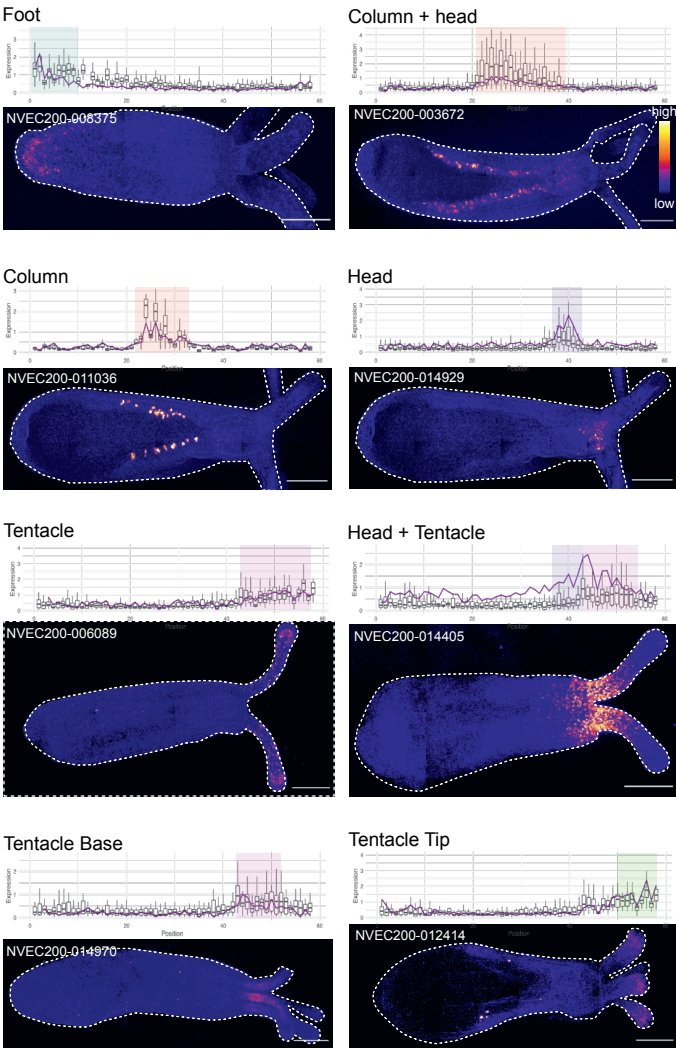


Figure 2. Validation of the tomo-seq data. Bar plots show the median z-score value of genes present in each gene cluster. Line plot over-lay shows the expression of the specified gene in the reference polyp. Maximum projection images of whole mount HCR in-situ for the specified genes (LUT = fire; scale bar = 100 microns) are shown.

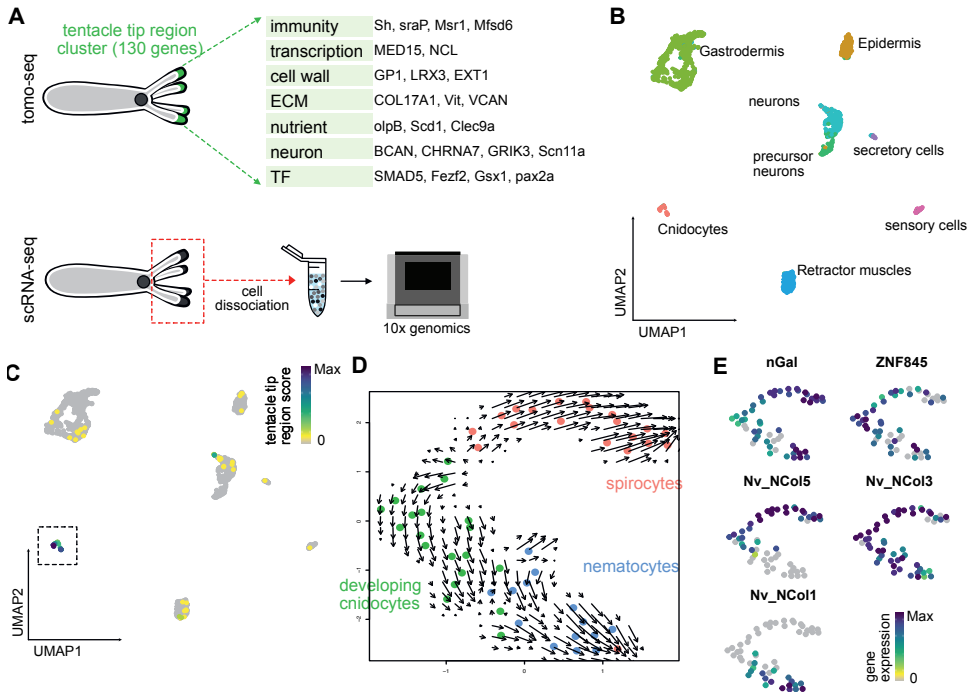


Figure 3. scRNA-seq of tentacle tissue combined with tentacle tip region genes reveal an enrichment of actively developing cnidocyte cells at the tip. (a) Schematic showing the annotated gene groups from the tentacle tip region cluster (top), and the protocol for generating single cell RNA-seq (scRNA-seq) data from tentacle tissue. (b) UMAP embedding of single-cell transcriptomic data of tentacle tissue shows cell type heterogeneity. (c) Mapping tentacle tip cluster genes onto scRNA-seq data as tip score (see Methods) shows an enrichment of tip cluster genes exclusively in cnidocytes. (d) RNA velocity map of cnidocyte cell cluster shows two developmental trajectories from developing cnidocytes branching into mature spirocytes and mature nematocytes. Colors mark de novo clustering of cnidocytes into 3 groups. (e) UMAP embedding of cnidocyte cell cluster showing the relative expression levels of specific genes marking different cnidocyte populations (nGal - cnidocyte maturation marker; ZNF845 - cnidocyte precursors; Nv_NCo15 - spirocytes marker; Nv_NCo13 - maturing cnidocyte; Nv_NCo11 - nematocytes)

varying speeds, tomo-seq data contain gene expression patterns that appear in a determined order but at varying spatial distances. We used the 292 genes identified to have a distinct spatial expression pattern to define the polyp body in our alignment analysis. After alignment, the six polyps (with initial lengths varying from 50 to 60 slices) all had a length of 58 slices of the reference polyp. To test the quality of our alignment method, we generated a tomo-seq dataset of a polyp lacking tentacles. Alignment of this “tentacle-less” polyp indeed showed no slices aligning to the oral-most region of the reference polyp (Figure S1).

With the unified coordinate system for six polyps, we reassessed the consistency of the 292 genes with distinct spatial expression patterns identified in the reference polyp. We compared the genes from each of the eight gene clusters across all samples and found the spatial expression pattern to be highly robust across samples while the level of gene expression varied greatly. To assess the ability of tomo-seq to capture gene expression patterns across the body of a *Nematostella* polyp, we compared the expression pattern detected in our tomo-seq dataset with published mRNA *in-situ* hybridization data (Figure 1e). We curated a total

of 54 genes with published in-situ images that showed a clear expression pattern in primary polyps (Table S1). Genes with low gene counts (< 10 counts per polyp) or poor sequence homology were removed from further analysis. Of the remaining 39 genes, 34 genes (87%) showed comparable expression patterns between the published in-situ data and our tomo-seq dataset. Three genes (RGMB, TCF15, Wnt4a) were already included in the eight gene clusters identified in our reference polyp.

Spatial clustering of gene expression defines both sub- and cross-anatomical boundaries

While tomo-seq analysis identified spatially restricted expression patterns that define discrete anatomical regions of the polyp (Figure 1c), there were also genes whose expression spanned multiple anatomical regions (i.e., head and column) and genes that showed expression restricted to a sub-anatomical region (i.e., base of the column, base of the tentacle; Figure 2). Some genes were expressed in both the head and column tissue which may stem from the fact that both regions contain tissue of a similar developmental origin, namely the pharyngeal ectoderm²³. Differential gene expression present in the base of the body column and the base of the tentacle suggests that those tissues may serve a specialized function. However, majority of the genes in these clusters are not annotated to any known gene, making it difficult to postulate the function of these tissue regions.

To further validate the anatomical marker genes and better define their expression location within the polyp, we performed in-situ HCR (hybridization chain reaction) for several genes from each cluster. Out of 17 genes tested, 16 genes showed the expected expression pattern except one gene for which no in-situ signal could be detected (HSPA12A). Genes from the column cluster were detected only in the mesentery tissue, with high expression within specific cells (Figure 2 and S2). In contrast, tentacle tip and foot markers showed uniform expression across their corresponding regions. Two genes tested from the tentacle-base cluster showed graded expression in the base of the tentacle, however one gene also had expression in the adjacent head region. Since the reads of a given gene are normalized to total transcript counts within a slice, to account for the heterogeneity of tissue density along the main axis, the large difference in total transcript counts between the head and tentacle can impact estimated expression levels at tissue boundaries. This could also affect how the boundary between the foot and column region are defined but we did not detect such an issue between these two regions.

Tentacle tip exhibits a rich repertoire of spatially restricted transcripts

Strikingly, over 40% of the anatomical marker genes show restricted expression in the tentacle tip (Figure S3), although this region has a relatively low cell density compared to other body parts such as the head and column. The large number of spatially restricted transcripts may indicate the tentacle tip is a developmentally active region or consists of highly specialized cells (akin to pancreatic islet cells²⁴ or erythrocyte precursor cells²⁵ whose highly specialized function results in the production of a highly distinct transcriptome).

In order to link gene expression and cellular identity in the tip region, we generated a single cell RNA-sequencing data from dissected tentacles (Figure 3a). A 2D projection plot of this single cell dataset reveals seven isolated cell clusters (Figure 3b). Using the marker genes reported for the eight major cell types in *Nematostella* polyps¹, we classified each of the clusters to their cell type identity. No digestive filament cells were detected in our dataset,

likely because these cell types are often found only in the body column. To identify which of these cells correspond to the tentacle tip region, we mapped the tentacle tip cluster genes onto the UMAP clusters and found that the tip cluster genes were almost exclusively found in the cnidocyte cell cluster (Figure 3c). Further analysis into the expression of individual genes from the tip cluster reveals that ~70% of tip cluster genes are highly enriched in cnidocyte cells (Figure S5). These results suggest that the rich repertoire of spatially restricted transcripts in the tip is driven by a dominant cell type composition.

Tentacles show continuous differentiation in homeostatic polyps

Next, we subset our scRNA-seq data for the cells reporting high expression of tentacle tip cluster genes and investigated the cell type variability within these cells. Clustering of these cells in a 2D plot shows a clear bifurcation into two branches. RNA velocity²⁶ analysis of this cell cluster suggests that the two branches represent two maturation trajectories (Figure 3d). To investigate if there is indeed a heterogeneity of cnidocyte cell states, we mapped on the expression levels of various individual genes specific to different cnidocyte cells. Expression of nGal¹⁸ (a marker for cnidocyte maturation) is detected in a gradient-like manner with highest expression at the very end of each branch. Expression of ZNF845²⁷, a marker for early developing cnidocytes is enriched in the cells at the bifurcation. Taken together, this supports that the two branches represent maturation trajectories from progenitor cnidocytes into potentially two types of mature cnidocytes. The top branch was found to be enriched in Nv_NCo15¹ expression, a reported marker gene for spirocytes (a specific type of cnidocyte) (Figure 3e). The lower branch shows high levels of Nv_NCo11^{18,19}, Nv_NCo14^{18,19}, and NEP10¹ expression, marker genes specific to nematocytes (Figure 3e and Figure S6). Expression of foxl2¹, a marker gene for spirocysts and developing cnidocytes, was detected both at the fork head and the end of the top branch (Figure S6). Taken together, by combining single-cell RNA-sequencing and tomo-seq data, we demonstrated that the tentacle tip is a region enriched in cells that are actively developing into two types of mature cnidocytes, nematocytes and spirocysts.

As cell differentiation and proliferation are strongly connected processes^{28,29}, we were curious about the spatial pattern of cell proliferation leading to cnidocyte differentiation in the tentacles. We calculated a mitosis score for each slice of the reference polyp and found the highest mitosis scores at the base of the tentacle (Figure S7). Since cell proliferation and differentiation was often reported to share an inverse relationship³⁰, we wondered if the spatial distribution of proliferating and differentiating cells within the tentacle represents a differentiation trajectory moving from the base to the tip of the tentacle. To test this hypothesis, we generated a Nv_CyclinB-eGFP reporter line to mark cycling cells in a homeostatic polyp. To do so, we tagged eGFP with the first 100 amino acids of Nv_Cyclin B (Nv_CyB) and expressed this construct under a ubiquitous promoter³¹ (Figure S8). Cyclin B is a highly conserved cyclin gene that is upregulated in late s-phase and peaks in late G2 phase³². We confirmed the cycling nature of this reporter construct during early embryogenesis, where Nv_CyB-eGFP signal peaks right before cytokinesis (Figure S9). In polyps, Nv_CyB-eGFP+ cells were found to be enriched at the head region and near the tentacle tips (Figure 4a). Nuclear staining intensity quantification of Nv_CyB-eGFP+ and Nv_CyB-eGFP- cells in the tentacle showed that Nv_CyB-eGFP predominantly marks cells in S-phase and early G2 (an expression pattern that would be expected from Cyclin A protein rather than Cyclin B) (Figure 4b). Interesting, Nv_CyB-eGFP+ cells near the tentacle tip often co-expressed Nv_

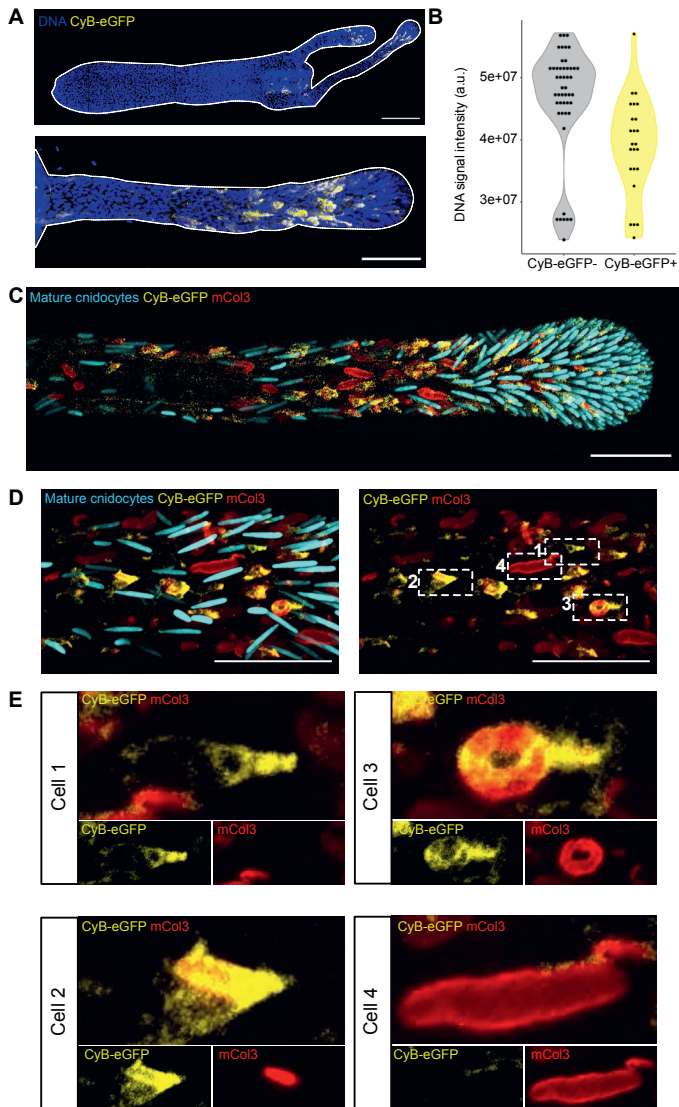


Figure 4. Terminal differentiation of cnidocytes initiates during the cell cycle. (a) Maximum projection images of CyB-eGFP polyps. (scale bar = 50 microns). (b) DNA staining intensity quantification of CyB-eGFP+ and CyB-eGFP- cells in the tentacle. (c) Maximum projection image of CyB-eGFP polyps stained for mCol3 and mature cnidocytes (d) Zoom in on a subregion of the tentacle (e) Highlight 4 cells with varying CyB-eGFP and mCol3 intensities

NCol3, a marker of cnidocyte precursors (Figure 4c). The relative intensity of Nv_CyB-eGFP and Nv_NCol3 seemed to share an inverse relationship, suggesting Nv_CyB-eGFP+ cells directly differentiate into Nv_NCol3+ cnidocyte precursors (Figure 4e). Based on the DNA content, we also noticed that most Nv_CyB-eGFP- cells are in G2 phase, suggesting there is a large proportion of G2-paused cells in the tentacle tissue. An abundance of G2-paused cells has also been reported in Hydra and shown to be important for head regeneration^{33,34}. Taken together, the spatial distribution of Nv_CyB-eGFP+ cells, cnidocyte precursors cells (Nv_NCol3+), and mature cnidocytes confirms the scRNA-seq data that the tentacle tip region consists is enriched in actively differentiating cnidocytes.

Discussion

A spatially resolved whole-transcriptome atlas of homeostatic polyps: a resource for tissue specific gene identification

We generated the first spatial transcriptomic atlas of homeostatic *Nematostella* primary polyps using tomo-seq. We identified eight gene clusters showing distinct spatial expression patterns across the oral-aboral axis. We were able to capture the expression patterns of known genes, while establishing more than 250 new region-specific gene markers. By taking an unbiased approach, our gene clusters have identified potentially new tissue regions that are restricted to a sub-anatomical region. For example, the aboral-end of the mesentery tissue and the base of the tentacle both show gene expression profiles distinct from its surrounding tissues. This suggests these tissues may serve a specialized function that has not yet been identified. Further studies of these genes and their biological function will be necessary to better understand the role of these expression states. While we have chosen to use an unbiased approach to cluster genes with restricted spatial expression patterns across the oral-aboral axis, a more targeted approach could also be used to mine this atlas for a specific gene of interest and identify other genes showing similar expression patterns.

In addition to the region-specific expression of these genes, the pattern of expression captured by our atlas may provide important insights into how tissue patterning is established and maintained during homeostasis. Many genes within the eight clusters are expressed in a gradient along the oral-aboral axis. The foot region in particular consists of genes that only show a graded expression, whereas the other regions show both graded and sharp expression changes across space. It would be interesting to disrupt these gene gradients to investigate their possible role in maintaining tissue identity.

Mapping the spatial distribution of cellular functions with both tomo-seq and scRNA-seq

Our transcriptomic atlas provides the spatial context for understanding tissue organization within the polyp; however, it lacks the cellular information scRNA-seq provides. Thus, in the second half of this study, we combined the spatial information from our tomo-seq dataset with scRNA-seq of tentacle tissue to identify the cellular composition of the tentacle tip region. By combining both spatial and single-cell datasets, we established that the rich repertoire of spatially restricted gene expression in the tip is largely driven by an enrichment of highly specialized cells called cnidocytes. Furthermore, we demonstrated that the tip region is a tissue with active differentiation of cycling cells into mature cnidocytes. This small example showcases the power of combining spatial transcriptomics with single-cell approaches. A more complete integration of our spatial atlas with scRNA-seq data of the whole polyp will provide further insight into the organization and function of different cells and tissues within the polyp.

In conclusion, our spatial transcriptomic atlas of homeostatic polyps should serve as a valuable resource for identifying region-specific genes for use in further studies of tissue function and generation of tissue-specific transgenic constructs. We envision this gene expression map to serve as the foundation for further spatial transcriptomic studies across developmental stages, regeneration time points, or even across species. Integration of this dataset with other -omics approaches will certainly provide important molecular insights into tissue patterning and maintenance during homeostasis.

Materials and Methods

Animal care and sample collection

Female and male adult animals were kept separately in the dark at 17C and spawned every 3 weeks as described previously³⁵. Spawned egg masses were collected and fertilized at room temperature, then kept at 23C in the dark. All experiments were done with unfed primary polyps 3 weeks after fertilization.

Tomography mRNA sequencing

Relaxed polyps were immobilized with 7% MgCl₂ in 12ppt artificial sea water (ASW). Mounting and storage of the samples were done as described in Ebbing et al., 2018⁸. Changes to the protocol are described below. Polyps were transferred via mouth pipette into the Tissue Freezing Medium (Leica) and oriented using a hair tool so that its tentacles are fully extended parallel to the body column. The ends of the animal were marked with red polyethylene microspheres (Cospheric, REDPMS-0.98 180-212um). Samples were frozen in liquid nitrogen and stored at -80C. Samples were warmed to -20C prior to cryosectioning into 20-micron thick slices. Each slice was transferred into a separate well of a 96-well TOMO-seq plate (Single Cell Discoveries, scdiscoveries.com). Processing of the plates and library preparation was then carried out by Single Cell Discoveries following a CEL-seq2 protocol³⁶ adapted for a low-input robotics system. Libraries were then multiplexed and sequenced on the Illumina NextSeq500 platform using the 40 bp paired-end set up. A sequencing depth of 50-80 million reads were generated per library.

in situ hybridization chain reaction (HCR)

For each gene target, probe sets for *in situ* HCR v3.0 with split-initiator probes were ordered from Molecular Instruments, Inc (molecularinstruments.com). DNA HCR amplifiers, hybridization, wash, and amplification buffers were also purchased from Molecular Instruments. The staining protocol used for *in situ* HCR was adapted from Molecular Instrument's protocol for whole mount zebrafish embryos and larva, based on Choi et al., 2018³⁷. Briefly, polyps were fixed with 4% PFA in PTw (1x PBS, 0.1% tween-20) for 1 hour at room temp. Samples were then permeabilized with 10% DMSO in PBS, followed by PTx0.5 (1x PBS, 0.5% triton X-100). Tissue was then clarified via MeOH washes (30%, 60%, 100%) and stored at -20C for >1 hour before rehydration back into PTw. Samples were then treated with 10ug/ml Proteinase K (Promega V3021) in PTw for 30min. Excess Proteinase K was removed by washing PTw. Animals were then refixed in 4% PFA in PTw for 25min and washed 3 times with PTw. Prehybridization was done in 200uL Probe Hybridization Buffer (Molecular Instruments) for 30min at 37C before hybridizing with the *in-situ* probe set (2pmol in 200uL Probe hybridization Buffer) overnight at 37C. Post-hybridization washes are as follows: 2 times 30min washes with 400uL Probe Wash Buffer (Molecular Instruments) at 37C, then 2 times 5 min washes with 500uL 5X SSCT (5x SSC pH 7, 0.1% Tween-20) at room temperature. Amplifier hairpins h1 and h2 (18pmol) were heated separately to 95C for 90sec then snap cooled to room temperature before being added to 300uL Probe Amplification Buffer (Molecular Instruments). Samples were then incubated with this amplification solution overnight at room temperature. Excess hairpins were removed by the following washes: 2 times 5min, then 2 times 30min with 500uL 5X SSCT. DNA counter staining was done by incubating samples overnight with Hoechst (1:1000) in PTw at 4C. Samples were then mounted into 85% glycerol or Vectashield Plus for imaging.

Transgenic animals

The cell cycle reporter line, *CyclinB(1-100)-eGFP*, was generated using the I-SceI meganuclease system as described before²¹. The DNA sequence corresponding to the first 100 amino acids of the *Nv_CyclinB* gene was fused directly to eGFP with a SV40 polyA sequence. Expression was driven by the *Nv_EF1* promoter sequence. Cloning of the transgene into the transgenesis plasmid was done using the NEBuilder HiFi DNA assembly kit (NEB, E2621). Fertilized embryos were injected with the transgenesis plasmid and I-SceI enzyme at the one-cell stage. F1 transgenic animals were selected based on their GFP fluorescence. F2 polyps were used for regeneration experiments. GFP signal was visualized via immunohistochemistry using the anti-eGFP antibody (Torry Pines TP401).

Immunohistochemistry

Animals were fixed and stained using a modified protocol adapted from Genikhovich and Technau³⁸. Briefly, samples were fixed in a solution of 4% paraformaldehyde (PFA; Electron Microscopy Sciences E15710) in Ptw (1x PBS, 0.1% tween-20) for 1 hour at room temperature before being permeabilized with 10%DMSO in PBS for 20min followed by Ptx0.5 (1X PBS, 0.5% TritonX-100) for 20min. Then they were incubated in blocking buffer (5% normal goat serum, 1% BSA, 1% DMSO, 0.1% tritonX-100 in 1X PBS) for 1 hour at room temperature before incubating with primary antibodies (anti-eGFP 1:500, Torry Pines TP401; anti-mini collagen3 1:400, gift from Dr. Suat Ozbek¹⁹) overnight at 4C. Samples were then washed 3 times with cnidocyte wash buffer (10mM TrisHCl pH 7.7, 10mM EDTA, 0.1% tween20) before incubating with secondary antibodies (goat anti-rabbit alexa488, 1:500, Thermo Fisher A-11008; goat anti-guineapig alexa647 1:1000, Thermo Fisher A-21450) and DNA stain (DAPI 1:1000 Sigma Aldrich D9542). EDTA (10mM final concentration) and DAPI (3:1000) were added to the sample and incubated for 30min at room temperature to stain the mature cnidocyte capsules. Samples were then washed with cnidocyte wash buffer 3 times and mounted into 85% glycerol or Vectashield Plus (Vector via Biozol VEC-H-1900-10) for imaging.

Confocal imaging and image analysis

Confocal stacks of *in situ* HCR samples were acquired on a Leica TCS SP8 confocal microscope using a 40x 1.1NA water objective using the tile scan function. Images of *Nv_CyB-eGFP* tentacles co-stained for eGFP and *Nv_NCol3* were collected in a similar way. Images of whole *Nv_CyB-eGFP* transgenic polyps were acquired on a Leica LSM780-NLO microscope using a 40x water objective, while high resolution images of tentacles were collected using a 63x oil objective for DNA intensity quantification. Image analysis was performed using FIJI (<https://imagej.net/software/fiji/>)³⁹. Nuclei segmentation was done via Cellpose⁴⁰.

Tom-seq data processing

Reads were mapped to the *Nematostella vectensis* transcriptome⁴¹ using the kallisto-BUStools method⁴². Full gene sequences were used for mapping as it resulted in consistently higher mapping rates compared to spliced transcripts when using exon-intron boundaries available in the genome annotation. Barcode (8bp) and UMI (6bp) locations in the sequence of the first read were specified accordingly for pseudoalignment. Barcodes were corrected to account for 1 substitution using the white list of barcodes. UMI were then counted for each gene to

provide a count matrix for each sample.

Sample boundaries

Tomo-seq data for each polyp includes gene counts for 96 slices, some of which do not contain the polyp. Sample boundaries were defined automatically using the dynamic threshold for each polyp defined as a local minimum of the density function of the number of genes per slice. Slices with high background signal above this threshold were marked and consequently filtered out manually. Data here as well as below was operated using tidyverse packages⁴³ and plotted using ggplot2⁴⁴.

Anatomical marker genes selection

Gene counts for the genes detected in at least three animals were normalized by total expression per slice and log-transformed, and highly variable genes (HVGs) were selected using the VariableFeatures function in Seurat v4⁴⁵. Additional genes found in the foot region of the polyp were identified via differential expression (DE) analysis comparing the aggregated gene expression in the five most aboral slices to the remaining slices in each animal performed with edgeR⁴⁶.

Polyp alignment

Dynamic time warping algorithm was used as implemented in the DTW package v1.22²². In particular, an open-ended alignment with an asymmetric step function was performed. Thus, we allowed for alignment of multiple slices within the query polyp to any given slice within the reference polyp in order to account for the possibility that certain regions along the polyp can be longer or shorter than in the reference polyp.

Single cell dissociation and RNA sequencing

Nematostella juvenile individuals were used for dissection and tentacles were cut at the base trying to exclude any tissue of the body column. The tentacle sample was dissociated in 300 uL filtered 12ppt artificial sea water (ASW) supplemented with Proteinase XIV (10 mg/mL) while mildly triturating every 10 minutes for a total of 45 minutes at 20 degrees, respectively. Three volumes of 12ppt ASW were added to stop the reaction. Afterwards, cells were briefly spun down at 1000g and resuspended in 1000 uL 12ppt ASW to wash debris and remaining protease off. In addition, the cell suspension was filtered through a 40 um strainer (Falcon) before spinning was repeated and cells were resuspended in 50 uL 12ppt ASW. Finally, cells were filtered with a 40 um flowmi strainer. Cell concentration was estimated manually using a hemocytometer and the cell suspension was diluted to aim for 10,000 cells on one lane of a 10x microfluidic chip device. Cells were loaded on one lane of a Chromium Cartridge (10X Genomics) and cDNA was generated following the Chromium Single Cell Kit protocol (10X Genomics, 3' library kit, v2 chemistry). The quality of the cDNA and resulting sequencing libraries were checked by bioanalyzer (High Sensitivity DNA Kit, Agilent). The libraries were sequenced using an Illumina NextSeq at the EMBL GeneCore facility.

Raw reads were mapped against the latest Nematostella (Nvec200) genome release (zimmerman (2020) using STARsolo⁴⁷. The R package 'Seurat' (v4)⁴⁸ was mostly used for analyses and visualizations unless stated differently. Cells with less than 500 or more than 3,000 RNA counts were removed from the data set. Data was default log normalize and count differences were regressed out during default data scaling. A Principle Component Analysis

(PCA) was performed and the first 20 PCs (estimated by Seurat's Elbow plot analysis) were used as input for Louvain clustering (resolution of 2) and dimensionality reduction by a UMAP embedding.

The FindAllMarkers function was used to identify genes that are differentially expressed between clusters identified based on a Wilcoxon Rank Sum test. Cell type identities were inferred by canonical markers and by scoring clusters for marker genes¹ published recently using Seurat's AddModuleScore function.

Cells associated with the stinging cell cluster were selected based on the location on the UMAP embedding and re-normalized and scaled as described above. PCA was performed and top 10 PCs were used as input for Louvain clustering (resolution of 1) and dimensionality reduction by a UMAP embedding. Seurat's FeaturePlot function was used to visualize gene expression intensities on top of the UMAP embeddings.

RNA velocity estimates and plots were generated using velocity.R²⁶ (fit.quantile 0.1, n 100, ngrid 50) with spliced and unspliced data matrices being generated using STARsolo⁴⁷.

References

1. Sebé-Pedrós, A. *et al.* Cnidarian Cell Type Diversity and Regulation Revealed by Whole-Organism Single-Cell RNA-Seq. *Cell* **173**, 1520-1534.e20 (2018).
2. Genikhovich, G. & Technau, U. The starlet sea anemone *Nematostella vectensis*: An anthozoan model organism for studies in Comparative genomics and functional evolutionary developmental biology. *Cold Spring Harb. Protoc.* **4**, 1–10 (2009).
3. Ståhl, P. L. *et al.* Visualization and analysis of gene expression in tissue sections by spatial transcriptomics. *Science (80-.)*. **353**, 78–82 (2016).
4. Marx, V. Method of the Year: spatially resolved transcriptomics. *Nat. Methods* **18**, 9–14 (2021).
5. Chen, K. H., Boettiger, A. N., Moffitt, J. R., Wang, S. & Zhuang, X. Spatially resolved, highly multiplexed RNA profiling in single cells. *Science (80-.)*. **348**, 1360–1363 (2015).
6. Kruse, F., Junker, J. P., van Oudenaarden, A. & Bakkers, J. *Tomo-seq: A method to obtain genome-wide expression data with spatial resolution. Methods in Cell Biology* **135**, (Elsevier Ltd, 2016).
7. Junker, J. P. *et al.* Genome-wide RNA Tomography in the Zebrafish Embryo. *Cell* **159**, 662–675 (2014).
8. Ebbing, A. *et al.* Spatial Transcriptomics of *C. elegans* Males and Hermaphrodites Identifies Sex-Specific Differences in Gene Expression Patterns. *Dev. Cell* **47**, 801-813.e6 (2018).
9. Wu, C. C. *et al.* Spatially Resolved Genome-wide Transcriptional Profiling Identifies BMP Signaling as Essential Regulator of Zebrafish Cardiomyocyte Regeneration. *Dev. Cell* **36**, 36–49 (2016).
10. Passamanek, Y. J. & Martindale, M. Q. Cell proliferation is necessary for the regeneration of oral structures in the anthozoan cnidarian *Nematostella vectensis*. *BMC Dev. Biol.* **12**, 1 (2012).
11. Amiel, A. R. *et al.* Characterization of morphological and cellular events underlying oral regeneration in the sea anemone, *Nematostella vectensis*. *Int. J. Mol. Sci.* **16**, 28449–28471 (2015).
12. Warner, J. F., Amiel, A. R., Johnston, H. & Rottinger, E. Regeneration is a partial redeployment of the embryonic gene network. *BioRxiv* (2019). doi:10.1017/CBO9781107415324.004
13. Schaffer, A. A., Bazarsky, M., Levy, K., Chalifa-Caspi, V. & Gat, U. A transcriptional time-course analysis of oral vs. aboral whole-body regeneration in the Sea anemone *Nematostella vectensis*. *BMC Genomics* **17**, 1–22 (2016).
14. Dubuc, T. Q., Traylor-knowles, N. & Martindale, M. Q. Initiating a regenerative response ; cellular and molecular features of wound healing in the cnidarian *Nematostella vectensis*

- Initiating a regenerative response ; cellular and molecular features of wound healing in the cnidarian *Nematostella vectensis*. **12**, 1–20 (2014).
15. Kusserow, A. *et al.* Unexpected complexity of the Wnt gene family in a sea anemone. *Nature* **433**, 156–160 (2005).
 16. Richards, G. S. & Rentzsch, F. Transgenic analysis of a SoxB gene reveals neural progenitor cells in the cnidarian *Nematostella vectensis*. *Development* **141**, 4681–4689 (2014).
 17. Rentzsch, F., Fritzenwanker, J. H., Scholz, C. B. & Technau, U. FGF signalling controls formation of the apical sensory organ in the cnidarian *Nematostella vectensis*. *Development* **135**, 1761–1769 (2008).
 18. Babonis, L. S. & Martindale, M. Q. PaxA, but not PaxC, is required for cnidocyte development in the sea anemone *Nematostella vectensis*. *Evodevo* **8**, 1–20 (2017).
 19. Zenkert, C., Takahashi, T., Diesner, M. O. & Özbek, S. Morphological and molecular analysis of the *Nematostella vectensis* cnidom. *PLoS One* **6**, (2011).
 20. He, S. *et al.* An axial Hox code controls tissue segmentation and body patterning in *Nematostella vectensis*. *Science (80-.)*. **361**, 1377–1380 (2018).
 21. Renfer, E., Amon-Hassenzahl, A., Steinmetz, P. R. H. & Technau, U. A muscle-specific transgenic reporter line of the sea anemone, *Nematostella vectensis*. *Proc. Natl. Acad. Sci. U. S. A.* **107**, 104–108 (2010).
 22. Toni, G. Computing and Visualizing Dynamic Time Warping Alignments in R: The dtw Package. *J. Stat. Softw.* **31**, (2009).
 23. Steinmetz, P. R. H., Aman, A., Kraus, J. E. M. & Technau, U. Gut-like ectodermal tissue in a sea anemone challenges germ layer homology. *Nat. Ecol. Evol.* **1**, 1535–1542 (2017).
 24. Muraro, M. J. *et al.* A Single-Cell Transcriptome Atlas of the Human Pancreas. *Cell Syst.* **3**, 385–394.e3 (2016).
 25. Yang, Y. *et al.* Transcriptome dynamics during human erythroid differentiation and development. *Genomics* **102**, 431–441 (2013).
 26. La Manno, G. *et al.* RNA velocity of single cells. *Nature* **560**, 494–498 (2018).
 27. Babonis, L. S., Enjolras, C., Ryan, J. F. & Martindale, M. Q. A novel regulatory gene promotes novel cell fate by suppressing ancestral fate in the sea anemone *Nematostella vectensis*. *bioRxiv* (2021). doi:10.1101/2021.08.29.458124
 28. Soufi, A. & Dalton, S. Cycling through developmental decisions: How cell cycle dynamics control pluripotency, differentiation and reprogramming. *Dev.* **143**, 4301–4311 (2016).
 29. Muhr, J. & Hagey, D. W. The cell cycle and differentiation as integrated processes: Cyclins and CDKs reciprocally regulate Sox and Notch to balance stem cell maintenance. *BioEssays* **43**, 1–12 (2021).
 30. Ruijtenberg, S. & van den Heuvel, S. Coordinating cell proliferation and differentiation: Antagonism between cell cycle regulators and cell type-specific gene expression. *Cell Cycle* **15**, 196–212 (2016).
 31. Klochendler, A. *et al.* A Transgenic Mouse Marking Live Replicating Cells Reveals In Vivo Transcriptional Program of Proliferation. *Dev. Cell* **23**, 681–690 (2012).
 32. King, R. W., Jackson, P. K. & Kirschner, M. W. Mitosis in Transition Review. *Cell* **79**, 563–571 (1994).
 33. Buzgariu, W., Crescenzi, M. & Galliot, B. Robust G2 pausing of adult stem cells in Hydra. *Differentiation* **87**, 83–99 (2014).
 34. Buzgariu, W., Wenger, Y., Tcaciuc, N., Catunda-Lemos, A. P. & Galliot, B. Impact of cycling cells and cell cycle regulation on Hydra regeneration. *Dev. Biol.* **433**, 240–253 (2018).
 35. Fritzenwanker, J. H. & Technau, U. Induction of gametogenesis in the basal cnidarian *Nematostella vectensis* (Anthozoa). *Dev. Genes Evol.* **212**, 99–103 (2002).
 36. Hashimshony, T. *et al.* CEL-Seq2: Sensitive highly-multiplexed single-cell RNA-Seq. *Genome Biol.* **17**, 1–7 (2016).
 37. Choi, H. M. T. *et al.* Third-generation in situ hybridization chain reaction: Multiplexed, quantitative, sensitive, versatile, robust. *Dev.* **145**, 1–10 (2018).

38. Genikhovich, G. & Technau, U. Induction of spawning in the starlet sea anemone *Nematostella vectensis*, in vitro fertilization of gametes, and dejellying of zygotes. *Cold Spring Harb. Protoc.* **4**, 1–4 (2009).
39. Schneider, C. A., Rasband, W. S. & Eliceiri, K. W. NIH Image to ImageJ: 25 years of image analysis. *Nat. Methods* **9**, 671–675 (2012).
40. Stringer, C., Wang, T., Michaelos, M. & Pachitariu, M. Cellpose: a generalist algorithm for cellular segmentation. *Nat. Methods* **18**, 100–106 (2021).
41. Zimmermann, B. *et al.* Sea anemone genomes reveal ancestral metazoan chromosomal macrosynteny. *bioRxiv* (2022). doi:10.1101/2020.10.30.359448
42. Melsted, P. *et al.* Modular, efficient and constant-memory single-cell RNA-seq preprocessing. *Nat. Biotechnol.* **39**, 813–818 (2021).
43. Wickham, H. *et al.* Welcome to the Tidyverse. *J. Open Source Softw.* **4**, 1686 (2019).
44. Wickham, H. *ggplot2: Elegant Graphics for Data Analysis*. (Springer-Verlag New York, 2016).
45. Satija, R., Farrell, J. A., Gennert, D., Schier, A. F. & Regev, A. Spatial reconstruction of single-cell gene expression data. *Nat. Biotechnol.* **33**, 495–502 (2015).
46. Robinson, M. D., McCarthy, D. J. & Smyth, G. K. edgeR: A Bioconductor package for differential expression analysis of digital gene expression data. *Bioinformatics* **26**, 139–140 (2009).
47. Kaminow, B., Yunusov, D. & Dobin, A. STARsolo: accurate, fast and versatile mapping/quantification of single-cell and single-nucleus RNA-seq data. *bioRxiv* (2021). doi:10.1101/2021.05.05.442755
48. Butler, A., Hoffman, P., Smibert, P., Papalexi, E. & Satija, R. Integrating single-cell transcriptomic data across different conditions, technologies, and species. *Nat. Biotechnol.* **36**, 411–420 (2018).
49. Richards, G. S. & Rentzsch, F. Regulation of *Nematostella* neural progenitors by SoxB, Notch and bHLH genes. *Dev.* **142**, 3332–3342 (2015).
50. Ryan, J. F. *et al.* Pre-bilaterian origins of the hox cluster and the hox code: Evidence from the sea anemone, *Nematostella vectensis*. *PLoS One* **2**, (2007).
51. Matus, D. Q., Magie, C. R., Pang, K., Martindale, M. Q. & Thomsen, G. H. The Hedgehog gene family of the cnidarian, *Nematostella vectensis*, and implications for understanding metazoan Hedgehog pathway evolution. *Dev. Biol.* **313**, 501–518 (2008).
52. Marlow, H., Roettinger, E., Boekhout, M. & Martindale, M. Q. Functional roles of Notch signaling in the cnidarian *Nematostella vectensis*. *Dev. Biol.* **362**, 295–308 (2012).
53. Matus, D. Q., Thomsen, G. H. & Martindale, M. Q. FGF signaling in gastrulation and neural development in *Nematostella vectensis*, an anthozoan cnidarian. *Dev Genes Evol* **217**, 139–148 (2007).
54. Magie, C. R., Pang, K. & Martindale, M. Q. Genomic inventory and expression of Sox and Fox genes in the cnidarian *Nematostella vectensis*. *Dev. Genes Evol.* **215**, 618–630 (2005).
55. Martindale, M. Q., Pang, K. & Finnerty, J. R. Investigating the origins of triploblasty: ‘Mesodermal’ gene expression in a diploblastic animal, the sea anemone *Nematostella vectensis* (phylum, Cnidaria; class, Anthozoa). *Development* **131**, 2463–2474 (2004).
56. Moran, Y. *et al.* Cnidarian microRNAs frequently regulate targets by cleavage. *Genome Res.* **24**, 651–663 (2014).
57. Faltine-Gonzalez, D. Z. & Layden, M. J. Characterization of nAChRs in *Nematostella vectensis* supports neuronal and non-neuronal roles in the cnidarian-bilaterian common ancestor. *Evodevo* **10**, 1–18 (2019).
58. Mazza, M. E., Pang, K., Reitzel, A. M., Martindale, M. Q. & Finnerty, J. R. A conserved cluster of three PRD-class homeobox genes (homeobrain, rx and orthopedia) in the Cnidaria and Protostomia. *Evodevo* **1**, 1–15 (2010).
59. Matus, D. Q., Pang, K., Daly, M. & Martindale, M. Q. Expression of Pax gene family members in the anthozoan cnidarian, *Nematostella vectensis*. *Evol. & Dev.* **9**, 25–38 (2007).

60. Leclère, L. & Rentzsch, F. RGM Regulates BMP-Mediated Secondary Axis Formation in the Sea Anemone *Nematostella vectensis*. *Cell Rep.* **9**, 1921–1931 (2014).
61. Lee, P. N., Pang, K., Matus, D. Q. & Martindale, M. Q. A WNT of things to come: Evolution of Wnt signaling and polarity in cnidarians. *Semin. Cell Dev. Biol.* **17**, 157–167 (2006).
62. Layden, M. J., Meyer, N. P., Pang, K., Seaver, E. C. & Martindale, M. Q. Expression and phylogenetic analysis of the *zic* gene family in the evolution and development of metazoans. *Evodevo* **1**, 1–16 (2010).
63. Pukhlyakova, E. A., Kirillova, A. O., Kraus, Y. A., Zimmermann, B. & Technau, U. A cadherin switch marks germ layer formation in the diploblastic sea anemone *Nematostella vectensis*. *Dev.* **146**, 1–15 (2019).

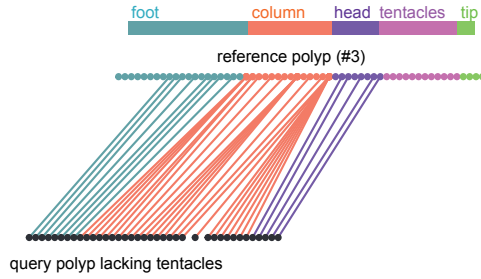


Figure S1. Sample alignment of tentacle-less polyp to the reference polyp using DTW. Each dot represents one slice.

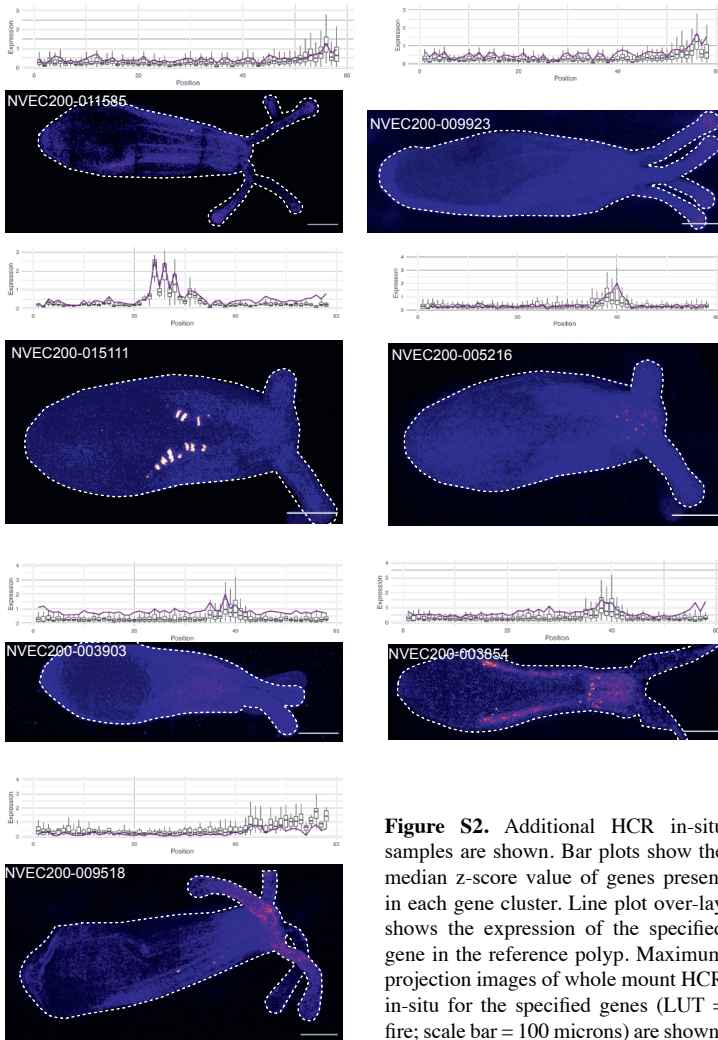


Figure S2. Additional HCR in-situ samples are shown. Bar plots show the median z-score value of genes present in each gene cluster. Line plot overlay shows the expression of the specified gene in the reference polyp. Maximum projection images of whole mount HCR in-situ for the specified genes (LUT = fire; scale bar = 100 microns) are shown.

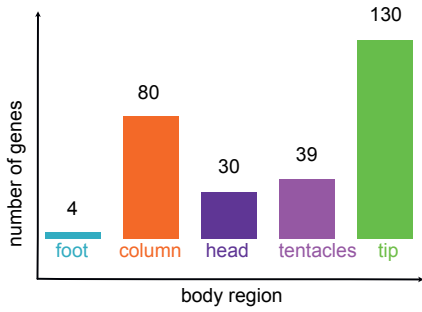


Figure S3. Bar plot showing the number of HVGs (highly variable genes) with specific expression in each anatomical region

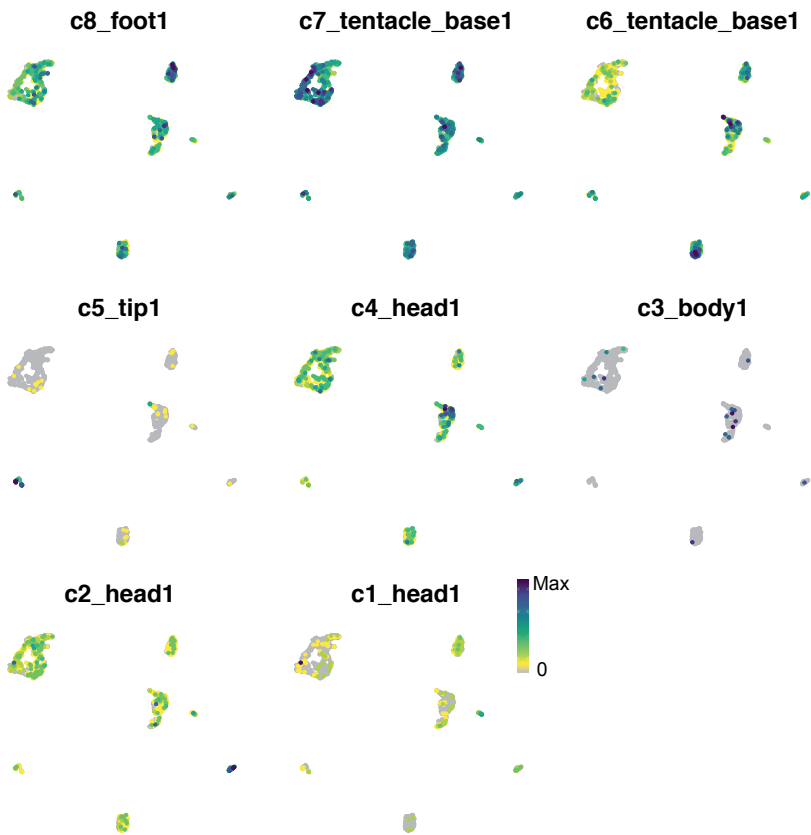


Figure S4. Mapping of the anatomical region marker genes onto scRNA-seq data of tentacle tissue. Cluster numbers are indicated along with their anatomical region.

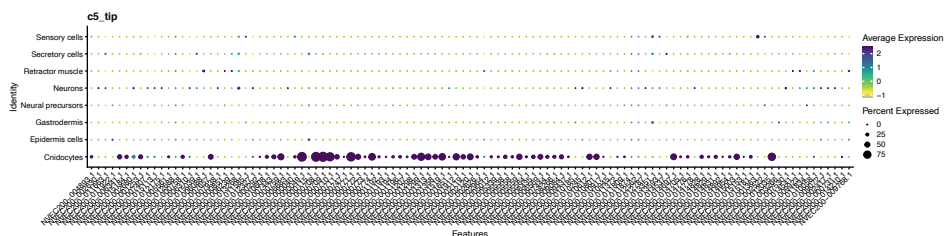


Figure S5. Dot plot of scRNA-seq data showing the expression pattern of tentacle tip cluster genes across the eight cell clusters.

2

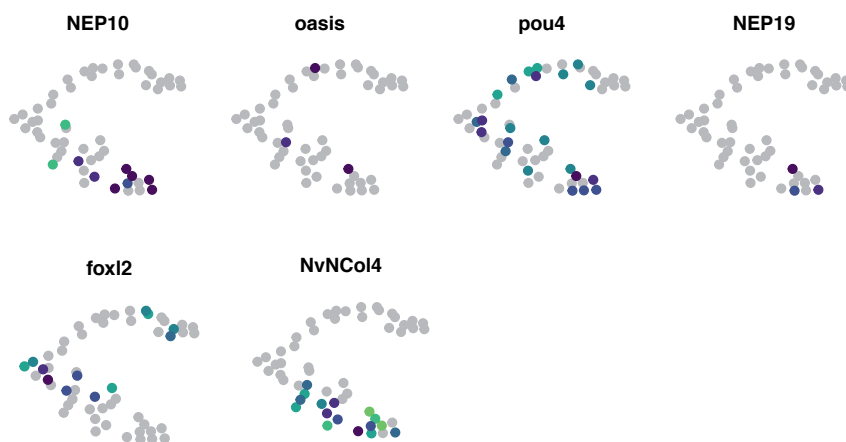


Figure S6. UMAP embedding of cnidocyte cell cluster showing the expression levels of various cnidocyte specific genes.

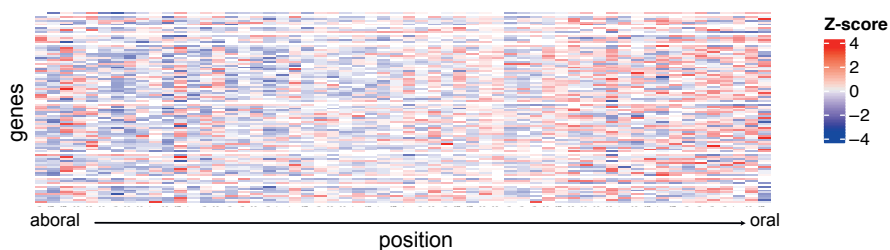
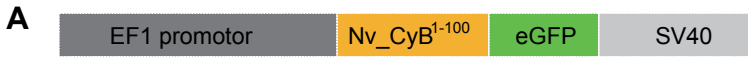


Figure S7. Heat map of showing the expression pattern of genes used to calculate the mitosis score in the reference polyp.



B Nv_CyB(1-100)

MAAVRRLTAQTVPAQENVLDLTKAKHGQNTRFGRAALGDIANKDKAVLPGKRIALGT
RGLTRNEAFTALPKPERPASKPEPMDMADFSEALNECFPTDVE

Figure S8. (a) Schematic showing the Nv_CyB-eGFP construct used to generate the cell cycle report line. (b) The amino acid sequence of the first 100 amino acids of Nv_CyB

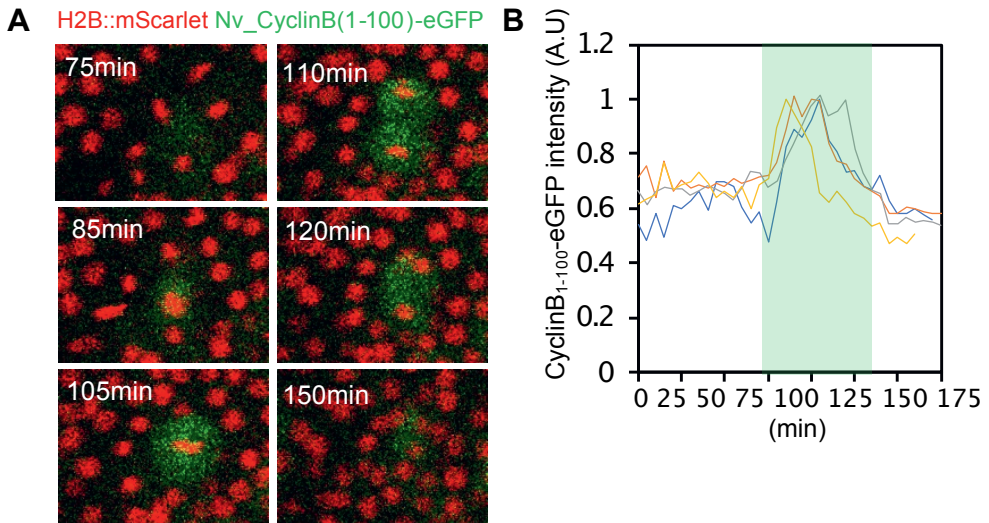


Figure S9. (a) Still images from live imaging video of early cell divisions of Nv_CyB-eGFP embryos (red = H2B::mScarlet, Green = Nv_CyB(1-100)-eGFP; time from beginning of video is noted in the top left corner). (b) Line plot showing the CyB-eGFP intensity changes over the time of a single cell division. Each line represents one cell division event.



“The real purpose of scientific method is to make sure Nature hasn’t misled you into thinking you know something you don’t actually know.”

- Robert M. Pirsig, *Zen and the Art of Motorcycle Maintenance*, p.131

Chapter 3

Heat shock treatment initiates dormant regeneration in the sea anemone *Nematostella vectensis*

Stephanie Cheung^{1*}, Danila Bredikhin^{2*}, Petrus Steenbergen¹, Hendrik C. Korswagen³, Oliver Stegle^{2,4#}, Aissam Ikmi^{1#}

¹ Developmental Biology Unit, European Molecular Biology Laboratory, Heidelberg 69117, Germany

² Genome Biology Unit, European Molecular Biology Laboratory, Heidelberg 69117, Germany

³ Hubrecht Institute- KNAW (Royal Netherlands Academy of Arts and Sciences) and University Medical Center Utrecht, Uppsalalaan 8, 3584 CT Utrecht, The Netherlands

⁴ Division of Computational Genomics and Systems Genetics, German Cancer Research Center (DKFZ), Heidelberg 69120, Germany

*These authors contributed equally

#Corresponding authors

Abstract

In highly regenerative species, wound healing leads to regeneration initiation. However, which wound signals are responsible for activating regenerative programs in these species is still poorly understood. Here we present the first organism-wide spatial transcriptomic study on a highly regenerative Cnidarian species, *Nematostella vectensis*, during foot regeneration to better understand what body-wide responses contribute to regeneration. We investigate both wound-localized gene expression as well as genes differentially expressed in a non-wound localized manner. By taking such a spatial transcriptomic approach, we were able to identify the presence of injury-related genes in the tentacle region during homeostasis and discover the selective up-regulation of wound-related genes at distant locations from the wound site during regeneration. Furthermore, we demonstrate that the oral tissues in *Nematostella* exhibit similar changes in gene expression and cell proliferation upon heat shock treatment and foot amputation. Strikingly, both foot amputation and heat shock treatment were independently sufficient to initiate head regrowth in regeneration arrested polyps. Our results challenge the paradigm that wounding is required for regeneration and suggests that other stress inducing factors may also be able to activate regenerative programs in the absence of wounding.

Introduction

Regeneration describes a remarkable phenomenon whereby a lost body structure is regrown following amputation or injury. The process of regeneration generally proceeds through three major modules starting with wound healing, regeneration initiation, and finally, morphogenesis¹. The first step, wound healing, is a conserved process found throughout the evolutionary tree². However, the ability of wounding signals to initiate regenerative programs is what separates highly regenerative tissues from non-regenerative ones. Despite being the focus of scientific research since the 1700s, how animals initiate regeneration following wounding remain poorly understood.

The study of early wounding signals has identified calcium signaling, ROS (reactive oxygen species), inflammation/immune response, and nerve-related factors as common responses activated immediately after injury^{3,4}. Disruption to any of these processes often blocks successful regeneration of the lost structure suggesting that having the correct wound signals is important for regeneration initiation⁵⁻⁸. The context in which a wound is induced also has grave implications toward regeneration initiation. Initially, it was observed that only wounds that resulted in the loss of tissue led to regeneration initiation and thus, it was thought that the size of the wound determined its ability to initiate regeneration⁹. However, more recently, it was shown in Planaria and Zebrafish that all wounds are capable of inducing regeneration if there is a missing tissue context¹⁰. Thus, while all wounding may elicit the same generic signals, how a given tissue interprets those signals is key to initiating regeneration.

Recently, wounding signals were also found in non-wounded tissues. Following the amputation of a single hind limb in *Xenopus* froglets, the uninjured contralateral limb showed similar levels of depolarization signals as detected in the amputated limb¹¹. Similarly, cell proliferation was found to be upregulated in both the amputated and uninjured contralateral limb of axolotls¹². One function of this mirroring wounding effect in amphibian seems to be a role in “priming” the uninjured limb for regeneration, however it’s unclear whether such “priming” is sufficient to also induce regeneration. If true, this would suggest that local wounding in one area can induce regeneration in distant tissues, thus disentangling regeneration initiation from the wound site. The relationship between local wounding signals and its long-range effects on the rest of the organism is only beginning to be addressed. Transcriptomic studies during regeneration have demonstrated how gene expression dynamically changes throughout the course of regeneration^{13,14}. However, these studies often focus only on the wound site. An investigation into organism-wide gene expression changes occurring during regeneration across time and space is still missing. The closest example is a recent spatial transcriptomic study of the Zebrafish heart during regeneration¹⁵.

Here we present the first comprehensive organism-wide spatial transcriptomic analysis of regeneration. Owing to its small size, high regenerative capacity, and abundant transcriptomic and genomic resources available, we conducted our study on *Nematostella vectensis*, a sea anemone from the phylum Cnidaria¹⁶. We first characterized the time course for aboral regeneration and then performed tomography RNA-seq (tomo-seq) on primary polyps at five different time points (uncut, 12, 24, 48, 96hpa) during aboral regeneration. Wound-localized genes at 12hpa were found to exhibit dramatically different spatial expression patterns during homeostasis, with many genes showing restricted expression at the tentacles in uncut animals. Further analysis for genes specifically upregulated beyond the wound location

revealed several stress-related genes are selectively upregulated in the tentacles during aboral regeneration, indicating the presence of long-range communication of wound signals across the animal body. Strikingly, global heat shock treatment and aboral amputation both elicit a similar polarized response in stress genes and cell proliferation at the tentacles. We then tested if heat shock treatment can serve as a generic wound signal to initiate regeneration. Using a dormant regeneration assay, we surprisingly find that heat shock alone was sufficient to induce oral regeneration in polyps. Our results demonstrate that generic stress signals are sufficient to initiate regeneration, challenging the paradigm that an open wounding is required for regeneration.

Results

Wound-localized genes show diverse expression patterns during homeostasis

The aim of this study is to capture the dynamic gene expression changes that occur across the body of an animal during regeneration. Traditionally, *Nematostella* polyps have been used to study oral regeneration where half of the polyp is removed during amputation. Since we wished to observe body-wide responses to wounding, we chose to utilize a smaller amputation site. By amputating part of the foot region, we are able to retain >80% of the polyp after amputation for spatial transcriptomic analysis. Since foot regeneration has not been reported before, we first established a regeneration time line following foot amputation. The foot is characterized by the presence of Fgfrb-eGFP+ cells at the very aboral end of the polyp (Figure 1a). Using this landmark, we were able to stage regeneration of the foot region and determine that regeneration is complete by ~96hpa (Figure 1a).

3 With the timeline for regeneration established, we performed tomo-seq on four time points (12, 24, 48, 96hpa) spanning the full course of foot regeneration. Tomo-seq is a spatial transcriptomic method that combines cryosectioning with low-input RNA-seq to generate transcriptome-wide expression atlases along a single body axis. Four polyps were sequenced per time point, yielding a total of 20 tomo-seq samples. Sample quality was comparable across all time points, with similar distributions of total gene counts detected per slice (Figure 1b).

First, we looked for genes upregulated at the wound site at 12hpa. We identified a total of 226 genes with wound-localized expression at 12hpa (Figure 1c). GO term enrichment analysis revealed that unfolded protein responses (i.e., GO:0036500, GO:0036499, GO:0006986), transcription regulation (i.e., GO:1902895, GO:1902893, GO:0045893), and stress responses (i.e., GO:0034976, GO:0140467) are enriched in the differentially expressed (DE) wound-localized genes (Figure S1). To determine whether these genes show a wound-specific expression pattern, we determined the expression patterns of these genes in uncut animals and found that up to ~30% of wound-localized genes at 12hpa already showed localized expression in the aboral region during homeostasis (Figure 1g). Interestingly, ~25% of wound-localized genes were found enriched at the tentacle region during homeostasis (Figure 1d-e). The remaining wound-localized genes either showed no clear enrichment at any body region in uncut animals, or did not show a consistent expression pattern across all samples (Figure 1f). Taken together, this data shows how wound-localized genes can have very different expression patterns in the absence of wounding. We were able to categorize these genes by their changes in expression pattern into four robust classes: 1) enriched expression at the

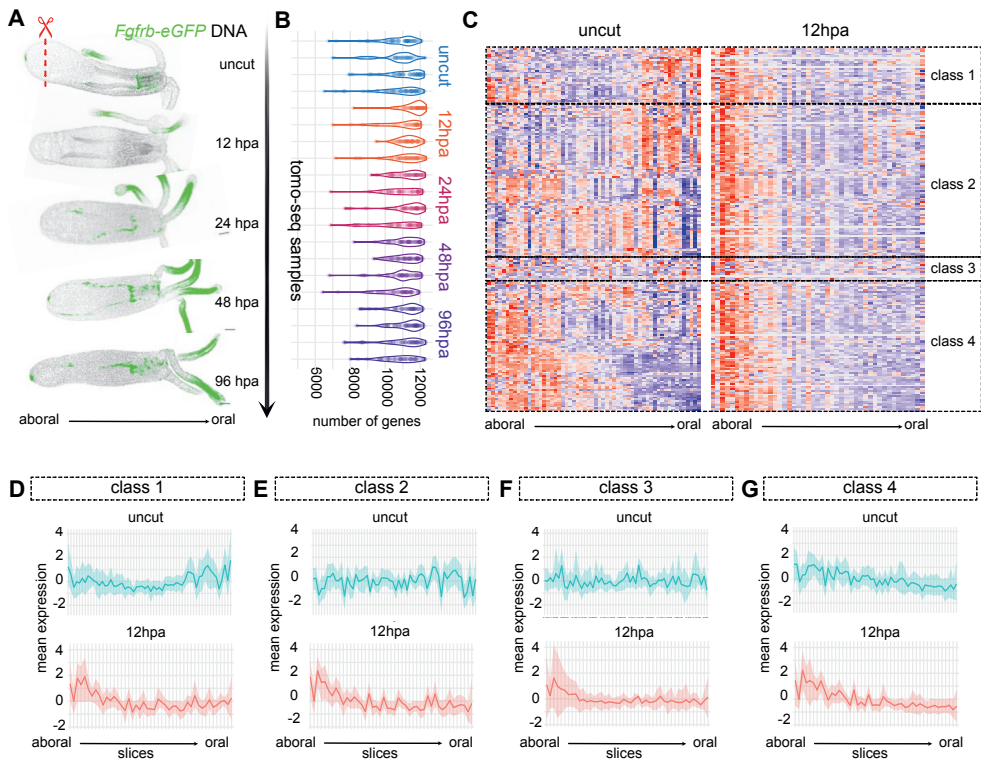


Figure 1. Tomo-seq of foot regenerating polyps reveal wound-localized genes at 12hpa have very different expression patterns during homeostasis. (a) Maximum projection images of Fgfrb-eGFP polyps at various time points (uncut, 12hpa, 24hpa, 48hpa, 96hpa) following foot amputation (Green = Fgfrb-eGFP, gray = DNA, scale bar = 50 microns). (b) Violin plot of tomo-seq samples showing the number of genes detected in each slice per sample (each dot represents one slice). (c) Heat maps showing the gene expression pattern of wound-localized DE (differentially expressed) genes in an uncut (left) and 12hpa (right) polyp. K-means clustering of the genes into 4 classes are highlighted. (d-g) Wound-localized DE genes are clustered into 4 robust groups. Line plots show the mean expression pattern of genes within the group for an uncut polyp (blue) and a 12hpa polyp (red), shading shows the expression value range of all genes.

foot, 2) enriched expression in the whole tentacle, 3) enrichment in the tentacle base and 4) no clear enrichment across the body.

Systemic changes in gene expression are deployed during regeneration

To determine if gene expression changes were occurring in other areas of the animal during foot regeneration, we performed DE analysis on the five body regions of the polyp: tentacle tips, tentacles, head, column and foot. Previously, we established gene marking the five major anatomical regions of the polyp (Chapter 1). Using these gene, we were able to align each of our samples to the reference polyp and annotate each slice within our samples to these 5 body regions (Figure 2a). Pooling the slices within each region and subsequent 2D plotting of these pooled slices showed that these marker genes robustly annotated each anatomical region in regenerating animals (Figure S2).

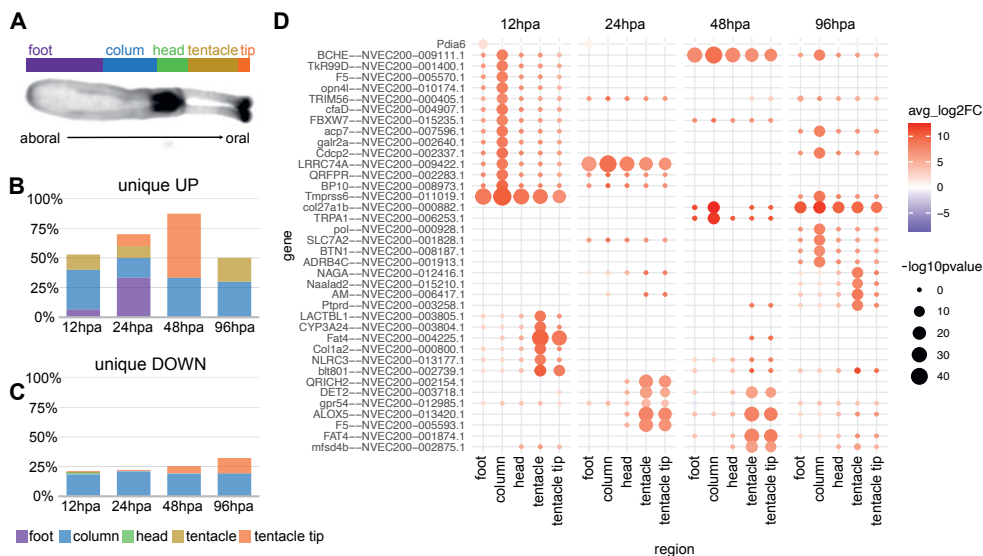


Figure 2. Regional DE analysis captures organism-wide changes in gene expression during foot regeneration (a) Image of a uncut polyp from the tomo-seq dataset with the five anatomical regions annotated. (b-c) Stacked bar plot showing a summary of regional DE analysis. The percentage of genes uniquely up-regulated (b) and down-regulated (c) in each region at each time point is shown. (d) Dot plot of regional DE analysis showing the expression profiles of genes specifically up-regulated in one anatomical region within the polyp at a given time point (tentacle and tentacle tip are grouped).

3

Next, we performed DE analysis between each region across all time points to determine whether genes are differentially expressed in a particular region at a given time point. We found over 4600 DE genes (<1% FDR) with a roughly even distribution across all regions and time points (Figure S3). Upregulated genes are more often specifically upregulated in a particular region within a time point, while downregulated genes are often downregulated across multiple anatomical regions within a time point (Figure 2b-c).

To simplify the many patterns of gene expression changes captured by our regional DE analysis, we decided to focus only on genes that were significantly upregulated (adjusted p-value <0.00001, \log_2 fold change > 2) in a single region at a given time point. This yield a total of 46 genes, with 26 genes being upregulated only in the column region, 19 genes upregulated in the tentacles/tip regions, and 1 gene upregulated only in the foot region (Figure 2d). Majority of the upregulated genes in the column region occur at 12hpa, while those found in the tentacles/tip are spread more equally across all four time points. Strikingly, the genes found specifically upregulated at the tentacles/tip show functions related to stress (i.e., *blt801*¹⁷), immunity (i.e., *NLRC3*¹⁸) and inflammation (i.e., *ALOX5*¹⁹). Genes specifically upregulated in the column region do not have such biological functions. Why such genes are upregulated in a non-wound location during regeneration is unclear, but is reminiscent of how the uninjured contralateral limbs of amphibians can exhibit similar responses found in the amputated limb^{11,12}. These results illustrate how wound signals can elicit dynamic gene expression changes in distant tissues throughout the entire time course of regeneration, suggesting that such responses are not merely acute effects caused by wounding.

Heat shock treatment and aboral amputation elicits similar responses in gene expression and cell proliferation

Both the wound-localized DE analysis and the regional DE analysis have revealed that the tentacle/tip region shows expression of stress related genes during homeostasis and regeneration. This led us to postulate if the expression of such genes during homeostasis could serve a “priming” function to facilitate faster regeneration in the event of wounding. Indeed, the tentacles are the only tissue exposed to the environment in the natural habitat of *Nematostella* polyps and thus are most prone to injury. To test this hypothesis, we focused on two heat shock proteins (HSP90B1 and HSPA5) that showed enriched expression at the tentacles during homeostasis but wound-localized expression at 12hpa (Figure 3a and Figure S4). Since a localized wound was enough to shift the expression of these two genes from one end of the polyp to the other, we wondered what would happen if we subjected the polyp to a global stress. Thus, we performed a heat shock on *Nematostella* polyps and measured the expression of HSP90B1 and HSPA5 at 12hphs (hours post heat shock). Both heat shock proteins showed increased expression at 12hphs compared to controls. Surprisingly, their pattern of expression was highly enriched at the tentacle/oral region compared to the rest of the body (Figure 3b). This demonstrates that a uniform stress can elicit a polarized response in the polyp, where the tentacle/oral region is more affected than the rest of the body.

Another well-known wound-localized response in *Nematostella* is cell proliferation, which is also upregulated after wounding²⁰. Since the pattern of cell proliferation has only been reported for oral regeneration in *Nematostella*, we wondered how cell proliferation is affected during foot regeneration and if the tentacle region will again show a similar response to the wound site. EdU labeling of polyps at 24hpa following foot amputation showed an increase in cell proliferation localized to two distinct areas compared to control: the wound site and the tentacle/oral tissues (Figure 4a). This pattern mirrors the gene expression pattern we observed for HSP90B1 and HSPA5 in our tomo-seq data. Intriguingly, heat shocked animals also showed an increase in cell proliferation at the tentacle/oral tissues, which is again similar to the response of HSP90B1 and HSPA5 to temperature stress (Figure 4b). Taken together, these results show that the tentacle/oral region responds to mechanical (i.e., foot amputation) and temperature (i.e., heat shock) stress in a similar fashion, indicating that the oral pole serves as a stress-responsive center in the polyp.

Heat shock is sufficient to induce regeneration in *Nematostella* polyps

Since both mechanical and temperature perturbations elicit similar responses in heat shock protein expression and cell proliferation, we sought to investigate if these responses are indeed involved in regeneration. Wounding in highly regenerative animals often leads to initiation of regeneration and regrowth of the missing tissues or structure. In *Planaria*, it was shown that different types of wounding all generate a “generic wound signal”, which can initiate regeneration when there is a missing tissue context¹⁰. In regeneration arrested *Planaria*, regeneration could be re-initiated with a small incision at the original wound site. Since heat shock was able to induce similar wounding responses as amputation in *Nematostella*, we wondered if heat shock would be sufficient to induce regeneration.

Previously, it was reported that *Nematostella* polyps treated with nocodazole (a drug involved in cell cycle arrest) after oral amputation failed to regenerate after wound healing²⁰.

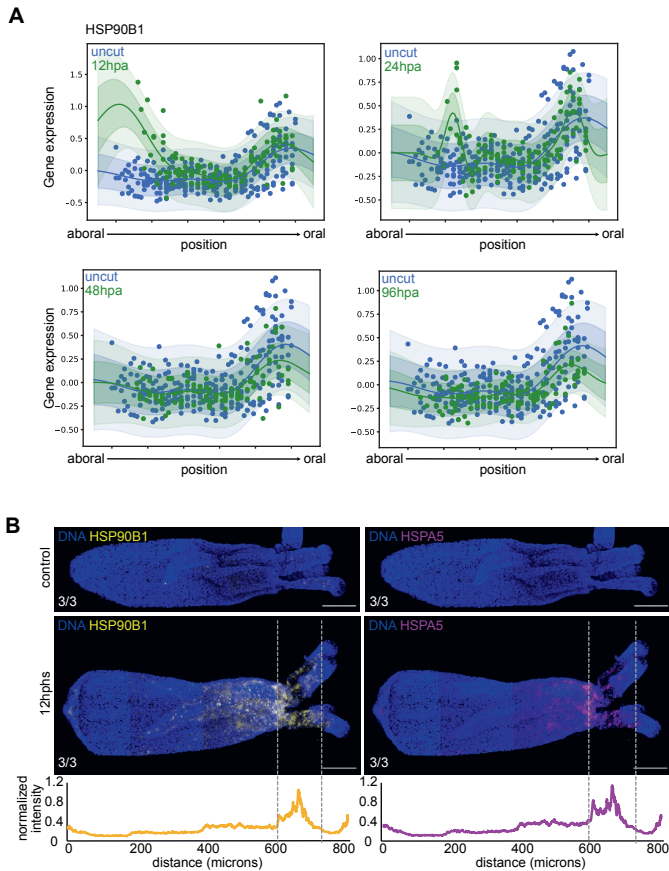


Figure 3. Two heat shock proteins respond in a polarized manner to foot amputation and heat shock treatment (a) Gaussian Processing analysis of HSP90B1 at each time point (12, 24, 48, and 96 hours post amputation, hpa) compared to control polyps (blue = uncut, green = time point) (b) Maximum projection images of in-situ HCR samples detecting expression of HSP90B1 (left) and HSPA5 (right) before and after heat shock treatment. Line plots below the images report the normalized intensity values (HSP intensity/DNA intensity) in the 12hphs (hours post heat shock) samples.

We adapted this protocol to arrest polyps after wound healing but before regeneration of the oral pole (Figure 5a). Similar to Planarians and Zebrafish, a secondary incision at the original wound site was able to induce regeneration of the oral pole in these arrested polyps (Figure 5b). Strikingly, a secondary incision at the aboral end of the polyp was also sufficient to induce regeneration. Heat shock treatment alone was also able to initiate regeneration in these arrested polyps. These results demonstrate that wounding is not required for regeneration initiation. Rather, generic stress signals caused by other environmental stresses are sufficient to induce regeneration.

Discussion

The first step of regeneration is wounding. Thus, many studies within regeneration focus

on the initial wound signals and the process of wound healing in order to understand how wounding is able to initiate regeneration. While such studies have been very informative about the process of wound healing, their narrow focus on the wound site has limited our understanding of how local wounds can induce systemic responses in the body. Here, we reported the first comprehensive spatial transcriptomic study of regeneration where we used tomo-seq to capture the spatial gene expression patterns of regenerating *Nematostella* polyps following foot amputation. Our dataset revealed the dynamic nature of wound-localized signals and showed that these wound-localized signals have a diversity of expression patterns during homeostasis. Thus, while most transcriptomic studies have focused on absolute changes in gene expression levels during regeneration, here we were also able to observe genes that showed a spatial change in expression pattern without necessarily showing a global change in expression levels. A striking finding from this wound-localized analysis of our spatial data was that many wound-localized genes showed enriched expression at the tentacle region during homeostasis.

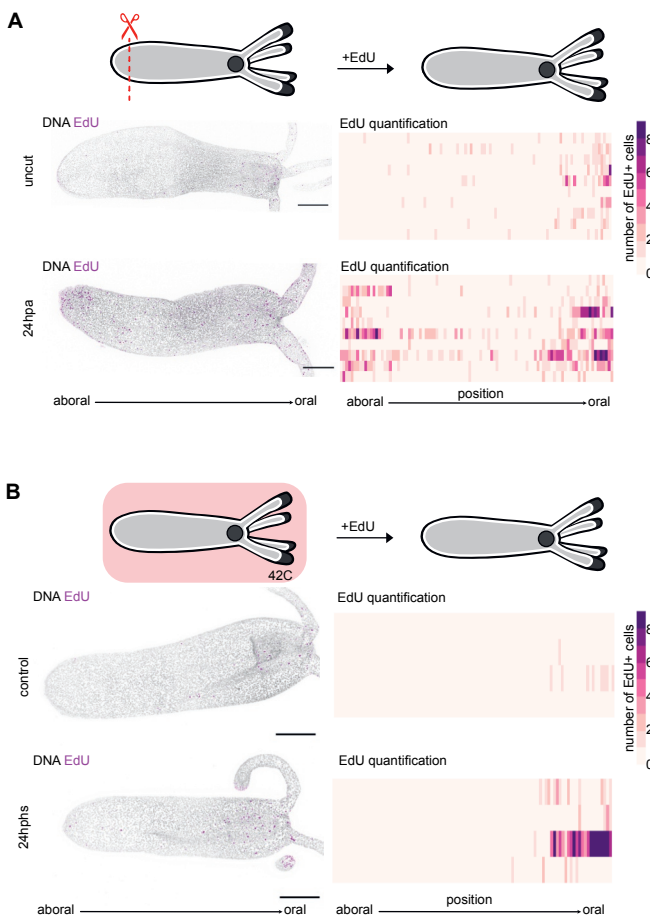


Figure 4. Cell proliferation is up-regulated at the oral tissues after heat shock treatment and foot amputation. (a) Maximum projection images of a control (top) and a foot amputated (bottom) polyp at 24hpa (hours post amputation) (magenta = EdU, gray = DNA; scale bar = 100 microns) with the corresponding quantification graphs of EdU+ cells across the polyp body (purple = high, light pink = low, each row = 1 polyp). (b) Maximum projection images of a control (top) and a heat shock treated (bottom) polyp at 12hphs (hours post heat shock) (magenta = EdU, gray = DNA; scale bar = 100 microns) with the corresponding quantification graphs of EdU+ cells across the polyp body (purple = high, light pink = low, each row = 1 polyp).

Interestingly, a number of genes were also selectively upregulated in the tentacle/tip region during regeneration. This result not only demonstrates how local wounding can induce long range signals across the entire body of an animal, but also that different tissues can interpret wound signals in significantly different ways. How these wound signals are able to communicate with distant tissues is largely unknown, but recently nerves were shown to be required for systemic activation of cell proliferation in un-injured contralateral limbs of axolotls¹². In *Nematostella*, longitudinal nerves also connect the foot region with the tentacle tissue²¹, but whether these nerve cells serve any role in relaying wound signals across the body has not been investigated. Further studies comparing different wound types and locations would also be needed to better understand whether these differential responses are intrinsic to the tissue type, or whether it is dependent on the relative distance from the wound. Moreover, it is important to investigate whether these long-range effects of foot amputation

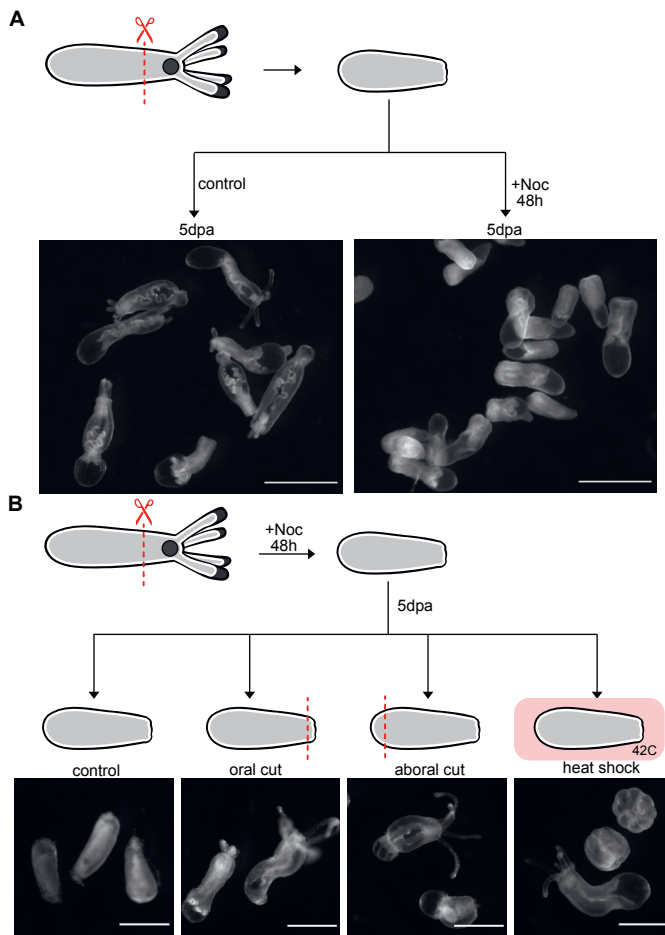


Figure 5. Heat shock treatment is sufficient to initiate oral regeneration in arrested polyps. (a) Polyps fail to regenerate the oral pole following transient treatment with 0.2 μ M nocodazole (scale bar = 1mm). Images of cut polyps at 5dpa (days post amputation). (b) Regeneration of the oral pole can be initiated in arrested polyps by inducing a secondary cut at the oral pole, the foot, or by heat shock treatment (scale bar = 0.5mm)

are specific to wounding and whether they play a role in regeneration.

Heat shock treatment was also sufficient to induce upregulation of some of the wound-localized genes found in our tomo-seq study. It was striking to find that a global stressor such as heat shock was able to elicit a polarized response in heat shock protein (HSP) upregulation. Similarly, we also saw a polarized response in cell proliferation following heat shock treatment enriched in the oral tissues. Upregulation of cell proliferation was previously reported to be wound-localized and required for successful oral regeneration in *Nematostella*²⁰. Here we showed that cell proliferation is upregulated at both the wound-site and the oral pole during foot regeneration. Taken together, we have demonstrated that both mechanical (via foot amputation) or temperature (heat shock) stresses are able to induce wound-like responses in the oral tissues, highlighting the role of the oral pole as a stress-responsive center.

Lastly, we challenged the assumption that wounds are required for regeneration by showing that heat shock treatment alone is sufficient to induce regeneration. The ability to separate the effects of wounding from the regeneration has not been possible until very recently¹⁰. And now we have shown that indeed in a missing tissue context, a generic cellular stress such as heat shock is sufficient to induce regeneration. Moreover, a wound induced at the opposite end of the animal is also able to induce regeneration, suggesting that both local and global stress signals initiate a systemic regenerative response in *Nematostella*. In addition, given that an environmental input triggers regeneration, we propose this process might have originated from developmental processes that respond to environmental changes. Thus, regeneration might represent a derived form of development that is expressed in different degrees in animals depending on their environmental plasticity. Therefore, it would be important to see if this is a conserved mechanism across regenerative species. If such generic cellular stressors are able to initiate regeneration, it would provide a new context in which to approach regenerative medicine.

Materials and Methods

Animal care and foot amputation

Female and male adult animals were kept separately in the dark at 17C and spawned every 3 weeks as described previously²². Spawned egg masses were collected and fertilized at room temperature, then kept at 23C in the dark. All experiments were done with unfed primary polyps 3 weeks after fertilization. For regeneration experiments, unfed polyps were relaxed and immobilized using 7% MgCl₂ in 12ppt artificial sea water (ASW). Polyps were cut ~1mm from the aboral pole with a tungsten needle (Ted Pella, Inc. 13570-10). The cut polyps were then washed with fresh 12 ppt ASW 2x before putting at 23C.

Tomography mRNA sequencing

Relaxed polyps were immobilized with 7% MgCl₂ in 12ppt artificial sea water (ASW). Mounting and storage of the samples were done as described in Ebbing et al., 2018²³. Changes to the protocol are described below. Polyps were transferred via mouth pipette into the Tissue Freezing Medium (Leica) and oriented using a hair tool so that its tentacles are fully extended parallel to the body column. The ends of the animal were marked with red

polyethylene microspheres (Cospheric, REDPMS-0.98 180-212um). Samples were frozen in liquid nitrogen and stored at -80C. Samples were warmed to -20C prior to cryosectioning into 20-micron thick slices. Each slice was transferred into a separate well of a 96-well TOMO-seq plate (Single Cell Discoveries, scdiscoveries.com). Processing of the plates and library preparation was then carried out by Single Cell Discoveries following a CEL-seq2 protocol²⁴ adapted for a low-input robotics system. Libraries were then multiplexed and sequenced on the Illumina NextSeq500 platform using the 40 bp paired-end set up. A sequencing depth of 50-80 million reads were generated per library.

in situ hybridization chain reaction (HCR)

For each gene target, probe sets for *in situ* HCR v3.0 with split-initiator probes were ordered from Molecular Instruments, Inc (molecularinstruments.com). DNA HCR amplifiers, hybridization, wash, and amplification buffers were also purchased from Molecular Instruments. The staining protocol used for *in situ* HCR was adapted from Molecular Instrument's protocol for whole mount zebrafish embryos and larva, based on Choi et al., 2018²⁵. Briefly, polyps were fixed with 4% PFA in PTw (1x PBS, 0.1% tween-20) for 1 hour at room temp. Samples were then permeabilized with 10% DMSO in PBS, followed by PTx0.5 (1x PBS, 0.5% triton X-100). Tissue was then clarified via MeOH washes (30%, 60%, 100%) and stored at -20C for >1 hour before rehydration back into PTw. Samples were then treated with 10ug/ml Proteinase K (Promega V3021) in PTw for 30min. Excess Proteinase K was removed by washing PTw. Animals were then refixed in 4% PFA in PTw for 25min and washed 3 times with PTw. Prehybridization was done in 200uL Probe Hybridization Buffer (Molecular Instruments) for 30min at 37C before hybridizing with the *in-situ* probe set (2pmol in 200uL Probe hybridization Buffer) overnight at 37C. Post-hybridization washes are as follows: 2 times 30min washes with 400uL Probe Wash Buffer (Molecular Instruments) at 37C, then 2 times 5 min washes with 500uL 5X SSCT (5x SSC pH 7, 0.1% Tween-20) at room temperature. Amplifier hairpins h1 and h2 (18pmol) were heated separately to 95C for 90sec then snap cooled to room temperature before being added to 300uL Probe Amplification Buffer (Molecular Instruments). Samples were then incubated with this amplification solution overnight at room temperature. Excess hairpins were removed by the following washes: 2 times 5min, then 2 times 30min with 500uL 5X SSCT. DNA counter staining was done by incubating samples overnight with Hoechst (1:1000) in PTw at 4C. Samples were then mounted into 85% glycerol or Vectashield Plus for imaging.

Transgenic animals

Homozygous *Fgfrb-eGFP* adults were crossed with wild-type adults to generate transgenic polyps for staging foot regeneration. Full details on the generation of both mutant lines have been reported previously²⁶.

Sample fixation and immunohistochemistry

Animals were fixed and stained using a modified protocol adapted from Genikhovich and Technau²⁷. Briefly, samples were fixed in a solution of 4% paraformaldehyde (PFA; Electron Microscopy Sciences E15710) in Ptw (1x PBS, 0.1% tween-20) for 1 hour at room temperature before being permeabilized with 10%DMSO in PBS for 20min followed by Ptx0.5 (1X PBS, 0.5% TritonX-100) for 20min. Then they were incubated in blocking buffer (5% normal goat serum, 1% BSA, 1% DMSO, 0.1% tritonX-100 in 1X PBS) for 1 hour at room temperature before incubating with the primary antibody (anti-eGFP 1:500, Torrey Pines

TP401) overnight at 4C. Samples were then washed 3 times with PTw before incubating with the secondary antibody (goat anti-rabbit alexa488, 1:500, Thermo Fisher A-11008) and DNA stain (Hoechst34580 1:1000 Sigma Aldrich 63493). Samples were then washed with PTw 3 times and mounted into 85% glycerol or Vectashield Plus (Vector via Biozol VEC-H-1900-10) for imaging.

EdU staining and quantification

Staining with EdU was done as described previously²⁶. Briefly, animals were incubated with 50uM EdU in 12ppt ASW for 30 minutes before immobilizing with 7% MgCl₂ solution. Animals were then fixed with 4% PFA in PTw for 1 hour at room temperature before being permeabilized with 10%DMSO in PBS for 20min followed by Ptx0.5 (1X PBS, 0.5% TritonX-100) for 20min. Samples were then blocked for 15 min using 5% BSA (Sigma A2153-50G) in PBS. The Click-it reaction was then performed with alexa647-azide with the sample as specified in the Click-it EdU Cell Proliferation Kit for Imaging (Thermo Fisher C10340) for 30 min at room temperature. Excess labelling reagents were washed away with PTw for 5 min before mounting into 85% glycerol for imaging.

EdU+ cells were quantified using a FIJI. First a difference of gaussians was calculated for each sample by subtracting the gaussian blurred (sigma =2) maximum projection image from the gaussian blurred (sigma =4) maximum projection image. The “find maxima” function was then used to detect individual EdU+ cells and determine their location (x, y coordinates) along the animal body. The 2D Coordinates were then collapsed into 1D by taking only the coordinates corresponding to the oral-aboral axis. The coordinates were then normalized to the size of the animal for each sample to generate a uniform coordinate axis. The number of EdU+ cells were then binned into 100 bins and plotted as a heat map using ggplot2.

Heat shock treatment

Polyps were transferred to a 1.5mL Eppendorf tube containing ~1mL 12ppt ASW. Heat shock treatment was performed by incubating the polyps in an Eppendorf Thermomixer Dry Block Heating Shaker at 37C for 40min. Then the polyps were immediately transferred into a 10cm dish containing >10mL 12ppt ASW at room temperature. Samples were then kept at 23C.

Regeneration dormant polyps and stress treatments

Juvenile polyps containing 6-8 tentacles were immobilized using 7% MgCl₂ solution and then bisected ~1mm below the pharynx. Polyps were then immediately washed 3x with fresh 12ppt ASW and kept at 23C. To arrest polyps after wound healing, polyps were treated with 0.2uM nocodazole (Sigma M1404) at 3hpa. The drug solution was refreshed every 24h. After treatment with nocodazole for 48h, the polyps were washed and transferred to fresh 12ppt ASW and kept at 23C for 3 days. Secondary amputations (at the oral or foot region) or heat shock treatment (42C) was performed and then animals were imaged 9 days later.

Confocal imaging and image analysis

Confocal stacks of whole polyps were acquired on a Leica TCS SP8 confocal microscope using a 40x 1.1NA water objective using the tile scan function. Image analysis was performed using FIJI (<https://imagej.net/software/fiji/>)²⁸.

Tomo-seq data processing

Reads were mapped to the *Nematostella vectensis* transcriptome²⁹ using the kallisto-BUStools

method³⁰. Full gene sequences were used for mapping as it resulted in consistently higher mapping rates compared to spliced transcripts when using exon-intron boundaries available in the genome annotation. Barcode (8bp) and UMI (6bp) locations in the sequence of the first read were specified accordingly for pseudoalignment. Barcodes were corrected to account for 1 substitution using the white list of barcodes. UMIs were then counted for each gene to provide a count matrix for each sample. Sample boundary determination and subsequent polyp alignment was done as reported previously (see Chapter 1 Methods). Tomo-seq samples of homeostatic polyps reported in Chapter 1 were included in all analyses reported below.

Polyp alignment

Dynamic time warping algorithm was used as implemented in the DTW package v1.22³¹. In particular, an open-ended alignment with an asymmetric step function was performed. Thus, we allowed for alignment of multiple slices within the query polyp to any given slice within the reference polyp in order to account for the possibility that certain regions along the polyp can be longer or shorter than in the reference polyp.

Differential expression of the wound-localized genes

In order to find out which genes are expressed at the wound site, we looked into the wound-adjacent slices of the animals at the 12hpa time point. In particular, we aggregated gene expression in 5 slices from the aboral side and in all the other slices. This resulted in two corresponding measurements per polyp for each gene. Differential expression testing was then performed in edgeR, with a likelihood ratio test for identifying significant hits³². We also tested for differential gene expression at the foot in uncut animals using the same approach and excluded these significantly differentially expressed genes from the list of the wound-localized ones. We used hierarchical clustering to group these genes by their expression patterns in polyps at 2 time points (12hpa and uncut) and to demonstrate different patterns of expression of different groups of genes.

GO term enrichment

Significant hits from the DE analysis with gene annotations were used as an input to EnrichR^{33–35} for GO term enrichment analysis. Significant GO biological process 2021 terms with an adjusted p-value <0.05 were reported.

Gene expression with region resolution

Region labels for each polyp were defined by label transfer from the reference polyp using the output of the sample alignment procedure. Gene expression counts were aggregated per each region in each polyp thus producing a coarse-grained view on gene expression along the polyp's body. A 2D t-SNE representation of gene expression was computed using the first five principal components of the scaled gene expression matrix. Differential expression was performed using DESeq2 comparing gene expression in a region at a time point to gene expression in the same region in uncut polyps³⁶. P-values were adjusted using the Benjamini-Hochberg procedure. Unique up- or downregulated genes were considered to be the ones not significantly up- or downregulated (<1% FDR) in other regions at the same time point.

Modelling gene expression in time and space with Gaussian processes

As Gaussian processes provide a flexible framework for modelling spatial or temporal gene expression, we employed it to compare spatial expression patterns between time points. We

applied GPcounts³⁷ to fit a Gaussian process with a Gaussian likelihood per gene per time point on non-zero counts, log-normalised and centered, for polyps after alignment. We then used a two-sample test to compare between gene expression pattern at each time point to its pattern in uncut polyps.

References

1. Bideau, L., Kerner, P., Hui, J., Vervoort, M. & Gazave, E. Animal regeneration in the era of transcriptomics. *Cell. Mol. Life Sci.* **78**, 3941–3956 (2021).
2. Takeo, M., Lee, W. & Ito, M. Wound healing and skin regeneration. *Cold Spring Harb. Perspect. Med.* **5**, (2015).
3. Liu, Y., Lou, W. P. K. & Fei, J. F. The engine initiating tissue regeneration: does a common mechanism exist during evolution? *Cell Regen.* **10**, 1–12 (2021).
4. Niethammer, P. The Early Wound Signals Philipp. *Curr. Opin. Genet. Dev.* **40**, 17–22 (2016).
5. Tsai, S. L., Baselga-Garriga, C. & Melton, D. A. Blastemal progenitors modulate immune signaling during early limb regeneration. *Dev.* **146**, (2019).
6. Marchant, J. S. Ca²⁺ signaling and regeneration. *Cold Spring Harb. Perspect. Biol.* **11**, 1–12 (2019).
7. Jaenen, V. *et al.* Reactive oxygen species rescue regeneration after silencing the MAPK–ERK signaling pathway in *Schmidtea mediterranea*. *Sci. Rep.* **11**, 1–16 (2021).
8. Kumar, A. & Brockes, J. P. Nerve dependence in tissue, organ, and appendage regeneration. *Trends Neurosci.* **35**, 691–699 (2012).
9. Wenemoser, D. & Reddien, P. W. Planarian regeneration involves distinct stem cell responses to wounds and tissue absence. *Dev. Biol.* **344**, 979–991 (2010).
10. Owlarn, S. *et al.* Generic wound signals initiate regeneration in missing-tissue contexts. *Nat. Commun.* **8**, 1–13 (2017).
11. Busse, S. M., McMillen, P. T. & Levin, M. Cross-limb communication during xenopus hindlimb regenerative response: Non-local bioelectric injury signals. *Dev.* **145**, (2018).
12. Payzin-Dogru, D. *et al.* Nerve-mediated amputation-induced stem cell activation primes distant appendages for future regeneration events in axolotl. *bioRxiv* (2021). doi:10.1101/2021.12.29.474455
13. Wenemoser, D., Lapan, S. W., Wilkinson, A. W., Bell, G. W. & Reddien, P. W. A molecular wound response program associated with regeneration initiation in planarians. *Genes Dev.* **26**, 988–1002 (2012).
14. Dubuc, T. Q., Traylor-knowles, N. & Martindale, M. Q. Initiating a regenerative response ; cellular and molecular features of wound healing in the cnidarian *Nematostella vectensis* Initiating a regenerative response ; cellular and molecular features of wound healing in the cnidarian *Nematostella vectensis*. **12**, 1–20 (2014).
15. Wu, C. C. *et al.* Spatially Resolved Genome-wide Transcriptional Profiling Identifies BMP Signaling as Essential Regulator of Zebrafish Cardiomyocyte Regeneration. *Dev. Cell* **36**, 36–49 (2016).
16. Genikhovich, G. & Technau, U. The starlet sea anemone *nematostella vectensis*: An anthozoan model organism for studies in Comparative genomics and functional evolutionary developmental biology. *Cold Spring Harb. Protoc.* **4**, 1–10 (2009).
17. Dunn, M. A., Brown, K., Lightowers, R. & Hughes, M. A. A low-temperature-responsive gene from barley encodes a protein with single-stranded nucleic acid-binding activity which is phosphorylated in vitro. *Plant Mol. Biol.* **30**, 947–959 (1996).
18. Schneider, M. *et al.* The innate immune sensor NLRC3 attenuates Toll-like receptor signaling via modification of the signaling adaptor TRAF6 and transcription factor NF- κ B. *Nat. Immunol.* **13**, 823–831 (2012).
19. Hofheinz, K. *et al.* Conversion of pro-inflammatory murine Alox5 into an anti-inflammatory 15S-lipoxygenating enzyme by multiple mutations of sequence determinants. *Arch. Biochem.*

- Biophys.* **530**, 40–47 (2013).
20. Passamanek, Y. J. & Martindale, M. Q. Cell proliferation is necessary for the regeneration of oral structures in the anthozoan cnidarian *Nematostella vectensis*. *BMC Dev. Biol.* **12**, 1 (2012).
 21. Havrilak, J. A. *et al.* Characterization of NvLWamide-like neurons reveals stereotypy in *Nematostella* nerve net development. *Dev. Biol.* **431**, 336–346 (2017).
 22. Fritzenwanker, J. H. & Technau, U. Induction of gametogenesis in the basal cnidarian *Nematostella vectensis* (Anthozoa). *Dev. Genes Evol.* **212**, 99–103 (2002).
 23. Ebbing, A. *et al.* Spatial Transcriptomics of *C. elegans* Males and Hermaphrodites Identifies Sex-Specific Differences in Gene Expression Patterns. *Dev. Cell* **47**, 801–813.e6 (2018).
 24. Hashimshony, T. *et al.* CEL-Seq2: Sensitive highly-multiplexed single-cell RNA-Seq. *Genome Biol.* **17**, 1–7 (2016).
 25. Choi, H. M. T. *et al.* Third-generation in situ hybridization chain reaction: Multiplexed, quantitative, sensitive, versatile, robust. *Dev.* **145**, 1–10 (2018).
 26. Ikmi, A. *et al.* Feeding-dependent tentacle development in the sea anemone *Nematostella vectensis*. *Nat. Commun.* **11**, 1–13 (2020).
 27. Genikhovich, G. & Technau, U. Induction of spawning in the starlet sea anemone *Nematostella vectensis*, in vitro fertilization of gametes, and dejellying of zygotes. *Cold Spring Harb. Protoc.* **4**, 1–4 (2009).
 28. Schneider, C. A., Rasband, W. S. & Eliceiri, K. W. NIH Image to ImageJ: 25 years of image analysis. *Nat. Methods* **9**, 671–675 (2012).
 29. Zimmermann, B. *et al.* Sea anemone genomes reveal ancestral metazoan chromosomal macrosynteny. *bioRxiv* (2022). doi:10.1101/2020.10.30.359448
 30. Melsted, P. *et al.* Modular, efficient and constant-memory single-cell RNA-seq preprocessing. *Nat. Biotechnol.* **39**, 813–818 (2021).
 31. Toni, G. Computing and Visualizing Dynamic Time Warping Alignments in R: The dtw Package. *J. Stat. Softw.* **31**, (2009).
 32. Robinson, M. D., McCarthy, D. J. & Smyth, G. K. edgeR: A Bioconductor package for differential expression analysis of digital gene expression data. *Bioinformatics* **26**, 139–140 (2009).
 33. Chen, E. Y. *et al.* Enrichr: interactive and collaborative HTML5 gene list enrichment analysis tool. *BMC Bioinformatics* **14**, 128 (2013).
 34. Kuleshov, M. V. *et al.* Enrichr: a comprehensive gene set enrichment analysis web server 2016 update. *Nucleic Acids Res.* **44**, W90–7 (2016).
 35. Xie, Z. *et al.* Gene Set Knowledge Discovery with Enrichr. *Curr. Protoc.* **1**, e90 (2021).
 36. Love, M. I., Huber, W. & Anders, S. Moderated estimation of fold change and dispersion for RNA-seq data with DESeq2. *Genome Biol.* **15**, 1–21 (2014).
 37. BinTayyash, N. *et al.* Non-parametric modelling of temporal and spatial counts data from RNA-seq experiments. *Bioinformatics* **37**, 3788–3795 (2021).

Adj p-value	GO Biological Process
0.0003	ATF6-mediated unfolded protein response (GO:0036500)
0.0034	regulation of apoptotic process (GO:0042981)
0.0034	cellular response to glucose starvation (GO:0042149)
0.0127	PERK-mediated unfolded protein response (GO:0036499)
0.0162	positive regulation of pri-miRNA transcription by RNA polymerase II (GO:1902895)
0.0165	response to endoplasmic reticulum stress (GO:0034976)
0.0197	integrated stress response signaling (GO:0140467)
0.0262	negative regulation of programmed cell death (GO:0043069)
0.0262	regulation of pri-miRNA transcription by RNA polymerase II (GO:1902893)
0.0262	positive regulation of transcription, DNA-templated (GO:0045893)
0.0262	negative regulation of RNA splicing (GO:0033119)
0.0264	positive regulation of transcription by RNA polymerase II (GO:0045944)
0.0264	response to unfolded protein (GO:0006986)
0.0264	positive regulation of transcription from RNA polymerase II promoter involved in cellular response to chemical stimulus (GO:1901522)
0.0264	negative regulation of apoptotic process (GO:0043066)

Figure S1. GO term enrichment of wound-localized genes using EnrichR (see methods)

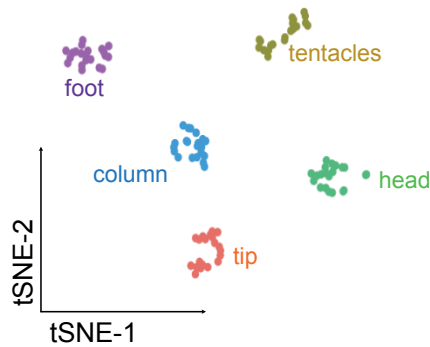


Figure S2. tSNE plot of the pooled slices from each anatomical region of all tomo-seq samples reveals 5 distinct clusters corresponding to each anatomical region.

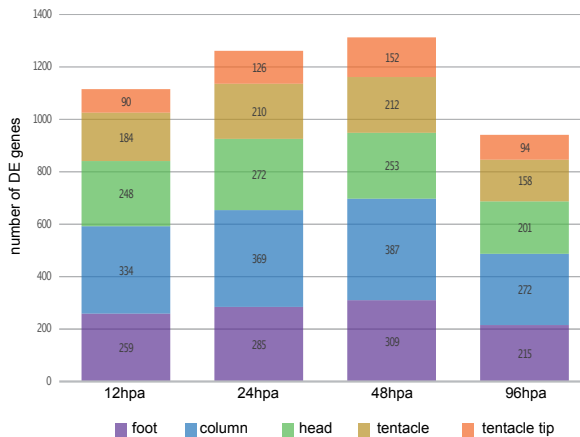


Figure S3. Stack bar plot showing the number of DE genes found in each region per time point.

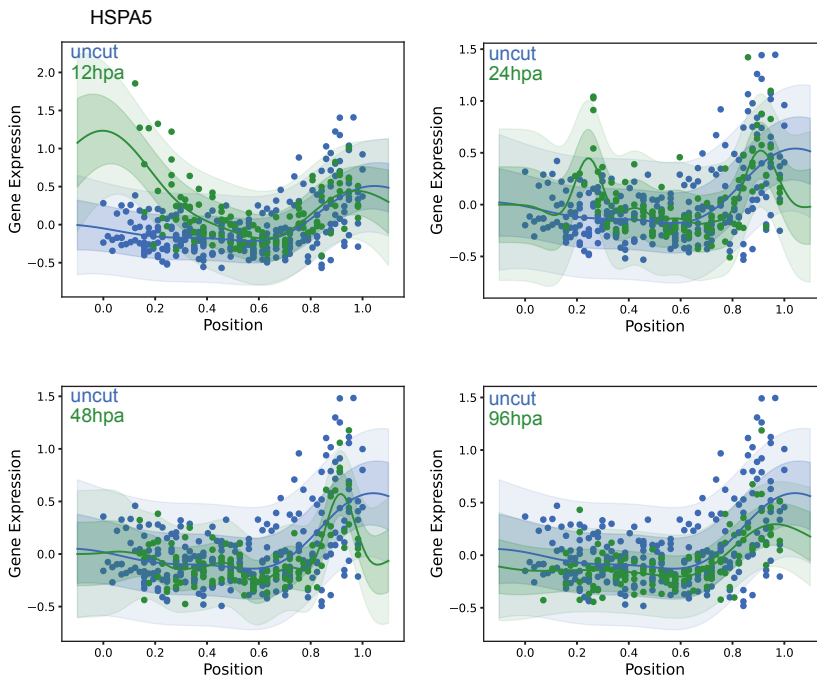
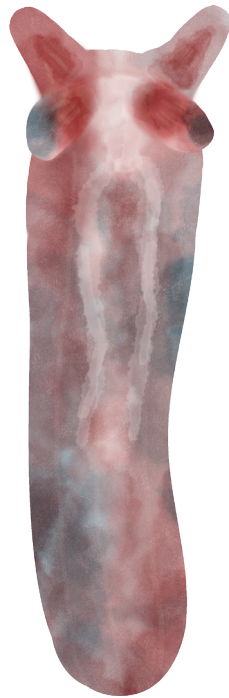


Figure S4. Gaussian Processing analysis of HSPA5 at each time point compared to control polyps (blue = uncut, green = time point). Dots show the expression value of a given slice. The line plots show the best fit line for the data.



“It is the time you have wasted for your rose that makes your rose so important.”

- Antoine de Saint-Exupéry, *The Little Prince*, p.64

Chapter 4

Tentacle tip regeneration can proceed via two distinct mechanisms in *Nematostella vectensis*

Stephanie Cheung¹, Giulia Bergamini^{1,2}, Omar Matar^{1,3}, Petrus Steenbergen¹, Aissam Ikmi^{1#}

¹ Developmental Biology Unit, European Molecular Biology Laboratory, Heidelberg, Germany

² Department of Life Sciences, University of Modena and Reggio Emilia, Modena, Italy

³ Department of Pharmacology, UCL School of Pharmacy, London WC1X 1AN, United Kingdom

[#]Corresponding author

Abstract

In cnidarians, tentacles armed with stinging cells (also called cnidocytes) are a hallmark of this phylum, which includes sea anemones, jellyfish and hydra. During feeding or defense, tentacles can be naturally subject to extensive injury and tissue loss, and the high regenerative capacity of cnidarians enables the restoration of damaged appendages. However, the mechanisms of tentacle regeneration have remained elusive. Here, we dissect the processes underlying tentacle tip regeneration in the sea anemone *Nematostella vectensis*, a powerful regeneration model with robust molecular genetic approaches^{1,2}. By combining *ex vivo* and *in vivo* experiments with transgenic reporter lines and molecular perturbations, we demonstrate that tip regeneration can proceed via two distinct mechanisms depending on the location of amputation. A fast regenerative response is possible due to the presence of a primed population of cnidocyte precursor cells near the tentacle tip, while a slower FGF-dependent mechanism is activated if this precursor population is removed. Furthermore, we identify a novel function of FGF signaling in cnidogenesis. Taken together, these findings illustrate how a cnidarian species has developed distinct regenerative strategies to cope with different types of insults.

Introduction

The tentacle is a unique anatomical structure characterized by its elongated morphology that extends from the main body of diverse groups of animals such as cnidarians, gastropods, and cephalopods. This appendage is typically used for a wide range of functions including locomotion, prey capture, sensing, and defense. In the metazoan tree, cnidarians are among the earliest animals that evolved the capacity to fully regenerate their tentacle appendages. This phylum can be broadly subdivided into two clades, the medusozoans (jellyfish and *Hydra* species) and Anthozoa (including sea anemones and corals). In both clades, tentacles are relatively simple extensions of the diploblastic body plan. The regenerative abilities of tentacles were already recognized in 1973, when the tentacles of the North Atlantic jellyfish, *Aurelia aurita*, were reported to be capable of regenerating into full polyps^{3,4}. Further studies investigating the cellular mechanism of tentacle regeneration in jellyfish has shown that localized cell proliferation at the tentacle bulbs is required for successful regeneration, which could indicate the involvement of resident stem/progenitor cell populations^{5,6}. Similarly in *Hydra*, proliferation of progenitor cells outside the tentacle underlies tentacle growth and maintenance⁷. While our current knowledge of tentacle regeneration mainly derives from medusozoan species, understanding this process in anthozoan species will shed new light on the cellular principle driving appendage regeneration in cnidarians.

Nematostella vectensis is an anthozoan species displaying remarkable regenerative abilities^{8,9}. *Nematostella* has emerged as an attractive regeneration model organism in past two decades

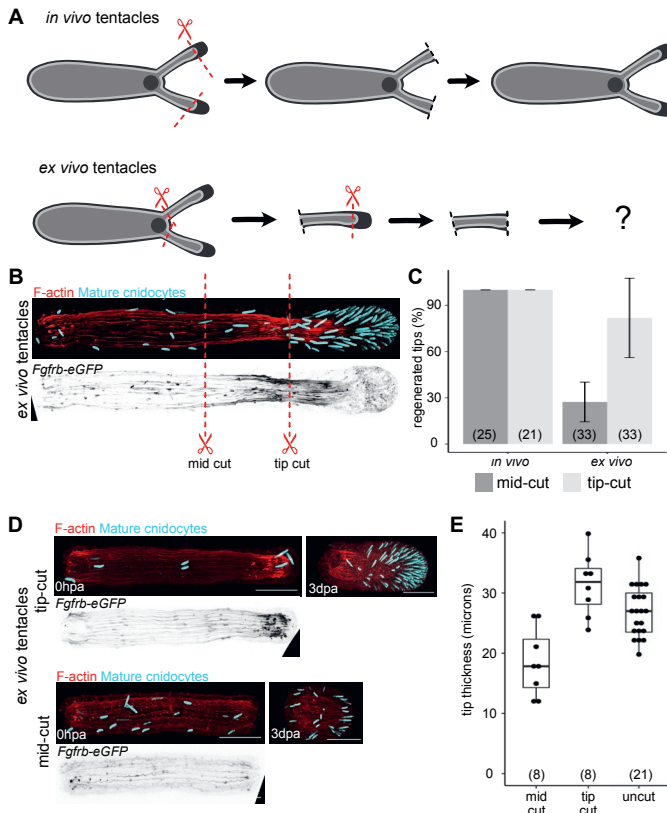


Figure 1. (A) Schematic showing the in vivo (top) and ex vivo (bottom) tentacle tip cut. (B) Maximum projection images of a detached tentacle with the approximate cut sites for “mid cut” and “tip cut” marked. Mature cnidocytes are clearly enriched at the tentacle tip (cyan) and Fgfrb-eGFP cells are enriched in the adjacent tissue (grays). Muscle fibers are visualized via F-actin staining (red). (Scale bar = 100 microns) (C) Bar graph showing the regeneration efficiency of in vivo (left) and ex vivo (right) tentacle tips after mid-cut (dark gray) or tip-cut (light gray) amputation. Sample numbers are given in parentheses. (D) Maximum projection images of ex vivo tentacles after tip-cut (top) or mid-cut (bottom) at 0 hpa (hours post amputation) and 3 dpa (days post amputation). (F-actin = red, mature cnidocytes = cyan, Fgfrb-eGFP = grays; scale bar = 100 microns). (E) Box plot showing the thickness of tentacle tips at 3 dpa following mid-cut (left) and tip-cut (right) amputation. Sample numbers are given in parentheses.

because of its ease of rearing^{10,11}, trackable developmental biology¹²⁻¹⁴, and robust molecular genetic approaches^{1,2}. During development, the oral pole of swimming larvae forms four-tentacle buds that generate the the initial appendages of the primary polyp¹⁵. The patterning of tentacles depends on an endodermal Hox code¹³ and the formation of pseudostratified ectodermal placode¹⁵. To generate the elongated tentacle, this thickened placode undergoes epithelial cell shape and arrangement. While undergoing morphogenesis, tentacle primordia also differentiate different cell types including longitudinal muscles¹⁶, hair cells¹⁷ and cnidocytes^{18,19}. At the primary polyp stage, the development of additional tentacles occurs in a feeding dependent manner, and relies on the interplay between TOR and *Fgfrb* signalling to control polarized cell proliferation that is critical for bud outgrowth²⁰. Such comparative studies in the same cnidarian species revealed that there are distinct morphogenetic trajectories leading to larval and feeding-dependent tentacle development, thus raising the question about which one of these mechanisms is deployed during tentacle regeneration. Furthermore, the regenerative potential of isolated tentacles in an anthozoan species has not been reported.

Here, we sought to elucidate the mechanism of tentacle regeneration in *Nematostella* polyps. To do so, we established an *ex vivo* system to study tentacle regeneration and showed the regenerative potential of an isolated tentacle depends on the location of amputation. Using molecular perturbations for cell proliferation and FGF signaling, we were able to establish that the mechanism of tentacle tip regeneration differs between the detached (*ex vivo*) and attached (*in vivo*) systems. We identify that a resident population of developing cnidocyte cells near the tentacle tip facilitate fast regeneration of the tip structure. Removal of this precursor population leads to slower regeneration due to the need to first re-establish this precursor population in the tentacle tissue. Taken together, we have identified two distinct mechanisms of regeneration for the tentacle tip and demonstrated how localized populations of precursor cells are involved in regeneration in *Nematostella vectensis*.

Results

Tip regeneration in *ex vivo* tentacles, but not *in vivo*, is highly dependent on the location of amputation

To test whether *Nematostella* appendages possess autonomous regenerative capacity, we generated *ex vivo* tentacles by surgically detaching them from the body column, and then challenged their ability to restore missing tip regions (Figure 1). In the tentacle, the tip region has distinct features characterized by a thickened, pseudostratified epidermis and an enrichment of mature cnidocytes (Figure 1b). Thus, we used these two features to score the reestablishment of tentacle polarity as a readout for successful tip regeneration. In primary polyps, amputation of the tentacle tip (*in vivo*) results in rapid regeneration of the structure within 3 days (Figure S1). Surprisingly, while shrinking over time, *ex vivo* tentacles also showed successful tip regeneration in this time frame. However, in contrast to *in vivo* tentacle tip regeneration, the success rate of *ex vivo* tentacle tip regeneration was highly variable from one tentacle to another (Figure S2). To determine the origins of this variability, we hypothesized that the regeneration of *ex vivo* tentacle might be dependent on the location of amputation and/or the size of the remaining tissue.

By taking advantage of the *Fgfrb*-eGFP transgenic line²⁰, we conducted cuts in defined regions along the tentacle. In this reporter line, *Fgfrb*-eGFP showed epidermal expression at

the tip and graded expression in the longitudinal muscles. We used this polarized expression pattern that expands beyond the tip region as a visual landmark to define two amputation sites (tip-cut and mid-cut; Figure 1d). Interestingly, we observed that amputated *ex vivo* tentacles that retained tissue with *strong Fgfrb-eGFP* expression (tip-cut) show a higher regenerative ability than amputated tentacles with tissue displaying low *Fgfrb-eGFP* expression (mid-cut) (Figure 1c). To rule out the effect of tissue size on regeneration, we normalized the length of *ex vivo* tentacles with tip-cut to a similar dimension as the mid-cut conditions (Figure 2). Despite unifying *ex vivo* tentacle lengths, the normalized tip-cut *ex vivo* tentacles still showed a higher success rate of regeneration than the mid-cut condition, but lower than tip-cut tentacles without length adjustment (Figure 2c). This suggests that while having more total tissue improves the success rate of tip regeneration, the spatial identity of the remaining tentacle tissue is also critical.

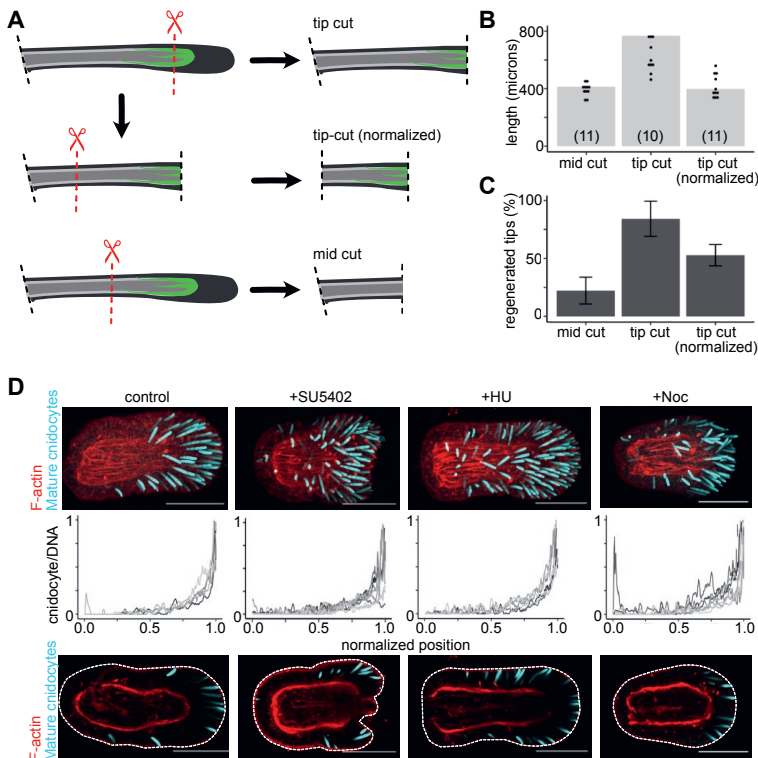


Figure 2. (A) Schematic showing the *ex vivo* tentacle amputation sites in *Fgfrb-eGFP* polyps for tip-cut, tip-cut (normalized), and mid-cut. (B) Bar plots with dot plot overlay showing the length of the tentacle tissue following mid-cut, tip-cut, and tip-cut (normalized) amputation at 0hpa. Sample numbers are given in parentheses. (C) Bar plots showing the regeneration efficiency of *ex vivo* tentacles at 3dpa for each amputation condition. Error bars show ± 1 standard deviation. Sample numbers are given in parentheses. (D) Maximum projection images (top row) of tip-cut *ex vivo* tentacles at 3dpa after treatment with no drug (control), SU5402, hydroxyurea (HU), or Nocodazole (Noc). Line plots (middle row) show the voxels of mature cnidocytes normalized to the voxels of nuclei along the tentacle (tentacle length is normalized to each tentacle; one line represents one tentacle). Image of a single confocal z-slice (bottom row) of the tentacles shown in the top row. Dotted white outline marks the tentacle tissue boundary.

Cell proliferation and FGF signaling are dispensable for tip regeneration in *ex vivo* tentacles

To investigate the mechanisms that underly the regenerative ability of *ex vivo* tentacles, we then sought to dissect the contribution of the Fgfrb-eGFP+ tissue region in tentacle tip regeneration. First, we assessed the role of FGF signaling by treating tentacles with SU5402, a multi-targeted receptor tyrosine kinase inhibitor. Tip regeneration was not inhibited in SU5402-treated *ex vivo* tentacles, as scored by the quantification of mature cnidocyte enrichment and epidermal thickening (Figure 2d and Figure S4). However, regenerated tentacles exhibited a disruption of the epidermis in the middle of the tentacle tip. Such an effect was not observed in uncut *ex vivo* tentacles treated with SU5402 (Figure S5), which suggests that FGF signaling is required to maintain epithelial integrity during regeneration. Second, based on the critical role of proliferative growth in oral regeneration of *Nematostella* polyps²¹, we wondered whether the Fgfrb-eGFP+ tissue region is important for cell proliferation in *ex vivo* tentacles. While an increase in EdU (a marker for s-phase cells) incorporation was observed across the tentacle (Figure S6), inhibition of cell cycle progression using hydroxyurea (HU) surprisingly did not disrupt *ex vivo* tentacle tip regeneration (Figure 2d), suggesting regeneration may be governed by multiple mechanisms in *Nematostella*.

The most well-known example of regeneration proceeding in the absence of cell proliferation is in Hydra, where a population of G2-paused cells residing near the head can undergo direct

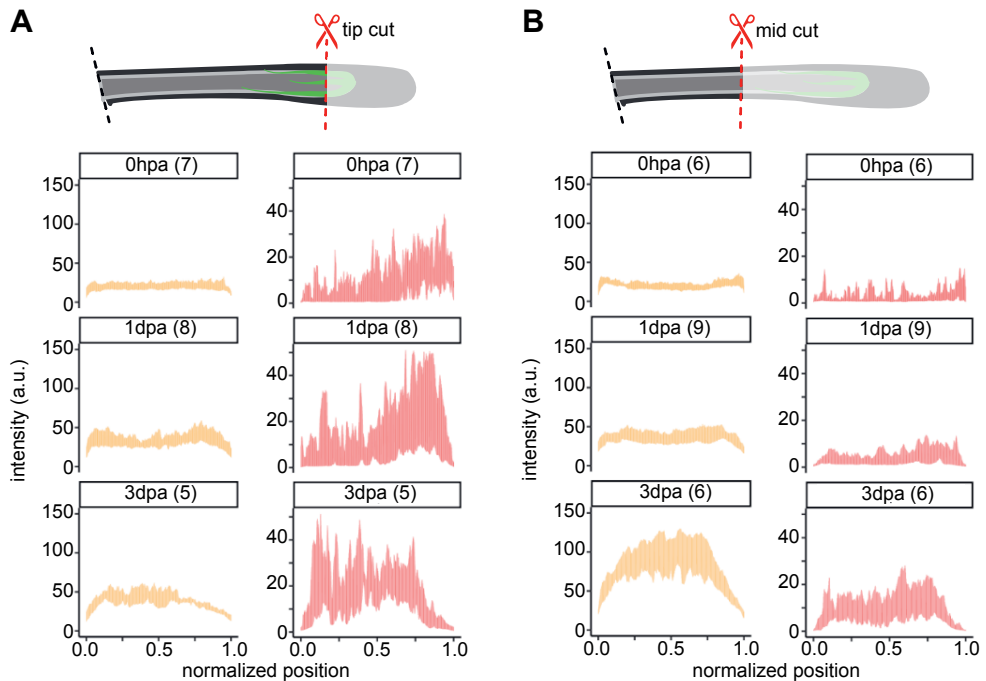


Figure 3. (A) Line plots showing the fluorescent intensity of CyB- eGFP (yellow) and Nv_NCol3 (red) stainings of *ex vivo* tentacles following tip-cut amputation at 0hpa (top), 1dpa (middle), 3dpa (bottom). Sample numbers are given in parentheses. (B) Line plots showing the fluorescent intensity of CyB- eGFP (yellow) and Nv_NCol3 (red) stainings of *ex vivo* tentacles following mid-cut amputation at 0hpa (top), 1dpa (middle), 3dpa (bottom). Sample numbers are given in parentheses.

differentiation to reform the missing tissues^{22,23}. Recently, we generated a transgenic line expressing a CyclinB-GFP (CyB-GFP) fusion reporter (see Chapter 1) that labels cells in the S/G2/M phases of the cell cycle^{24,25}. Combined with estimation of DNA content, we found that many cells near the tentacle tip reside in the G2-phase of the cell cycle (see Chapter 1 Figure 4). Since HU only blocks cell cycle progression through s-phase, we wondered if the G2-cells are the cellular source of tentacle tip regeneration. Strikingly, treatment of *ex vivo* tip-cut tentacles with nocodazole (Noc), which blocks progression through metaphase, also did not prevent tip regeneration (Figure 2d). These results suggest that cnidogenesis and epithelial thickening in *ex vivo* tentacle tip regeneration can take place without cell proliferation.

Spatial heterogeneity of precursor cells accounts for the distinct regenerative responses of tip-cut versus mid-cut *ex vivo* tentacles

The results described above also suggest that G2-cells might directly differentiate to restore tentacle tips without undergoing mitosis. To test this hypothesis, we used an antibody against Nv_NCol3 to detect developing but not fully mature cnidocytes. We identified a distinct population of cycling cells that show this differentiation marker for cnidocyte precursor cells (Nv_NCol3+ cells¹⁹) (Figure 4 in Chapter 1). Because these CyB-eGFP+, Nv_NCol3+ cells were found in approximately the same location as the Fgfrb-eGFP+ tissue region, we wondered if the presence of these precursor cells is critical for tip regeneration in *ex vivo* tentacles.

To assess the role of these precursor cells during regeneration, we performed the tip-cut and mid-cut experiments in *ex vivo* tentacles expressing CyB-eGFP, and stained for GFP and Nv_NCol3 at three different time points after amputation (0hpa, 1dpa, 3dpa). At 0hpa, an enrichment of Nv_NCol3+ cells could be found near the amputation plane of tip-cut tentacles but not mid-cut tentacles (Figure 3 and Figure S8). This population of Nv_NCol3+ cells increased near the tip at 1dpa but receded from the very tip by 3dpa leading to mature cnidocyte formation (Figure 3). In mid-cut tentacles, the number of Nv_NCol3+ cells increased over time but to a lesser extent and showed no spatial enrichment of Nv_NCol3+ signal near the tip (Figure 3). Interestingly, both tip-cut and mid-cut tentacles showed an increase in the number and intensity of CyB-eGFP+ cells over time. Taken together, these results suggest that tentacle tip regeneration requires the generation of a certain number of Nv_NCol3+ cnidocyte precursor cells and their appropriate spatial localization. However, it is still unclear what prevents mid-cut *ex vivo* tentacles from driving the differentiation of Nv_NCol3+ cells in the population of CyB-eGFP+ cells. Since Nv_NCol3+ cells directly develop into the mature cnidocytes enriched in the tentacle tip¹⁹, their presence in the tip-cut *ex vivo* tentacle may explain why cell proliferation is not required for tip regeneration.

FGF signaling is required for tip regeneration in mid-cut *in vivo* tentacles

While mid-cut *ex vivo* tentacles fail to regenerate tentacle tips, *in vivo* tentacles regenerate robustly following a mid-cut amputation (Figure 1c). This suggests that the body column is able to rescue the regeneration deficient mid-cut *ex vivo* tentacles. To determine how tip regeneration proceeds in attached tentacles, we analyzed the dynamics of CyB-eGFP+ and Nv_NCol3+ cells in *in vivo* tentacles after a mid-cut amputation (Figure 4 and Figure S8). Indeed, mid-cut *in vivo* tentacles showed a similar pattern of CyB-eGFP and Nv_NCol3 signal during regeneration. At 0hpa, *in vivo* mid-cut tentacles had very few CyB-eGFP+ or Nv_NCol3+ cells but by 1dpa an enrichment of CyB-eGFP+ cells was detected at the tip. By 5dpa a distinct population of CyB-eGFP+ cells were present near the tip, adjacent to a

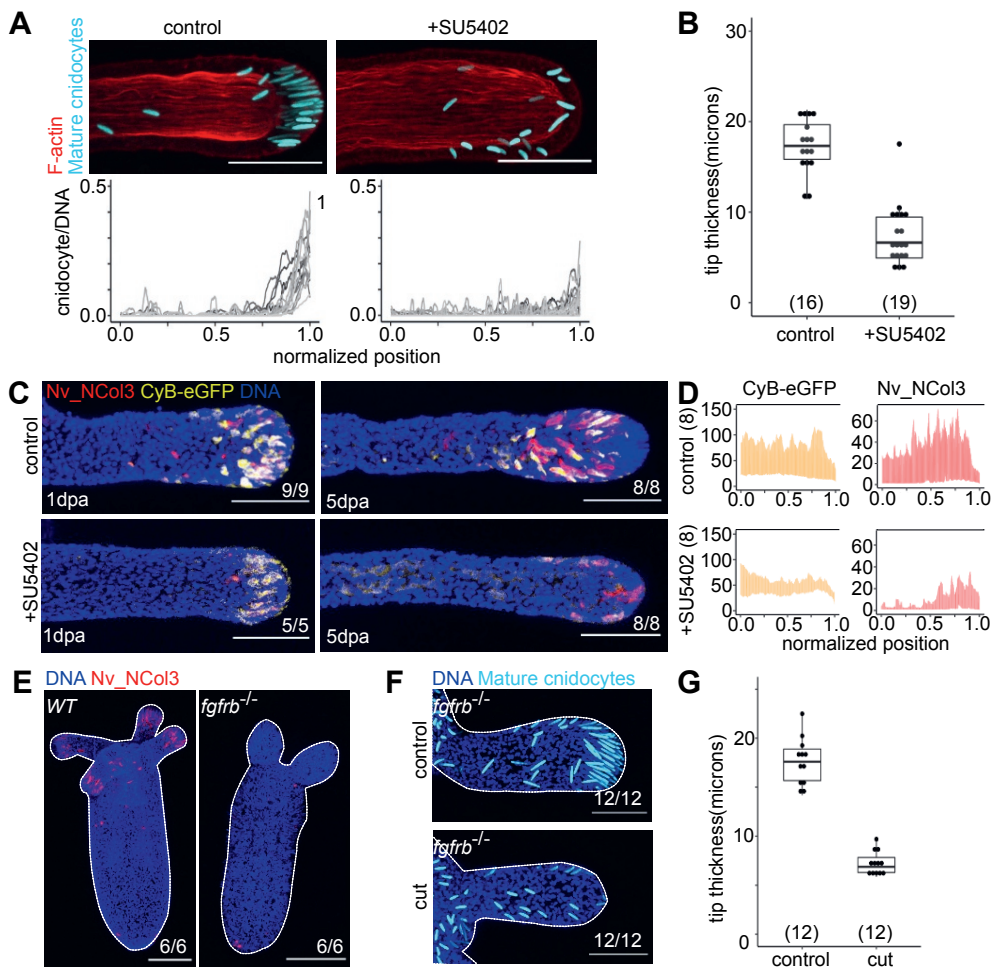


Figure 4 (A) Maximum projection images (top row) of control (left) and SU5402 (right) treated *in vivo* mid-cut tentacles at 5dpa (F-actin = red, mature cnidocytes = cyan; scale bar = 50 microns). Line plots (bottom row) show the voxels of mature cnidocytes normalized to the voxels of nuclei along the tentacle (tentacle length is normalized to each tentacle; one line represents one tentacle). (B) Box plot showing the tip thickness (microns) of *in vivo* mid-cut tentacles at 5dpa (one dot = 1 tentacle). Sample numbers are given in parentheses. (C) Maximum projection images of control (top row) and SU5402 (bottom row) treated *in vivo* mid-cut tentacles at 1dpa and 5dpa (Nv_NCol3 = red, CyB-eGFP = yellow, DNA = blue; scale bar = 50 microns). Number of imaged samples are indicated at the bottom right corner. (D) Line plots showing the fluorescent intensity of CyB-eGFP (yellow) and Nv_NCol3 (red) staining of control (top row) and SU5402 (bottom row) treated *in vivo* mid-cut tentacles at 5dpa. Tentacle lengths are normalized (normalized position 0.0 = tentacle base, 1.0 = tentacle tip). Sample numbers are given in parentheses. (E) Maximum projection images of wild-type (WT; left) and *Fgfrb*^{-/-} mutant (right) polyps (Nv_NCol3 = red, DNA = blue, scale bar = 100 microns). Number of imaged samples are indicated at the bottom right corner. Dotted white outline marks the polyp boundary. (F) Maximum projection images of control (top) and *in vivo* mid-cut tentacles (bottom) at 5dpa of *Fgfrb*^{-/-} polyps (mature cnidocytes = cyan, DNA = blue; scale bar = 50 microns). Number of imaged samples are indicated at the bottom right corner. Dotted white outline marks the tentacle boundary. (G) Box plots with dot plot overlay showing the tentacle tip thickness of control (left) and *in vivo* mid-cut tentacles (right) at 5dpa of *Fgfrb*^{-/-} polyps (each dot represents one tentacle). Sample numbers are given in parentheses.

population of Nv_NCol3+ cells followed by mature cnidocytes (Figure 4c). In contrast to *ex vivo* tentacles, Nv_NCol3+ cells were detected with high intensity and showed polarized localization near the tentacle tip. It is important to note that while *in vivo* tentacles required 5 days to fully regenerate the tentacle tip, *ex vivo* tentacles still did not regenerate at 5dpa (Figure S9).

To test the role of FGF signaling in tentacle tip regeneration, we treated polyps with SU5402 following mid-cut amputation. In stark contrast to *ex vivo* tip-cut tentacles, which were not affected by the inhibition of FGF signaling, the tentacle tips failed to regenerate in this *in vivo* condition (Figure 4a-b). When we checked the effect of FGF inhibition on formation of CyB-eGFP+ and Nv_NCol3+ cells, we found that CyB-eGFP+ cells arose at 1dpa at a similar pattern as controls, but very few Nv_NCol3+ cells were detected at 5dpa (Figure 4c-d). This suggests that the differentiation of Nv_NCol3+ cells requires FGF signaling. Intriguingly, the number of CyB-eGFP+ cells observed at 5dpa were also fewer than that observed in *ex vivo* mid-cut tentacles at 3dpa. To confirm the role of FGF signaling in cnidocyte precursor cell formation, we analyzed the pattern of Nv_NCol3+ cells in *Fgfrb*^{-/-} knockout animals. We found that *Fgfrb*^{-/-} primary polyps had almost no Nv_NCol3+ cells, despite showing mature cnidocytes (Figure 4e). This is in contrast to wild-type polyps where Nv_NCol3+ cells are found scattered throughout the body and highly enriched near the tentacle tips. The tentacle structure of *Fgfrb*^{-/-} polyps are also shorter and rounder than wild-type polyps. Consistent with the results of the pharmacological inhibition experiment, *Fgfrb*^{-/-} animals were not capable of tentacle tip regeneration (Figure 4f-g). Taken together, these findings suggest that FGFRb signaling is required for the renewal of Nv_NCol3+ cnidocyte precursor cells.

Discussion

By investigating tentacle tip regeneration via both an *in vivo* and *ex vivo* tentacle context, we were able to reveal two distinct mechanisms of tentacle tip regeneration in *Nematostella* polyps. A primed population of precursor cells present near the tip of the tentacle can directly differentiate into mature cnidocytes, providing a fast regenerative response to injury at the tip. Removal of this precursor cell population results in a slower regenerative response whereby body column tissue and FGF signaling are required to drive development of this precursor cell population. In its natural habitat, *Nematostella* polyps bury their bodies into the sand/mud and expose their tentacles to the environment to defend against predators and capture prey²⁶. Thus, the presence of a fast regenerative mechanism for the tentacle tip likely facilitates the high cell turnover of this tissue during homeostasis.

Interestingly, such a localized distribution of precursor cells next to the tentacle tip is not found in other Cnidarian species such as *Hydra* and *Clytia hemisphaerica*. Although *Hydra* tentacles share a similar morphology to *Nematostella* tentacles, cnidocyte precursor cells generated in the body column of *Hydra* migrate to the head region where it then undergoes maturation before migrating into the tentacle tissue²⁷⁻³¹. In *Clytia*, cnidocyte precursors proliferate and differentiate at the tentacle base structure (tentacle bulb) before migrating to the tip³². Since both *Hydra* and *Clytia* belong to the Hydrozoan branch of Cnidaria, while *Nematostella* belongs to the Anthozoan clade, it seems that there may be different mechanisms employed by the two sister groups to replenish tentacle tip cells. Further studies into other cnidarian species will be necessary for a more complete comparison.

Another key finding in our study is the role of FGF signaling in the formation of Nv_

NCoI3+ cnidocyte precursor cells. FGF signaling is required for the correct localization and differentiation of CyB-eGFP+ cells into Nv_NCoI3+ cells in mid-cut *in vivo* tentacles, suggesting that FGF signaling has a role both in development of Nv_NCoI3+ cells and determining their spatial organization. While the role of FGF signaling has been implicated in neurogenesis during *Nematostella* development^{33,34}, the function of FGF signaling in cnidogenesis has not been reported before. In Hydrozoans, cnidocyte differentiation has been associated with Wnt/B-catenin signaling^{32,35,36}. Our work also showed that the requirement of *Fgfrb* signalling is context-dependent during regeneration. While this developmental signalling is dispensable for tip-cut regeneration, it is required along with cell proliferation when a large portion of the tentacle tissue is removed. Interestingly, this situation mimics the mechanisms underlying the feeding-dependent tentacle development²⁰. In contrast, embryonic tentacle development takes place in the *Fgfrb*^{-/-} mutant background. Building on this comparative analysis, we propose that *de novo* tentacle morphogenesis in the polyp stage relies on a common mechanism involving *Fgfrb* signalling and cell proliferation.

In conclusion, by targeting a small and simple structure as a model for regeneration, we were able to dissect the relative contributions of different body regions and cell populations to achieving successful regeneration. The *ex vivo* tentacle system we established can serve as a novel reduced system in which to study regeneration. The relatively small size and simple morphology of the *ex vivo* tentacle would allow for live cell tracking studies to elucidate the potential contributions of cell migration and tissue rearrangement in tentacle tip regeneration. Establishment of such reduced systems in other regenerative species may also provide novel insight into the mechanism of complex structure regeneration.

Materials and Methods

Animal husbandry and tentacle amputation

N. vectensis animals were grown in 12ppt artificial seawater (Sea Salt, Instant Ocean) and adult animals were spawned as described previously³⁷. Fertilized embryos were grown at 23C until the primary polyp stage. The polyps were then fed with *Artemia* nauplii for 4 days at 27C, followed by a starvation period of 4 days at 27C. Immediately prior to amputation, polyps were immobilized with 7% MgCl₂ (Merck, 1.05833.1000) in 12ppt ASW. For the detached tentacle regeneration experiments, tentacles were first cut at the base of the tentacle with a tungsten needle (Ted Pella, Inc. 13570-10). The detached tentacles were then cut at either the tentacle tip or mid-tentacle. The MgCl₂ solution was immediately removed after amputation and the regenerating tissue was washed twice with 12ppt ASW and then kept at 23C. For the attached tentacle experiments, polyps are first bisected at the base of the pharynx using an ophthalmic scalpel (Micro Feather No.780). Then a mid-tentacle cut was done on the 4 primary tentacles. Glass petri dishes were used for detached tentacle cutting experiments, while plastic petri dishes were used for attached tentacle experiments.

Transgenic animals

The cell cycle reporter line, *CyclinB(1-100)-eGFP*, was generated using the I-SceI meganuclease system as described before³⁸. The DNA sequence corresponding to the first 100 amino acids of the *Nv_CyclinB* gene was fused directly to eGFP with a SV40 polyA sequence. Expression was driven by the *Nv_EF1* promoter sequence. Cloning of the

transgene into the transgenesis plasmid was done using the NEBuilder HiFi DNA assembly kit (NEB, E2621). Fertilized embryos were injected with the transgenesis plasmid and I-SceI enzyme at the one-cell stage. F1 transgenic animals were selected based on their GFP fluorescence. F2 polyps were used for regeneration experiments. GFP signal was visualized via immunohistochemistry using the anti-eGFP antibody (Torry Pines TP401).

Embryos from the *Fgfrb-eGFP* reporter line were first crossed with *Fgfrb^{+/+}* embryos to yield *Fgfrb^{+/+}Fgfrb-eGFP* animals. Embryos from these double mutants were crossed to generate *Fgfrb^{-/-}Fgfrb-eGFP* polyps. Homozygous *Fgfrb* knockout polyps were selected based on their short and rounded tentacle morphology. Full details on the generation of both mutant lines have been reported previously²⁰.

Immunohistochemistry and staining

Animals were fixed and stained using a modified protocol adapted from Genikhovich and Technau¹¹. Briefly, samples were fixed in a solution of 4% paraformaldehyde (PFA; Electron Microscopy Sciences E15710) in Ptw (1x PBS, 0.1% tween-20) for 1 hour at room temperature before being permeabilized with 10%DMSO in PBS for 20min followed by Ptx0.5 (1X PBS, 0.5% TritonX-100) for 20min. Then they were incubated in blocking buffer (5% normal goat serum, 1% BSA, 1% DMSO, 0.1% tritonX-100 in 1X PBS) for 1 hour at room temperature before incubating with primary antibodies (anti-eGFP 1:500, Torry Pines TP401; anti-mini collagen3 1:400, gift from Dr. Suat Ozbek¹⁹) overnight at 4C. Samples were then washed 3 times with cnidocyte wash buffer (10mM TrisHCl pH 7.7, 10mM EDTA, 0.1% tween20) before incubating with secondary antibodies (goat anti-rabbit alexa488, 1:500, Thermo Fisher A-11008; goat anti-guineapig alexa647 1:1000, Thermo Fisher A-21450) and DNA stain (DAPI 1:1000 Sigma Aldrich D9542). EDTA (10mM final concentration) and DAPI (3:1000) were added to the sample and incubated for 30min at room temperature to stain the mature cnidocyte capsules. Samples were then washed with cnidocyte wash buffer 3 times and mounted into 85% glycerol or Vectashield Plus (Vector via Biozol VEC-H-1900-10) for imaging.

Fgfrb-eGFP animals were fixed with 4% PFA in Ptw for 30min at room temperature then washed 3 times with cnidocyte wash buffer before incubating with phalloidin-alexa647 (1:100; Thermo Fisher A22287) and DAPI (1:50) in cnidocyte wash buffer overnight at 4C. Samples were then washed with cnidocyte wash buffer 3 times and mounted into Vectashield Plus mounting medium.

Imaging and image analysis

Confocal stacks were acquired on a Leica TCS SP8 confocal microscope using a 63x 1.4NA objective for the detached tentacle samples and 40x 1.1NA objective for the attached tentacle samples. Image analysis was performed using FIJI (<https://imagej.net/software/fiji/>)³⁹. Data here as well as below were plotted using ggplot2⁴⁰.

Detached tentacle images and zoomed-in images of attached tentacles were straightened using the straighten function. Quantification of the ratio of mature cnidocyte to DNA signal was done using a FIJI jython script. Briefly, a segmented line is manually drawn to span the length of the tentacle of interest from the tip to the base. The pixel volume containing mature cnidocyte staining is summed across the tentacle. The same is done for DNA staining. The ratio is then calculated by dividing the mature cnidocyte voxel value by the DNA voxel value

for each voxel across the tentacle. Length of each tentacle is then normalized to 1.

EdU staining and drug treatments

Staining with EdU was done as described previously²⁰. Briefly, animals were incubated with 50 μ M EdU in 12ppt ASW for 30 minutes before immobilizing with 7% MgCl₂ solution. Animals were then fixed with 4% PFA in PTw. For drug treatments, samples were incubated with 20mM hydroxyurea (Sigma Aldrich H8627) or 20 μ M SU5402 (Sigma Aldrich SML0443-5MG) in 12ppt ASW within 1h after amputation. Drug solutions were refreshed once a day.

References

1. Karabulut, A., He, S., Chen, C. Y., McKinney, S. A. & Gibson, M. C. Electroporation of short hairpin RNAs for rapid and efficient gene knockdown in the starlet sea anemone, *Nematostella vectensis*. *Dev. Biol.* **448**, 7–15 (2019).
2. Ikmi, A., McKinney, S. A., Delventhal, K. M. & Gibson, M. C. TALEN and CRISPR/Cas9-mediated genome editing in the early-branching metazoan *Nematostella vectensis*. *Nat. Commun.* **5**, 1–8 (2014).
3. Lesh-Laurie, G. E., Hujer, A. & Suchy, P. Polyp regeneration from isolated tentacles of *Aurelia scyphistomae*: a role for gating mechanisms and cell division. *Hydrobiologia* **216–217**, 91–97 (1991).
4. Laurie-Lesh, G. & Corriel, R. Scyphistoma Regeneration From Isolated Tentacles in *Aurelia Aurita*. *J. Mar. Biol. Assoc. United Kingdom* **53**, 885–894 (1973).
5. Fujita, S., Kuranaga, E. & Nakajima, Y. Regeneration potential of jellyfish: Cellular mechanisms and molecular insights. *Genes (Basel)*. **12**, (2021).
6. Fujita, S., Kuranaga, E. & Nakajima, Y. I. Cell proliferation controls body size growth, tentacle morphogenesis, and regeneration in hydrozoan jellyfish *Cladonema pacificum*. *PeerJ* **2019**, 1–20 (2019).
7. Dübel, S. Cell differentiation in the head of *Hydra*. *Differentiation* **41**, 99–109 (1989).
8. Amiel, A. R. *et al.* Characterization of morphological and cellular events underlying oral regeneration in the sea anemone, *Nematostella vectensis*. *Int. J. Mol. Sci.* **16**, 28449–28471 (2015).
9. Dubuc, T. Q., Traylor-knowles, N. & Martindale, M. Q. Initiating a regenerative response ; cellular and molecular features of wound healing in the cnidarian *Nematostella vectensis* Initiating a regenerative response ; cellular and molecular features of wound healing in the cnidarian *Nematostella vectensis*. **12**, 1–20 (2014).
10. Hand, C. & Uhlinger, K. R. The Culture, Sexual and Asexual Reproduction, and Growth of the Sea Anemone *Nematostella vectensis*. *Biol. Bull.* **182**, 169–176 (1992).
11. Genikhovich, G. & Technau, U. Induction of spawning in the starlet sea anemone *Nematostella vectensis*, in vitro fertilization of gametes, and dejellying of zygotes. *Cold Spring Harb. Protoc.* **4**, 1–4 (2009).
12. Leclère, L., Bause, M., Sinigaglia, C., Steger, J. & Rentzsch, F. Development of the aboral domain in *Nematostella* requires β -catenin and the opposing activities of *Six3/6* and *Friz/led5/8*. *Development* **143**, 1766–1777 (2016).
13. He, S. *et al.* An axial Hox code controls tissue segmentation and body patterning in *Nematostella vectensis*. *Science (80-.)*. **361**, 1377–1380 (2018).
14. Warner, J. F. *et al.* NvERTx: A gene expression database to compare embryogenesis and regeneration in the sea anemone *Nematostella vectensis*. *Development* **145**, (2018).
15. Fritz, A. E., Ikmi, A., Seidel, C., Paulson, A. & Gibson, M. C. Mechanisms of tentacle morphogenesis in the sea anemone *Nematostella vectensis*. *Dev.* **140**, 2212–2223 (2013).
16. Jähnel, S. M., Walzl, M. & Technau, U. Development and epithelial organisation of muscle cells in the sea anemone *Nematostella vectensis*. *Front. Zool.* **11**, 1–15 (2014).

17. Ozment, E. *et al.* Cnidarian hair cell development illuminates an ancient role for the class IV POU transcription factor in defining mechanoreceptor identity. *Elife* **10**, 1–34 (2021).
18. Babonis, L. S. & Martindale, M. Q. PaxA, but not PaxC, is required for cnidocyte development in the sea anemone *Nematostella vectensis*. *Evodevo* **8**, 1–20 (2017).
19. Zenkert, C., Takahashi, T., Diesner, M. O. & Özbek, S. Morphological and molecular analysis of the *Nematostella vectensis* cnidom. *PLoS One* **6**, (2011).
20. Ikmi, A. *et al.* Feeding-dependent tentacle development in the sea anemone *Nematostella vectensis*. *Nat. Commun.* **11**, 1–13 (2020).
21. Passamanek, Y. J. & Martindale, M. Q. Cell proliferation is necessary for the regeneration of oral structures in the anthozoan cnidarian *Nematostella vectensis*. *BMC Dev. Biol.* **12**, (2012).
22. Buzgariu, W., Crescenzi, M. & Galliot, B. Robust G2 pausing of adult stem cells in Hydra. *Differentiation* **87**, 83–99 (2014).
23. Buzgariu, W., Wenger, Y., Tcaciuc, N., Catunda-Lemos, A. P. & Galliot, B. Impact of cycling cells and cell cycle regulation on Hydra regeneration. *Dev. Biol.* **433**, 240–253 (2018).
24. Klochender, A. *et al.* A Transgenic Mouse Marking Live Replicating Cells Reveals In Vivo Transcriptional Program of Proliferation. *Dev. Cell* **23**, 681–690 (2012).
25. King, R. W., Jackson, P. K. & Kirschner, M. W. Mitosis in Transition Review. *Cell* **79**, 563–571 (1994).
26. Stefanik, D. J., Friedman, L. E. & Finnerty, J. R. Collecting, rearing, spawning and inducing regeneration of the starlet sea anemone, *Nematostella vectensis*. *Nat. Protoc.* **8**, 916–923 (2013).
27. Bode, H. R. & Flick, K. M. Distribution and dynamics of nematocyte populations in Hydra attenuata. *J. Cell Sci.* **21**, 15–34 (1976).
28. Broun, M. & Bode, H. R. Characterization of the head organizer in hydra. *Development* **129**, 875–884 (2002).
29. David, C. N. & Challoner, D. Distribution of interstitial cells and differentiating nematocytes in nests in Hydra attenuata. *Integr. Comp. Biol.* **14**, 537–542 (1974).
30. Engel, U. *et al.* A switch in disulfide linkage during minicollagen assembly in hydra nematocysts. *EMBO J.* **20**, 3063–3073 (2001).
31. David, C. N. & Gierer, A. Cell cycle kinetics and development of Hydra attenuata. III. Nerve and nematocyte differentiation. *J. Cell Sci.* **16**, 359–375 (1974).
32. Denker, E., Manuel, M., Leclère, L., Le Guyader, H. & Rabet, N. Ordered progression of nematogenesis from stem cells through differentiation stages in the tentacle bulb of *Clytia hemisphaerica* (Hydrozoa, Cnidaria). *Dev. Biol.* **315**, 99–113 (2008).
33. Matus, D. Q., Thomsen, G. H. & Martindale, M. Q. FGF signaling in gastrulation and neural development in *Nematostella vectensis*, an anthozoan cnidarian. *Dev Genes Evol* **217**, 139–148 (2007).
34. Layden, M. J. *et al.* MAPK signaling is necessary for neurogenesis in *Nematostella vectensis*. *BMC Biol.* **14**, 1–19 (2016).
35. Hobmayer, B. *et al.* WNT signalling molecules act in axis formation in the diploblastic metazoan Hydra. *Nature* **407**, 186–189 (2000).
36. Plickert, G., Frank, U. & Müller, W. A. Hydractinia, a pioneering model for stem cell biology and reprogramming somatic cells to pluripotency. *Int. J. Dev. Biol.* **56**, 519–534 (2012).
37. Fritzenwanker, J. H. & Technau, U. Induction of gametogenesis in the basal cnidarian *Nematostella vectensis* (Anthozoa). *Dev. Genes Evol.* **212**, 99–103 (2002).
38. Renfer, E., Amon-Hassenzahl, A., Steinmetz, P. R. H. & Technau, U. A muscle-specific transgenic reporter line of the sea anemone, *Nematostella vectensis*. *Proc. Natl. Acad. Sci. U. S. A.* **107**, 104–108 (2010).
39. Schneider, C. A., Rasband, W. S. & Eliceiri, K. W. NIH Image to ImageJ: 25 years of image analysis. *Nat. Methods* **9**, 671–675 (2012).
40. Wickham, H. *ggplot2: Elegant Graphics for Data Analysis*. (Springer-Verlag New York, 2016).

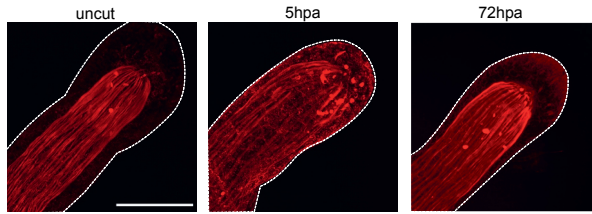


Figure S1. Maximum projection images of F-actin staining of in vivo tentacle tip regeneration in uncut samples (left), 5hpa (hours post amputation) (middle), and 72hpa (right). The tentacles are outlined using a white dotted line (scale bar = 50 microns, same scale for all images)

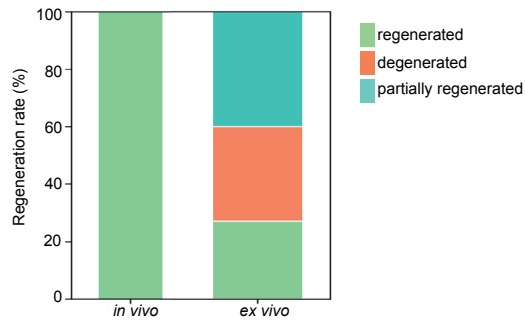


Figure S2. Stacked bar plot showing the regeneration efficiencies of in vivo (left) versus ex vivo (right) tentacle tip regeneration at 3dpa when cut sites were not standardized. (green = regenerated, red = degenerated, blue = partial regeneration).

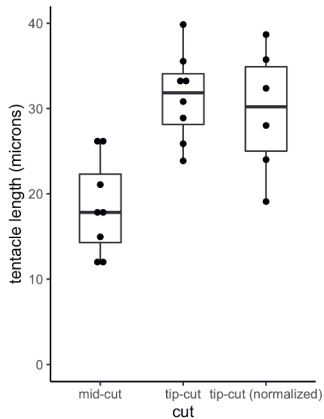


Figure S3. Ex vivo tip-cut tentacles normalized to the mid-cut tentacle length regenerates more robustly than mid-cut tentacles.

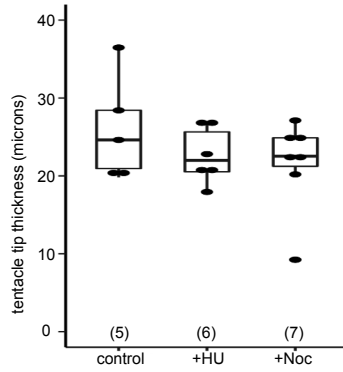


Figure S4. Box plot showing the thickness of tip-cut ex vivo tentacle tips at 3dpa in control samples, and samples treated with Hydroxyurea (HU) or nocodazole (Noc). Sample numbers are given in parentheses.

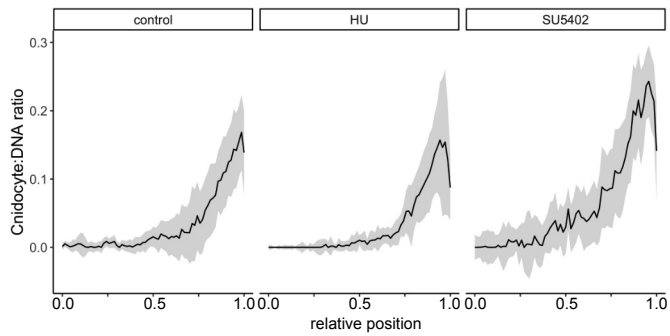


Figure S5. Treatment of uncut in vivo tentacle tips with HU and SU5402 does not affect spatial distribution of mature cnidocytes along the tentacle

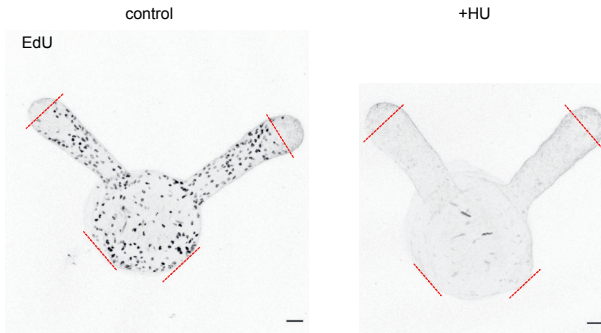


Figure S6. Maximum projection images of EdU staining of regenerating polyps at 24hpa (Grays = EdU, invert LUT; scale bar = 20 microns). Two tentacle tips were amputated, while the other two tentacles were cut at the tentacle base (red dotted lines mark the approximate cut sites for each tentacle).

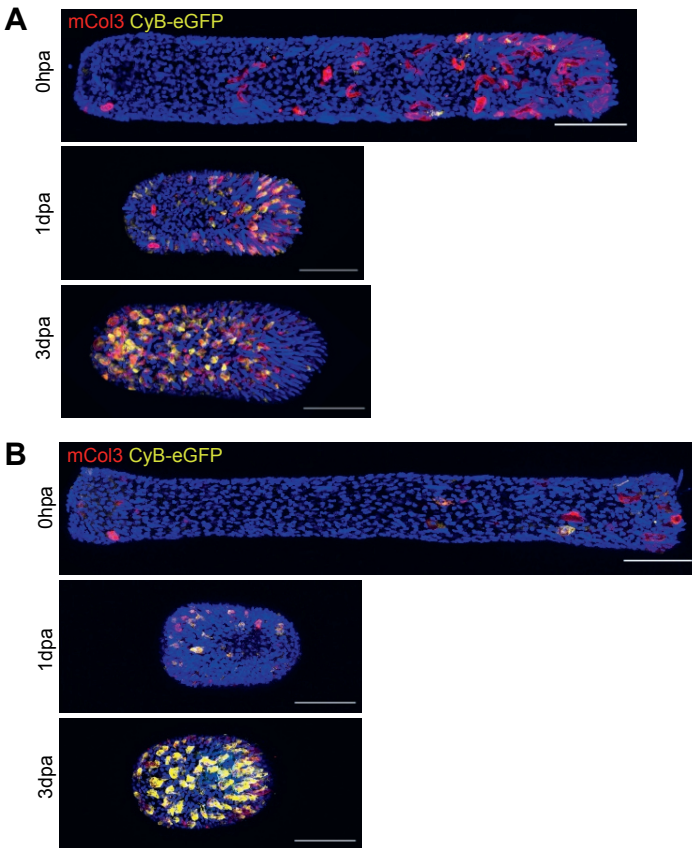


Figure S7. (A) Maximum projection images of ex vivo tip-cut tentacles of Cyb-eGFP polyps at 0hpa, 1dpa, and 3dpa (Nv-NCol3 = red, CyB-eGFP = yellow, DNA = blue; scale bar = 50 microns). (B) Maximum projection images of ex vivo mid-cut tentacles of Cyb-eGFP polyps at 0hpa, 1dpa, and 3dpa (Nv-NCol3 = red, CyB-eGFP = yellow, DNA = blue; scale bar = 50 microns).

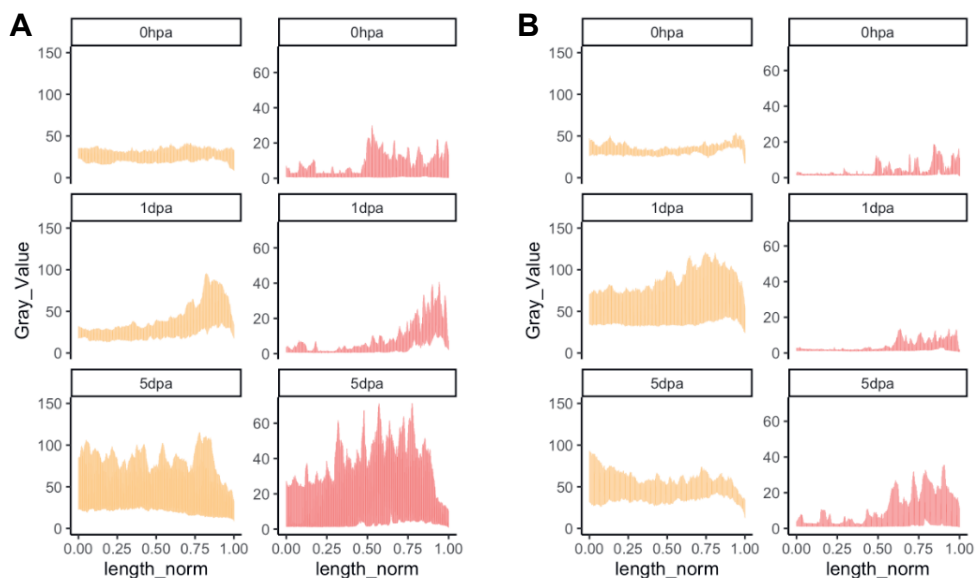


Figure S8. Tentacles treated with SU5402 show lower Cyb-eGFP and mCol3 intensities during regeneration. Intensity quantification of CyB-eGFP and mCol3 signal in amputated in vivo tentacles at 0hpa, 1dpa, and 5dpa. (A) Control samples (B) Samples treated with SU5402

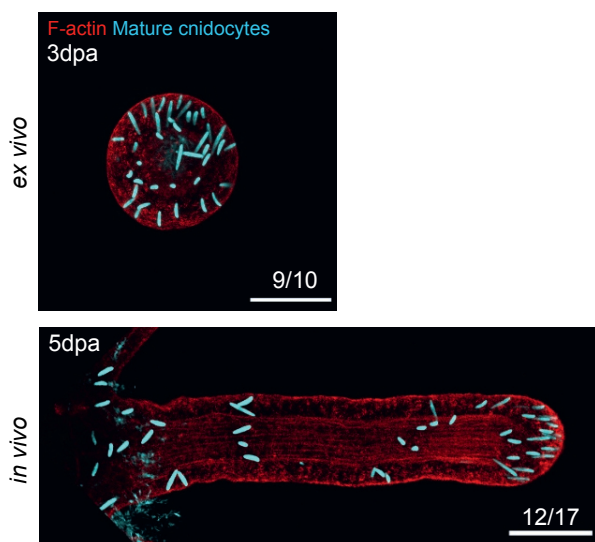


Figure S9. Maximum projection images of ex vivo (top) and in vivo (bottom) mid-cut tentacles at 5dpa and 3dpa respectively (F-actin = red, mature cnidocytes = cyan; scale bar = 50 microns). Number of tentacles imaged is indicated in the bottom right corner.



5

“When I think of formal scientific method an image comes to mind of an enormous juggernaut, a huge bulldozer - slow, tedious, lumbering, laborious, but invincible.”

- Robert M. Pirsig, *Zen and the Art of Motorcycle Maintenance*, p.129

Chapter 5

General Discussion

Stephanie Cheung

The results in this thesis aimed to investigate the mechanisms governing regeneration by taking an organism-level approach. We utilized a relatively new model organism, *Nematostella vectensis*, for our studies owing to its small size, simple body plan, complexity of cell types, and range of genetic tools available^{1,2}. By combining modern spatial transcriptomics and bioinformatics methods with traditional molecular biology techniques, we were able to discover new modalities involved in regeneration of this sea anemone. In this chapter I will summarize some of the major findings from my PhD work and discuss its implications for future research.

The first spatial transcriptomic atlas of *Nematostella* polyps

The explosion of transcriptomic studies in the last two decades has provided invaluable insight into a plethora of biological systems. However, since these methods rely on the mastication of tissues or dissociation of cells, information on the spatial gene expression patterns of the tissue/organism are lost. To understand how cells communicate across tissues and relay information such as wounding, the ability to capture the spatial context of gene expression changes is essential. Recently, a number of spatial transcriptomic methods capable of capturing gene expression changes on the whole transcriptome level while preserving their spatial context have become available³. One of the first methods developed is tomography RNA-sequencing (tomo-seq), which combines low-input RNA-sequencing with cyrosectioning to generate spatially resolved transcriptome maps along a single axis⁴. In **Chapter 2**, we utilize this method to generate the first organism-wide transcriptomic atlas of homeostatic *Nematostella* polyps. By capturing the expression profiles of the whole transcriptome along the major (oral-aboral) body axis, we identified almost 300 gene markers corresponding to various anatomical regions across the polyp. We clustered these genes into 8 major clusters and validated their expression patterns via *in situ* HCR. We further explore one of these gene clusters, the tentacle tip cluster, to investigate if these regional marker genes provide insight into the biological function of those tissues. We combine the spatial transcriptomic information from our tomo-seq dataset with single cell RNA sequencing (scRNA-seq) to determine the relative cell type composition of the tentacle tip tissue. By combining both spatial and single-cell transcriptomic methods, we were able to determine that the tentacle tip is enriched in a cluster of actively differentiating stinging cells (cnidocytes). This investigation into the tentacle tip cluster is only one example of how the information from our transcriptomic atlas can be utilized to explore new biology in *Nematostella* polyps.

Investigating regeneration across time and space

Having established the transcriptomic landscape of homeostatic polyps, we then turned to investigate how gene expression patterns change during foot regeneration. The wound site is often the focus of regeneration studies because that is the location in which new tissues arise and undergo patterning to reform the missing structure. However, recent studies in salamanders have shown that wound-like changes can also occur in non-wound locations such as the uninjured contralateral limb upon limb amputation^{5,6}. Furthermore, the effect of systemic factors such as insulin signaling and thyroid function has also been shown to have a significant effect on the regenerative ability of animals^{7,8}. These observations inspired us to take an organism-level approach to studying regeneration and thus we performed tomo-seq on foot regenerating polyps at four different time points (12, 24, 48, 96 hours post amputation) spanning the entire time course of regeneration (**Chapter 3**).

We first identified genes showing wound-localized expression at 12 hours post amputation (hpa) and compared their expression pattern in uncut polyps. By doing so, we were able to cluster these wound-localized genes into 4 distinct classes defined by their expression pattern in uncut polyps. It is interesting to be able to determine the expression pattern of wound-localized genes in uncut polyps because such information may shed light into the function of these genes during homeostasis. It also opens up new questions about whether the function of these genes change upon injury and how such a change may be regulated. For example, we

found two heat shock proteins (HSP90B1 and HSPA5) showing wound-localized expression at 12hpa have enriched expression in the tentacles during homeostasis. To investigate whether these heat shock proteins serve a stress sensing role, we looked at how their expression is affected after heat shock treatment. Interestingly, we saw that polyps at 12 hours after heat shock showed a polarized upregulation of these two heat shock proteins with the highest expression found in the tentacle region. Since these heat shock proteins are usually enriched at the wound location at 12hpa, it is interesting that the tentacles seem to be responding like a wound after heat shock treatment. This prompts us to investigate if the tentacle region shows any other similar responses to the wound-site upon injury. Strikingly, we found that both foot amputation and heat shock treatment cause an upregulation of cell proliferation at the tentacle region. These results led us to speculate whether the tentacle tissues are “primed” for regeneration and whether a global stress such as heat shock is sufficient to activate wounding signals in *Nematostella*. Considering the fact that the tentacles are naturally under constant battery from the environment during its function in defense and prey capture, it seemed possible to imagine that this tissue is in a constant state of repair or regeneration. However, more molecular studies into the function of these wound-localized genes during homeostasis will be needed to better understand if this is indeed the case.

Next, we exploited our spatial transcriptomic atlas to investigate if there were any non-wound localized changes resulting from foot amputation. Interestingly, we found over 4600 genes differentially expressed (<1% FDR) in the different anatomical regions at each time point during regeneration. When we isolated the most significantly up-regulated genes that were differentially expressed only within a single anatomical region, we found that the tentacles showed up-regulation of “wound-like” genes involved in the inflammation response, stress sensing, and polarity establishment. This was very unexpected because the tentacles are the spatially most distant tissue from the wound site. These results reveal that local wounds are able to initiate long-range communication across the body and induce vast changes in gene expression across the entire animal. Whether these transcriptional changes have a direct role in regeneration or if they resulted from a secondary effect will require further investigation.

While we have demonstrated that heat shock treatment is able to elicit similar changes as foot amputation in gene expression of two heat shock proteins and cell proliferation, it is unclear if these are isolated effects or if temperature stress is able to induce other wound signals. One of the most spectacular functions of wound signals in *Nematostella* is regeneration initiation. Thus, to test if heat shock treatment is able to elicit other wound signals, we challenged the ability of such a global stress to activate regenerative programs in *Nematostella* polyps arrested during head regeneration. Strikingly, we found that heat shock treatment was sufficient to induce regeneration in *Nematostella* polyps. This is the first example to our knowledge where regeneration was initiated in the absence of wounding.

Wounding is the first step to regeneration. This has been the paradigm in the field of regeneration since its inception. Recently, it was shown that injury induces generic wound signals that are able to initiate regeneration in a tissue permissive context⁹. Using MAPK inhibitors, Owlarn *et al* was able to arrest *Planaria* and *Zebrafish* regeneration after wound healing. Induction of a secondary incision at the original wound site was sufficient to induce full regeneration of the missing structures. Now we have shown that heat shock treatment is also sufficient to induce regeneration in dormant *Nematostella* polyps, suggesting that the

wound signals required for regeneration initiation could be generated by exposure to other environmental stresses. It would be important to determine if this response is a conserved phenomenon among other regenerative species. If so, this result will surely challenge us to think about regeneration in a brand-new light.

Dissecting local and systemic contributions to appendage regeneration

In **Chapter 4**, we take a more direct approach to studying how different areas of the body may contribute to regeneration. By studying tentacle tip regeneration in detached tentacles as well as whole polyps, we showed that tentacle tip regeneration can proceed via two distinct mechanisms: 1) a fast response driven by the presence of an enriched cluster of developing cnidocyte cells near the tip, and 2) a slower response dependent on FGF signaling. By physically removing the tentacle from the body, we were able to generate a reduced system in which to study tip regeneration. Combined with the use of transgenic lines marking *Fgfrb* expression and cell cycle progression, we were able to identify a population of developing cnidocyte cells present near the tip that directly contributed to the regrowth of the tentacle tip. When these precursor cells were removed, regeneration required input from the rest of the body in order to reform these precursor cells. Interestingly, we found that these precursor cnidocyte cells were undergoing differentiation during the cell cycle (late G1 to early G2). This was an unexpected finding because terminal cell differentiation usually occurs after cell cycle exit¹⁰. Further work into defining the molecular and transcriptional signatures of these differentiating cnidocyte precursors would be needed to better understand how differentiation of these cells are regulated in *Nematostella* and how cell cycle progression may be linked to differentiation programs. Furthermore, it would be interesting to investigate why generation of these precursor cells requires input from the polyp body. Can we identify the molecular or cellular components the body contributes to the formation of these cells?

Concluding remarks

Taken as a whole, the work in this thesis has demonstrated the value of taking an organism-level approach to studying regeneration. Indeed, regeneration of a body structure is not an isolated event at the wound but rather a highly orchestrated phenomenon involving the whole animal. With the recent and ongoing advances in imaging technology and sequencing methods, the monitoring of whole-organisms throughout the time course of regeneration is no longer an impossible dream. As these methods approach molecular resolution, we will no doubt be able to unravel the mysteries of biology at ever greater precision. In my PhD work, I have utilized some of these modern technological advances to generate two datasets of spatial transcriptomic atlases of regenerating *Nematostella* polyps. We have only begun to scratch the surface of the biological insights that can be gleaned from this data. I hope these will serve as valuable resources for future investigations to understanding regeneration as well as other fundamental processes such as cellular communication. Furthermore, I hope our results will inspire others to consider applying such an organism-level approach to their field of study.

References

1. Genikhovich, G. & Technau, U. The starlet sea anemone *Nematostella vectensis*: An anthozoan model organism for studies in Comparative genomics and functional evolutionary developmental biology. *Cold Spring Harb. Protoc.* **4**, 1–10 (2009).
2. Sebé-Pedrós, A. *et al.* Cnidarian Cell Type Diversity and Regulation Revealed by Whole-Organism Single-Cell RNA-Seq. *Cell* **173**, 1520–1534.e20 (2018).
3. Rao, A., Barkley, D., França, G. S. & Yanai, I. Exploring tissue architecture using spatial transcriptomics. *Nature* **596**, 211–220 (2021).
4. Junker, J. P. *et al.* Genome-wide RNA Tomography in the Zebrafish Embryo. *Cell* **159**, 662–675 (2014).
5. Busse, S. M., McMillen, P. T. & Levin, M. Cross-limb communication during xenopus hindlimb regenerative response: Non-local bioelectric injury signals. *Dev.* **145**, (2018).
6. Payzin-Dogru, D. *et al.* Nerve-mediated amputation-induced stem cell activation primes distant appendages for future regeneration events in axolotl. *bioRxiv* (2021). doi:10.1101/2021.12.29.474455
7. Easterling, M. R., Engbrecht, K. M. & Crespi, E. J. Endocrine Regulation of Epimorphic Regeneration. *Endocrinology* **160**, 2969–2980 (2019).
8. Losner, J., Courtemanche, K. & Whited, J. L. A cross-species analysis of systemic mediators of repair and complex tissue regeneration. *npj Regen. Med.* **6**, 1–11 (2021).
9. Owlarn, S. *et al.* Generic wound signals initiate regeneration in missing-tissue contexts. *Nat. Commun.* **8**, 1–13 (2017).
10. Myster, D. L. & Duronio, R. J. Cell cycle: To differentiate or not to differentiate? *Curr. Biol.* **10**, 302–304 (2000).



“Anyone whose goal is ‘something higher’ must expect some day to suffer vertigo.”
- Milan Kundera, *The Unbearable Lightness of Being*, p.58

Chapter 6

Addendum

Nederlandse samenvatting

Regeneratie in het dierenrijk houdt in dat dieren een lichaamsdeel, zoals een arm of een staart, kunnen hergroeien nadat ze deze zijn kwijtgeraakt. Hoewel we vaak over regeneratie denken als de hergroei van een ledemaat, kunnen ook kleinere structuren (zoals een onderdeel van een zenuw of een orgaan) regenereren. Sommige dieren kunnen ook veel grotere structuren hergroeien. De platworm *Planaria* kan bijvoorbeeld in 279 kleine stukken gesneden worden, waarna elk stukje weer uit kan groeien tot een volledige platworm. Het vermogen om een compleet lichaam te kunnen hergroeien uit een klein stukje weefsel wordt “whole-body regeneration” genoemd. Van de verschillende regeneratie types is dit de meest indrukwekkende omdat een heel klein stukje weefsel het vermogen heeft om alle verschillende onderdelen van het lichaam te hergroeien. Hoe dit kleine stukje weefsel precies weet welke lichaamsdelen er precies missen en hoe het lichaam er uit zag is nog steeds niet veel over bekend.

Officieel begon de studie van regeneratie in het midden van de 18de eeuw. Wetenschappers waren gebiologeerd door het vermogen van verschillende dieren om missende lichaamsdelen te hergroeien en zochten naar manieren om te begrijpen hoe regeneratie plaatsvindt in deze dieren. *Hydra*, een zoetwater diertje met een simpel buisachtig lichaam met tentakels aan een uiteinde, was het eerste dier waarbij de regeneratieve vermogens beschreven werden. Na deze ontdekking bleken meer dieren lichaamsdelen te kunnen hergroeien. De platworm *Planaria*, de Zebravis en de salamander zijn een aantal van de meest populaire model systemen die gebruikt worden om regeneratie te bestuderen. Door te onderzoeken hoe al die dieren lichaamsdelen kunnen hergroeien hebben wetenschappers geleerd hoe regeneratie kan beginnen beginnend met een wond. Elk dierlijk modelsysteem heeft zijn eigen specifieke gebreken en limitaties wat wetenschappers van ze kunnen leren. Daarom worden er nog steeds nieuwe dieren geïntroduceerd om regeneratie te bestuderen en beter te begrijpen welke factoren belangrijk zijn.

Nematostella vectensis, een kleine zeeanemoon, is een van deze nieuwe diermodellen die gebruikt worden om regeneratie te bestuderen. Deze zeeanemoon is een eenvoudig diertje maar deelt nog steeds veel genetische eigenschappen met mensen. Het is ook een makkelijk dier om mee te werken en het kan zijn hele lichaam regenereren. Vanwege deze handige eigenschappen is *Nematostella* onze keuze geweest om regeneratie te bestuderen. Ik heb deze zeeanemoon gebruikt tijdens mijn promotieonderzoek om beter te begrijpen hoe de verschillende delen van het anemonen lichaam reageren op verwonding en regeneratie. In plaats van alleen naar het regenererende deel van het lichaam te kijken, hebben we gekozen voor een meer holistische aanpak door naar het complete anemoon lichaam te kijken.

In **Hoofdstuk 1** van dit proefschrift geef ik een algemene introductie voor regeneratie onderzoek.

Hoofdstuk 2 beschrijft hoe we nieuwe sequencing technologie gebruikt hebben om te achterhalen welke genen ge-exprimeerd worden in het anemoon lichaam als er geen regeneratie plaatsvindt. We hebben meer dan 200 genen gevonden die zeer specifieke expressie patronen vertoonden over de belangrijkste lichaamsas. Onze resultaten

hebben ertoe geleid dat we een ruimtelijke genexpressie kaart hebben kunnen maken, wat een belangrijke kennisbron kan zijn voor de *Nematostella* onderzoek gemeenschap.

In **Hoofdstuk 3** hebben we gekeken naar hoe genexpressie veranderd tijdens regeneratie op verschillende tijdstippen en plekken. Hoewel veel gen activiteit veranderd bij de wondlocatie, hebben we ook gezien dat er zeer veel veranderingen plaatsvinden in lichaamsdelen verder weg van de wond. Deze veranderingen die ver weg van de wond plaatsvinden zijn interessant genoeg vergelijkbaar met de veranderingen bij de wondlocatie. Daarna hebben we laten zien dat deze reacties ook plaatsvinden als de anemoon op een andere manier schade ondervindt (door middel van hitte) en dat schade zonder een wond ook regeneratie kan induceren in *Nematostella*.

In **Hoofdstuk 4** hebben we ontdekt dat de *Nematostella* tentakels ook kunnen regenereren nadat ze van het lichaam zijn afgehakt. Door middel van klassieke biologie methodes hebben we laten zien dat tentakels kunnen regenereren zonder signalen van de rest van het lichaam zolang er maar een speciale groep cellen in de tentakel aanwezig zijn. Als deze cellen verwijderd worden zijn er daarentegen wel signalen van de rest van het lichaam nodig om de tentakel te regenereren.

Ik eindig dit proefschrift in **Hoofdstuk 5** waar ik de resultaten van mijn promotie onderzoek uitleg in de context van het brede regeneratie onderzoek.

English summary

Animal regeneration describes the ability of animals to regrow a missing body part, such as an arm or a tail. While we often think about regeneration to mean regrowth of limbs, regeneration can also describe the regrowth of smaller structures (such as part of a nerve, or part of an organ like the liver). Some animals are also able to regrow much larger structures. For example, when the flatworm *Planaria* is cut into 279 little pieces, each piece is able to regrow into a full worm again. This ability to reform an entire body from a small fragment of tissue is called whole-body regeneration. This is the most impressive type of regeneration because in this case, a very small bit of tissue is able to regrow all the different parts of the whole body. How the small piece of tissue knows which body parts are missing and what the body used to look like is still poorly understood.

The study of regeneration formally started in the mid 1700s. Scientists were captivated with the ability of various animals' ability to regrow missing body parts and sought to understand how regeneration happens in these animals. The first animal to have its regenerative abilities documented is the Hydra, a freshwater creature with a simple tube-like body with tentacles extending from one end. Since the discovery of Hydra's impressive regenerative abilities, many animals have been found to be able to regrow body parts. Some of the most popular animals used to study regeneration include a flatworm (*Planaria*), a small fish (zebrafish), and a lizard (salamander). By studying how each of these animals are able to regrow lost body parts, scientists have learned a lot about how wounding can lead to regeneration. However, each of these animals has its shortcomings and limitations in terms of what scientists can learn from them. Thus, new animals are still being introduced into the field of regeneration to allow scientists to better understand the many factors involved in successful regeneration.

Nematostella vectensis, a small sea anemone, is one of these new animals being used to study regeneration. This sea anemone is very simple but it still shares many genetic similarities with humans. It is also very easy to work with and is capable of whole-body regeneration. Because of these advantages, *Nematostella* became our animal of choice to study regeneration. During my PhD I used this sea anemone to better understand how different parts of the animal respond to injury and regeneration. Rather than focusing on only the regrowing body part, we take a more holistic approach by looking at the entire body of the animal.

In **Chapter 1** of this thesis, I give a general introduction to the field of regeneration.

Chapter 2 describes how we used new sequencing technology to find out what genes are being expressed throughout the animal when it is not regenerating. We identified over 200 genes that had very specific expression patterns across the major body axis. Our results allowed us to generate a spatial gene map of the animal, which would serve as a powerful resource for the *Nematostella* community.

In **Chapter 3**, we looked at how genes changed over time and space during regeneration. We learned that while a lot of genes change at the wound site, there are also many changes

happening in distant body parts. Interestingly, these changes in distant body parts are similar to the response at the wound site. We then showed that these responses are also present when the animal is stressed in a different way (i.e. heat shock) and that non-wounding stresses can also initiate regeneration in *Nematostella*!

In **Chapter 4**, we discover that the tentacles of *Nematostella* can regenerate when detached from the body. Using classical biology techniques, we show that the tentacles can regenerate without input from the body when a very special group of cells are present. When these cells are removed, input from the body is required for successful regeneration.

I conclude this thesis in **Chapter 5** where I put the results of my PhD work into the context of the field of regeneration.

Acknowledgements

My PhD journey has truly been eventful. I have met so many wonderful, smart, interesting, and funny people throughout my post graduate years and I have learned and grown so much as a person and scientist. There are so many people to give thanks to for being a part of my PhD journey. I will use the next few pages to acknowledge all those who have shared their time with me and I apologize now if I forget anybody!

First of all, thank you to **Aissam** for all your support throughout my PhD. I remember we first met online via Skype to chat about opportunities in your new lab at EMBL. I don't think you were too certain about me at that initial meeting. But luckily, we met again at the predoc interviews and ended up having great conversations filled with ideas for things to explore using the little starlet sea anemone. It's been a great 4.5 years in the Ikmi lab and I have to thank you for creating and maintaining such a great lab atmosphere!

Annik!! We started together at EMBL and now we are leaving together back to Holland! I'm so glad we did our PhDs together! I am eternally enviously of your patience and dedication to your work. You were the best lab mate, bench mate, and friend I could ask for to have shared my PhD with. And now thank you for being my paranymp!

To **Peter**, you were the backbone of our lab. Thanks for keeping everything running smoothly these past 4.5 years, even during the crazy corona times. **Marie**, it was so nice having you in the lab. I really enjoyed our many conversations about Japan and food and of course it was so much fun meeting your parents and staying with them in Tokyo! **Soham**, you have been so much fun to have in the lab. I really enjoyed our many little talks and all the great Indian food you have introduced me to. **Kaushik**, thank you for all your great input at lab meetings and fun lunch conversations. **Richard**, thank you for getting HCR to work in the lab! It really saved my project. **Jaro**, it was so nice to have you as a regeneration buddy. **Giulia**, you are always a ray of sunshine in the lab. It was great working with you on the tentacle project. To my students, **Sofie** and **Pauline**, I'm really glad I got to be a part of your internship at EMBL and I have learned so much from you two. **Omar**, thanks for all the super sweet cakes :) To the rest of the Ikmi lab members: **Melody**, **Julia**, **Paulo**, **Florian**, **Carlotta**, and **Irie** thanks for being a part of our little lab family. I hope I didn't bully you guys too much during your internships :)

Thank you to the Ephrussi lab for being so nice throughout my PhD and for always being happy to lend equipment or chemicals when we needed something. I'm very happy to have been a part of your little lab family. **Jane** and **Vaishali**, thanks for all the fun times during the predoc course. **Anna** and **Ale**, thanks for always being available to answer any questions I had about the unit. **Brana**, it been so much fun getting to know you and for the awesome bread recipe! **Lucia**, thanks for all the fun talks and car rides! **Alex**, you are always fun to talk to. I will miss our long talks about science and politics and life.

To the members of the Hiiragi lab (**Allison**, **Ester**, **Hui Ting**, **Dimitri**, **Prachiti** and **Vlad**),

thanks for the great joint meetings and scientific discussions. It's been great having you guys down the hall, we missed you after your move but luckily you didn't go far. I'm looking forward to seeing some of you in Utrecht!

To the Aulehla lab, you guys were like the big brother lab when we first started. I loved our joint lab parties. **Gregor** and **Ivica**, you guys always gave the best BBQs. I will miss hanging out in your back yard. **Takehito** and **Silvia**, I will miss our random chats on the bus and the DB kitchen. **Nobuko**, I will miss your smiley face and our kimchi exchanges! **Hide**, **Christine**, **Paul**, and **Carina**, thanks for all the good times and for always welcoming me to crash your lab lunches. **Emilia**, I'm so glad to have gotten to know you and your family these last few years. You are like our extended family in Heidelberg; Ollie's second mama ;)

Tobi, thanks for working with me to combine our tomo-seq data with single cell sequencing. It was really nice to have someone else to discuss the project with. **Leslie**, thank you for being like a mama duck to me. I will miss seeing you and Hannes on the bus! **Kevin**, thanks for the great chats. You are always fun to talk to and have helped keep me sane during the crazy corona times.

Annabel and **Marco**, thank you so much for helping me set up tomo-seq for Nematostella. You two made me feel very welcome during my visit to your lab and my PhD couldn't have been possible without it.

Rik, thank you for being my promotor and for all your support for the tomo-seq project! And thank you to the rest of my PhD committee members, **Kerstin**, **Alexander A.**, and **Alba** for the great feedback and discussions at my TAC meetings. Also many thanks to my reading committee members (**Takashi**, **Alexander van A.**, **Eugene**, **Jeroen**, and **Mike**) for looking through my thesis and being there for my defense ceremony!

Stefano, thanks for being such a good friend these past few years and for rides to EMBL. I will miss our lunch discussions. **Walt**, it's been great getting to know you these last few years. Thanks for all the great meals and conversations.

Danila, for all the fun times and for joining me on my tomo-seq project. The project would not have been possible without your master computational skills. I'm so glad I bothered you during the predoc course and we became friends. Thanks for all the books and dinners and lunches and interesting conversation throughout the years.

Thank you to **Oliver** for all the great discussions about the Tomo-seq project.

Hanh, **James** and **Joey**, it's been so nice getting to know all of you. I will miss our little family hang outs. To **Eva**, **Richardo**, and **David**, thanks for all sharing all your kid's insights. It's so great our kids got along so well! And to **Christina**, thanks for all the good conversations on the bus and around EMBL! You are always fun to talk to!

Marieke and **Chris**, thanks for being so awesome and helping us with our big move! You two are always so nice to be around. And of course, thanks for being my paranymp!

Jess, you are always so much fun to talk to. Thank you for being there since my MIT days. We finally did it! To **Barbara** and the rest of the Imperiali lab (**Michelle, Vinita, Austin, Philip, Andrew, Elke**) at MIT, thanks for memories and for teaching me about biochemistry. I learned so much from all of you. I really think my time at MIT is when my PhD journey really began. Now, almost 10 years later I am finally getting those three extra letters behind my name.

To **Dorus** and the rest of the **MolCyto** crew (**Orry, Daphne, Lindsey, Natalie, Marieke, Linda, Laura, Anna, Anna, Joachim, Mark, Ronald, Marten, Anoeska, Rene, Sergei, Amber, Nika, and Katrin**), thank you so much for teaching me all about microscopy. I had lots of fun at our borrels and Sinterklaas parties and will always remember the poffertjes!

And of course, I must thank my family in Hawaii for all their support. 爸爸妈妈，感谢你们的牺牲，使我有机会在美国长大。感谢你们在我学习期间的所有支持。Thank you to my brother, **Edmond**, for always being a great big brother and looking after your little sister. I still can't believe you will all be here for my defense! I'm so looking forward to hanging out with you and **Vanda** and **Lia**!

To my parents-in-law, **Tonny** and **Peter**, thanks for being such cool in-laws. It's always fun to hang out with you and I always enjoy your visits and our Christmas holidays. To **Marlon, Haley, Addison, and Charlie**, I'm sad you won't make it to the defense but it's been a blast hanging out with you all this summer!

And the biggest thank you to **Dylan** for being the best husband, father, and friend a girl could ask for. You make every day fun and I still think you are the smartest man I know. Thank you for putting up with my constant bad spelling, mispronunciations, and old lady remarks. I am so lucky to have had your unwavering support during my pursuit of the PhD; none of this would have been possible without you! And finally, to my little boy **Ollie**, you have made these last 2 years a great adventure. Mommy loves you!

List of Publications

Published works

Van Gell, O.; **Cheung, S.**; Gadella TWJ. Combining optogenetics with sensitive FRET imaging to monitor local microtubule manipulations. Scientific Reports, 2020, 10(1):6034

de Picciotto, S.D.; Dickson, P.M.; Traxlmayr, M.W.; Marques, B.S.; Socher, E.; Zhao, S.; **Cheung, S.**; Kiefer, J.D.; Wand, A.J.; Griffith, L.G.; Imperiali, Wittrup, B.K.D. Design principles for SuCESsFul biosensors: Specific fluorophore/analyte binding and minimization of fluorophore/scaffold interactions. Journal of Molecular Biology. 2016, 428(20), 4228-4241.

Works in preparation

Cheung S., Bergamini G., Matar O., Steenbergen P., Ikmi, A.; Mechanisms of tentacle regeneration in the sea anemone *Nematostella vectensis*.

Cheung S.*, Bredikhin D.*, Steenbergen P., Korswagen H.C., Stegle O., Ikmi A.; Spatiotemporal transcriptomics link systemic stress response to regeneration in the sea anemone *Nematostella vectensis*

**these authors contributed equally*

Curriculum Vitae

Stephanie Cheung was born in Guangdong, China on May 15, 1989. At the age of 3.5, Stephanie immigrated with her family to the United States of America. She grew up in Honolulu, Hawaii and graduated from Roosevelt High School in 2007. Then she moved to Grinnell, Iowa to attend a small liberal arts college called Grinnell College where she double majored in Sociology and Chemistry. During her college years, Stephanie explored multiple areas of Chemistry via 3 internships focusing on synthetic organic chemistry and developing nanomaterials for hydrogen production. In 2011, she moved to Boston, Massachusetts to pursue a graduate degree in Biological Chemistry at MIT where she worked in Barbara Imperiali's lab developing fluorogenic biosensors to detect small ligands. After receiving her MSc, she moved to the Netherlands and worked as an R&D technician in a small biotech company called Dyadic, Inc. Stephanie then decided to return to academia to pursue a long-time passion of hers: microscopy. So, she took on the role of a research technician at the University of Amsterdam in Dorus Gadella's lab where she developed FRET sensors and novel fluorescent proteins. At this point, Stephanie knew she wanted to pursue a PhD somewhere where she could combine advanced microscopy techniques to study biology in live animals. Thus, in 2017 Stephanie began her PhD studies at EMBL in Heidelberg, Germany under the supervision of Aissam Ikmi. The results of her PhD work are described in this thesis.

“Well, sometimes science is more art than science, Morty. A lot of people don’t get that.”

- Rick Sanchez (Rick and Morty)

